JESCEE
Journal of Emerging Supply Chain, Clean Energy, and Process Engineering

p-ISSN 2963-8577

Vol 1. No 1. 2022

JESCEE | Vol. 1 | No. 1 | pp. 1-83 | JAKARTA 2022 | ISSN 2963-8577

Faculty of Industrial Technology
Universitas Pertamina

Universitas Pertamina

Journal of

Emerging Supply Chain, Clean Energy and Process Engineering

Vol 1, No 1, 2022

Journal of
Emerging Supply Chain, Clean Energy and Process Engineering
Vol 1, No 1, 2022

Journal of

Emerging Supply Chain, Clean Energy and Process Engineering

Vol 1, No 1, 2022

Reviewers

1. Dr. Indar Chaerah Gunadin, S.T., M.T. (Universitas Hasanuddis, Indonesia)
2. Dr. Eng. Imam Wahyudi Farid, S.T., M.T. (Institut Teknologi Sepuluh Nopember, Indonesia)
3. Dr. Eng. Lusi Ernawati, S.T., M.Sc. (Institut Teknologi Kalimantan, Indonesia)
4. Anak Agung Ngurah Perwira Redi, Ph.D (Sampoerna University, Indonesia)
5. Dr. Eng. Murman Dwi Prasetyo, S.T, M.B.A. (Universitas Telkom, Indonesia)
6. Judha Purbolaksono, S.T., M.T., Ph.D (Universitas Pertamina, Indonesia)
7. Dr. Eng. Agus Susanto, S.Pd., M.T. (Politeknik Negeri Madiun, Indonesia)
8. Agung Nugroho, S.T., Ph.D (Universitas Pertamina, Indonesia)
9. Dr. Soni Prayogi, M.Si. (Universitas Pertamina, Indonesia)
10. Dr. Eng. Aditya Tirta Pratama, S.Si, M.T. (Swiss German University, Indonesia)
11. Teuku Muhammad Roffi, S.T, M.Eng., Ph.D (Universitas Pertamina, Indonesia)
12. Dr. Eng. Wahyu Kunto Wibowo, S.T., M.Eng. (Universitas Pertamina, Indonesia)
13. Eduardus Budi Nursanto, S.T., M.Eng. Ph.D (Universitas Pertamina, Indonesia)

Imprint

JESCEE is published by Faculty of Industrial Technology, Universitas Pertamina, Jakarta Selatan, Indonesia.

Postal Address

JESCEE Secretariat:

Universitas Pertamina

Jl. Teuku Nyak Arief, Simprug, Kebayoran Lama, Jakarta Selatan, 12220

Indonesia

Business hour: Monday to Friday

07:00 to 17:00 GMT+7

e-mail: jescee@universitaspertamina.ac.id

Journal of

Emerging Supply Chain, Clean Energy and Process Engineering

Vol 1, No 1, 2022

PREFACE

The Journal of Emerging Supply Chain, Clean Energy and Process Engineering (JESCEE) is a journal of the Faculty of Industrial Technology, Universitas Pertamina that promotes communication between researchers, dissemination of research results, development of academic culture, and development of new ideas in the fields of mechanical, electrical, chemical, and logistics. This journal's volume 1, issue no. 1 has captivated the attention of numerous researchers interested in publishing their work.

On behalf of the Editor-in-Chief, I would like to thank the people who support this journal, especially the Dean of the Faculty of Industrial Technology Industrial for their direct and indirect assistance, the editors who work well and are dedicated, the reviewers who provide suggestions and constructive criticism for each paper collected, and the authors who entrust JESCEE with the publication of their research results.

We hope that this publication will continue to expand and present the most recent information in the fields of mechanical, electrical, chemical, and logistical. We also welcome collaboration from parties who are pleased with the existence of this journal and wish for its further growth.

Jakarta, August 2022
Editor-in-Chief

Dr. Eng. Muhammad Abdillah

Journal of

Emerging Supply Chain, Clean Energy, and Process Engineering

Vol 1, No 1, 2022

List of Contents

Vol. 1, No. 1, August 2022, pp. 1-6
p-ISSN: 2963-8577
DOI: 10.57102/jescee.v1i1.3

THE EFFECT OF ADDITION OF SnO2 DOPING ON THE ELECTRONIC STRUCTURE OF TiO2 THIN FILM AS PHOTO-ANODE IN DSSC APPLICATIONS

Soni Prayogi[1*], Marza Ikhsan Marzuki[1]
[1]Department of Electrical Engineering, Faculty of Industrial Engineering, Universitas Pertamina

Abstract
Photoanode is a component of the dye-sensitized solar cell (DSSCc) which is synthesized from metal oxide semiconductor material with nanoparticle size deposited on transparent conductive glass. TiO2 powder was synthesized by mixing 20 mL of Titanium (III) chloride (TiCl3) with 100 mL of the equator and stirred for 1 hour. TiO2-SnO2 thin films have been successfully synthesized using the coprecipitation method and coated on ITO (Indium Tin Oxide) substrate by doctor-blade technique. The structure and morphology of the films were investigated by XRD and SEM respectively. The analysis of optical characteristics shows that the absorbance of TiO2 photoanode is in the wavelength range of 300-600 nm while SnO2 is in the wavelength range of 300-870 nm. The results showed that the synthesized film with SnO2 had a stronger anatase formation than the film with pure TiO2. Finally, incorporating SnO2 into the TiO2 matrix is an effective strategy to improve the overall properties of solar cells in future applications.

Keywords:
DSSCs; photoanode; solar cells; thin film

Article History:
Received: July 31st, 2022
Revised: August 7th, 2022
Accepted: August 25th, 2022
Published: August 31st, 2022

Corresponding Author:
Soni Prayogi
Department of Electrical Engineering, Universitas Pertamina, Indonesia
Email:
soni.prayogi@universitaspertamina.ac.id

1. Introduction

The need for energy in Indonesia continues to increase. This is due to infrastructure development, regional expansion, road construction, etc[1]. At this time, the need for energy is obtained from energy sources that are conventional and non-renewable, such as coal, gas, and oil[2]. Reserves from these energy sources will decrease, while the need for energy will increase[3]. To overcome these problems, alternative energy sources are needed that can help reduce dependence on non-renewable energy sources[4]. Renewable energy that is growing rapidly in the world today is wind energy and solar energy[5]. Wind and solar energy sources are clean and freely available renewable energy sources.

Dye-sensitized solar cell (DSSCs) is a type of third-generation solar cell that utilizes photoelectrochemical principles[6]. This type of solar cell is believed to be able to provide an alternative energy concept with a more affordable production cost and with a simpler fabrication technology than its predecessor solar cells made from crystalline silicon[7]. A typical DSSC consists of several microns thick nanostructured semiconductor that is deposited on a conductive substrate as a framework of DSSCs photoanode[8]. Titanium dioxide (TiO_2) is one of the most selected and studied extensively photoanodes materials in DSSCs[9]. TiO_2 can be found in its three polymorphs in nature: anatase, brookite, and rutile[10]. However, anatase is mostly used due to its excellent stability and photoactivity. Additionally, TiO_2 has proven as a fascinating material and has been used for many different applications in both gas sensors and DSSCs because of its biological, and chemical inertness, long-term stability against chemical and photo-corrosion

One of the factors that are still a problem in the manufacture of DSSC solar cells is the use of electrolytes, both gels, and solutions, which have an important role in converting light energy into electrical energy in these solar cells[11]. Because the shape is generally in the form of a solution, many problems arise related to the use of electrolytes, such as leakage, evaporation, the possibility of corrosion of the center-electrode, and so on[12]. Most of the problems above are related to the issue of stability of cell performance in the long term[13]. In addition, the selection of the right type of electrolyte solution is also one of the factors that are still widely studied by researchers [14]. In this work, we synthesized TiO_2 and TiO_2-SnO_2 nanocomposites by coprecipitation method, and their structures and morphology were characterized and compared with pure TiO2 photoanodes.

2. Experimental Details

TiO_2 powders were synthesized by mixing 20 mL of Titanium (III) chloride ($TiCl_3$) with 100 mL of equates and were stirred for 1 hour. To this mixture, NH_4OH *solution* was added *dropwise until pH reached* 9. The resultant solution was stirred until the resulting white precipitate. The precipitate was filtered and was then washed several times with distilled water, reaching a value of pH equal to 7. The removal process of residual organics and the stabilization of the materials were carried out by calcination for three hours at 450°C.

The equipment used includes a digital multimeter, hot plate with magnetic stirrer, hair dryer, ultrasonic cleaner, 10 ml and 50 ml beakers, pipettes, 5 ml glass bottles, digital scales, Whatman no.42 filter paper, column chromatography mortar, and spin coater ITO glass substrates were purchased from Mianyang Prochema Commercial Co., Ltd., China. ITO with a size of 1 × 1 cm^2 was thoroughly rinsed with deionized water and anhydrous ethanol and dried on a hot plate. The manufacture of ITO glass layer DSSC which has been coated with TiO2 and has been dipped in the extracted dye solution is called the working electrode. The working electrode is dripped with an electrolyte solution and then covered with a platinum-coated counter electrode called the counter electrode[15]. Then the DSSC device is clamped on both the right and left sides, so it doesn't come off. The DSSC device is shown in Fig. 1. The films were heated at 450°C for one hour and cooled naturally to obtain a nano-porous film. The structure and morphology of the films were characterized by XRD and SEM.

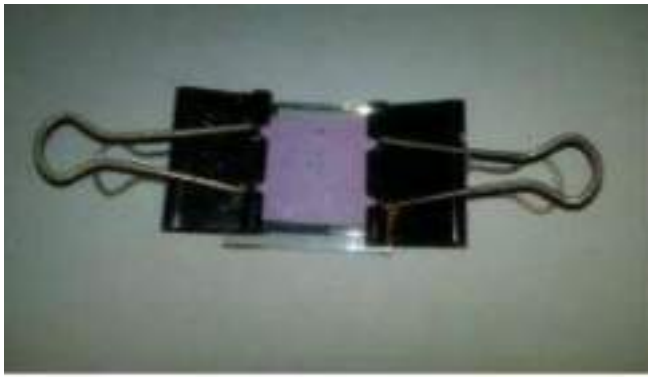

Figure 1. DSSC Device Display

3. Results and Discussion

The crystalline phase of photoanode films was evaluated by XRD analyses, and the result is shown in Fig. 2. It can be seen that the films are polycrystalline, and the diffraction peaks observed around 26 and 49 degrees correspond to the (101) and (200) reflexes of the anatase phase of TiO_2 with the tetragonal crystal structure. The TiO_2 film exhibits a new diffraction peak (222) plane around 31 degrees, which belongs to the ITO peak. These results agree with the analysis of the microstructure of pure TiO_2 film.

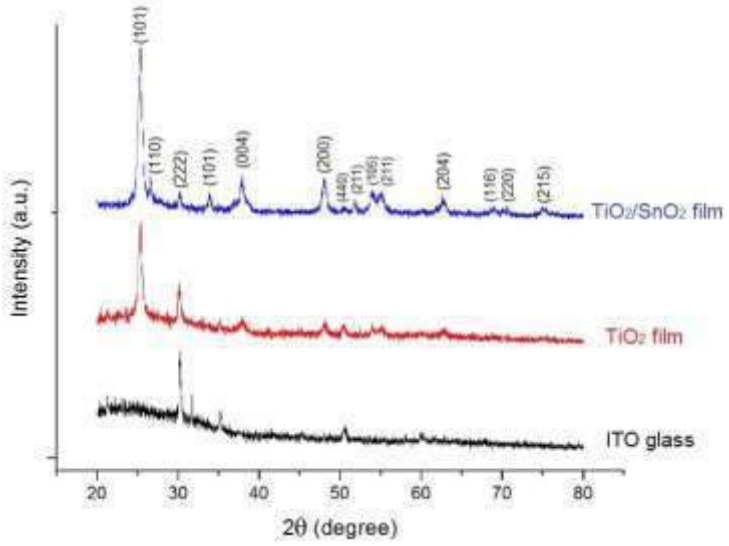

Figure 2. XRD spectra of pure and TiO2-SnO2 photoanodes

Furthermore, the diffraction peaks from rutile phase appear in the X-ray patterns due to the addition of the SnO_2 in the film. The (110), (101), and (211) planes at 2θ values 27, 34.1, and 53 degrees were observed as the characteristic peaks of SnO_2 in the doped TiO_2 film. Similar results have also been reported in previous studies. indicated that the increase of the concentration of dopant in the film has an effect on the transformation anatase to the rutile crystalline phase[16]. Nevertheless, the intensity of the (101) plane is higher than the intensity of pure TiO_2 film because of the electronegativity, and the ionic radius of Sn^{4+} ions is larger than Ti^{4+}[17]. It allowed easily for Sn^{4+} ions to replace and occupy the oxygen position in the TiO_2 lattice Thus, the spectrum shows the intensity of the (101) plane is gradually increased with the decreased ITO peak (222) plane, which indicated that better crystallinity than the pure TiO_2 film was obtained.

This feature gives a more stable chemical bond and permits excellent interconnection and continuity between titania nanoparticles, which in turn enhances electron transfer efficiency in photoanode[18]. This phenomenon showed that the inclusion of SnO_2 in the TiO_2 may stabilize the anatase as the main and strongest phase. The smaller radius of Ti^{4+} (0.68 Å) as compared to Sn^{4+} (0.69 Å) also made the crystallite size of doped TiO_2 film bigger than the pure one[20]. The average crystallite size, which is calculated from XRD data using the Rietveld method, is 34.2 and 10.3 nm for the doped TiO_2 and the pure TiO_2 films respectively.

Fig. 3 show represents the top-view SEM images of the doped and pure TiO_2 films. These images confirm that the microstructure of both samples exhibits spherical-shaped particles with irregular morphology due to the agglomeration of primary particles during the annealing treatment[21]. It can be seen that smaller particles with an average diameter of 10 − 11 nm were measured for pure TiO_2 and around 35 nm for SnO_2 doped TiO_2 film. The enlarging particle size of the doped TiO_2 film results in a larger surface area of the film, thus enabling a high dye loading capacity as well as enhancing the photosensitivity to solar radiation.

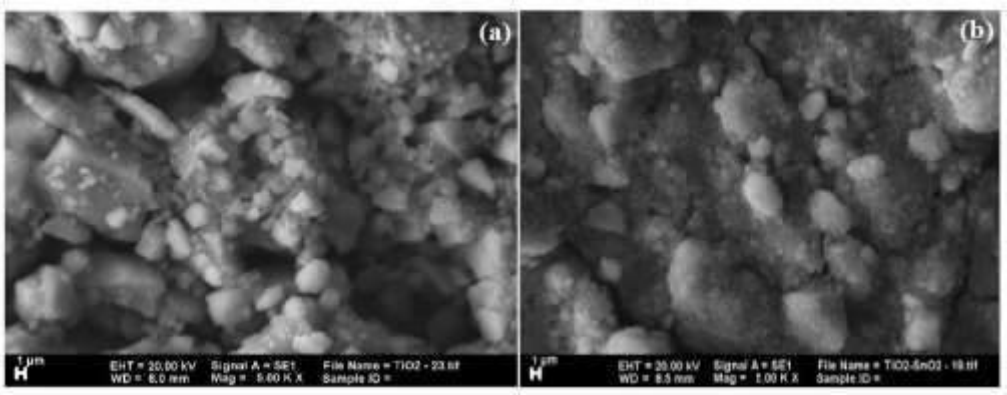

Figure 3. SEM micrographs of (a) pure TiO_2 and (b) TiO_2-SnO_2 films

The porous nature was observed in both films and this structure also plays a role in enhancing the surface area of the film photoanode. A bit rough, large and intense inhomogeneous agglomerations were formed in the pure TiO_2 film. In DSSC's system, these agglomerations decrease electron mobility and result in slow transport and recombination of photoexcited electrons[23]. On the other hand, TiO_2-SnO_2 exhibits smooth and rather well-distinguished uniform aggregates, although also there are a few voids and cracks which may be due to the loss of the binder during the annealing process[24]. These results indicate that the presence of SnO_2 can effectively suppress the grain growth of anatase compared with pure TiO_2.

The results of the analysis of the optical characteristics and band gap of the photoanode are obtained in the form of absorbance and transmittance graphs that describe the optical characteristics of the photoanode. It can be seen that the absorbance of TiO2 photoanode is in the wavelength range of 300-600 nm while SnO2 is in the wavelength range of 300-870 nm.

The photoanode has a wavelength range of 300-870 nm and the highest absorbance value when compared to TiO2 and SnO2 photoanodes. This is because the photoanode is composed of two constituent layers, namely the TiO2 layer which has a high absorbance value and the SnO2 layer which has a wavelength range of 300-870 nm. Fig. 4 shows the absorbance values in a certain wavelength range of TiO2, SnO2, and photoanodes where the absorbance value of photoanodes is lower than that of TiO2 photoanodes in the 300-600 nm wavelength range, but higher than SnO2 photoanodes in the wavelength range. 300-870 nm. This is because the photoanode is composed of one constituent layer, namely the TiO2/SnO2 composite layer so that absorbance is lower than TiO2 photoanode but has the same wavelength range as SnO2 photoanode.

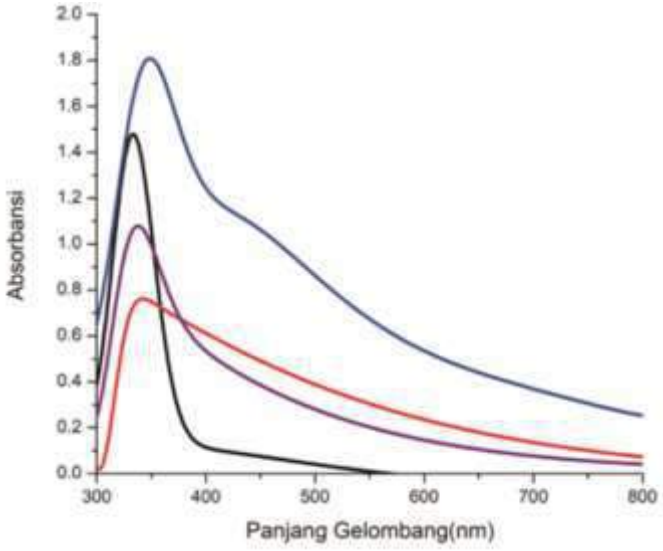

Figure 4. Photoanode absorbance value

In the photoanode the composite structure is layer by layer where there are 2 layers, namely SnO2 and TiO2 layers. SnO2 has a higher density than TiO2 so that the dye only sticks to TiO2. Because the dye only sticks to TiO2, SnO2 only accepts electron injection from TiO2. Meanwhile, in the SL photoanode the composite structure is a mixture of TiO2 and SnO2. So that the dye can stick to the surface of TiO2 and SnO2. This resulted in 2 recombination processes, namely from the TiO2 and SnO2 conduction bands to the HOMO dye level.

4. Conclusion

In summary, the proposed work compared the structural and morphological properties of the TiO2-SnO2 nanocomposite and the synthesized pure TiO2. The XRD pattern of the photoanode of TiO2 anatase with SnO2 shows superior crystallinity and stronger formation compared to the photoanode of pure TiO2 anatase. These results indicated that adding SnO2 could enhance the stability and microstructure of the photoanode. Additionally, the SEM analysis reveals the SnO2 dopants' existence in the TiO2 lattice. The surface of the doped TiO2 film showed a smooth and rather homogeneous aggregate; this explains that SnO2 content can suppress the crystal growth of TiO2 grains. Consequently, incorporating SnO2 into the TiO2 matrix was an effective strategy for enhancing the overall properties of solar cells in future applications.

Acknowledgment

One of the authors (SP) thankfully acknowledges the Pertamina University and Ministry of Finance of the Republic of Indonesia, through the Lembaga Pengelola Dana Pendidikan (LPDP), which has provided financial support through the Scholarship Indonesian.

References

[1] K. Nithyanandam and R. Pitchumani, "Analysis and design of dye-sensitized solar cell," *Sol. Energy*, vol. 86, no. 1, pp. 351–368, Jan. 2012, doi: 10.1016/j.solener.2011.10.009.

[2] C. C.-V. Pablo, R.-R. Enrique, A. R.-G. José, M.-P. Enrique, L.-H. Juan, and N. A.-M. Eddie, "Construction of Dye-sensitized Solar Cells (DSSC) with Natural Pigments," *Mater. Today Proc.*, vol. 3, no. 2, pp. 194–200, Jan. 2016, doi: 10.1016/j.matpr.2016.01.056.

[3] J. F. Kang *et al.*, "Design and optimization of larger-sized dye sensitized solar cell (DSSC)," in *2010 Photonics Global Conference*, Dec. 2010, pp. 1–3. doi: 10.1109/PGC.2010.5706115.

[4] M. Mazalan, M. M. Noh, Y. Wahab, M. N. Norizan, and I. S. Mohamad, "Development of dye-sensitized solar cell (DSSC) using patterned indium tin oxide (ITO) glass: fabrication and testing of DSSC," in *2013 IEEE Conference on Clean Energy and Technology (CEAT)*, Nov. 2013, pp. 187–191. doi: 10.1109/CEAT.2013.6775624.

[5] S. Prayogi, Ayunis, Kresna, Y. Cahyono, Akidah, and Darminto, "Analysis of thin layer optical properties of A-Si:H P-Type doping CH4 is deposited PECVD systems," *J. Phys. Conf. Ser.*, vol. 853, p. 012032, May 2017, doi: 10.1088/1742-6596/853/1/012032.

[6] N. Roslan, M. E. Ya'acob, M. A. M. Radzi, Y. Hashimoto, D. Jamaludin, and G. Chen, "Dye Sensitized Solar Cell (DSSC) greenhouse shading: New insights for solar radiation manipulation," *Renew. Sustain. Energy Rev.*, vol. 92, pp. 171–186, Sep. 2018, doi: 10.1016/j.rser.2018.04.095.
[7] D. Devadiga, M. Selvakumar, P. Shetty, and M. S. Santosh, "Dye-Sensitized Solar Cell for Indoor Applications: A Mini-Review," *J. Electron. Mater.*, vol. 50, no. 6, pp. 3187–3206, Jun. 2021, doi: 10.1007/s11664-021-08854-3.
[8] K. Hosseinpanahi, M. R. Golzarian, M. H. Abbaspour-Fard, and J. Feizy, "Improving The Efficiency of DSSC with A Novel Multi-dye layers Approach," *Optik*, vol. 208, p. 164068, Apr. 2020, doi: 10.1016/j.ijleo.2019.164068.
[9] R. Vasanthapriya, N. Neelakandeswari, K. Uthayarani, and M. Chitra, "Influence of pH on the DSSC Performance of Template Assisted SnO2 Nanostructures," *J. Inorg. Organomet. Polym. Mater.*, vol. 31, no. 11, pp. 4272–4280, Nov. 2021, doi: 10.1007/s10904-021-02031-z.
[10] F. Zanjanchi and J. Beheshtian, "Natural pigments in dye-sensitized solar cell (DSSC): a DFT-TDDFT study," *J. Iran. Chem. Soc.*, vol. 16, no. 4, pp. 795–805, Apr. 2019, doi: 10.1007/s13738-018-1561-2.
[11] D. Devadiga *et al.*, "Novel photosensitizer for dye-sensitized solar cell based on ionic liquid–doped blend polymer electrolyte," *J. Solid State Electrochem.*, vol. 25, no. 4, pp. 1461–1478, Apr. 2021, doi: 10.1007/s10008-021-04920-2.
[12] F. Job, S. Mathew, T. Meyer, and S. Narbey, "Performance and Stability analysis of Dye-Sensitized Solar Cell," in *2021 IEEE International Conference on Nanoelectronics, Nanophotonics, Nanomaterials, Nanobioscience & Nanotechnology (5NANO)*, Apr. 2021, pp. 1–4. doi: 10.1109/5NANO51638.2021.9491135.
[13] S. Prayogi, Y. Cahyono, D. Hamdani, and Darminto, "Effect of active layer thickness on the performance of amorphous hydrogenated silicon solar cells," *Eng. Appl. Sci. Res.*, vol. 49, no. 2, Art. no. 2, 2022.
[14] H. Jaafar, M. F. Ain, and Z. A. Ahmad, "Performance of dye-sensitized solar cell (DSSC) using carbon black-TiO2 composite as counter electrode subjected to different annealing temperatures," *Opt. Quantum Electron.*, vol. 52, no. 4, p. 221, Apr. 2020, doi: 10.1007/s11082-020-02341-5.
[15] S. Prayogi, Y. Cahyono, and Darminto, "Fabrication of solar cells based on a-Si: H layer of intrinsic double (P-ix-iy-N) with PECVD and Efficiency analysis," *J. Phys. Conf. Ser.*, vol. 1951, no. 1, p. 012015, Jun. 2021, doi: 10.1088/1742-6596/1951/1/012015.
[16] S. S. Singh and B. Shougaijam, "Recent Development and Future Prospects of Rigid and Flexible Dye-Sensitized Solar Cell: A Review," in *Contemporary Trends in Semiconductor Devices: Theory, Experiment and Applications*, R. Goswami and R. Saha, Eds. Singapore: Springer Nature, 2022, pp. 85–109. doi: 10.1007/978-981-16-9124-9_5.
[17] D. Devadiga, M. Selvakumar, P. Shetty, and M. S. Santosh, "Recent progress in dye sensitized solar cell materials and photo-supercapacitors: A review," *J. Power Sources*, vol. 493, p. 229698, May 2021, doi: 10.1016/j.jpowsour.2021.229698.
[18] W. Rahmalia, I. H. Silalahi, T. Usman, J.-F. Fabre, Z. Mouloungui, and G. Zissis, "Stability, reusability, and equivalent circuit of TiO2/treated metakaolinite-based dye-sensitized solar cell: effect of illumination intensity on Voc and Isc values," *Mater. Renew. Sustain. Energy*, vol. 10, no. 2, p. 10, Jun. 2021, doi: 10.1007/s40243-021-00195-9.
[19] A. Arunachalam, S. Dhanapandian, and C. Manoharan, "Effect of Sn doping on the structural, optical and electrical properties of TiO2 films prepared by spray pyrolysis," *Physics E*, pp. 35–46, 2016.
[20] D. Susanti, M. Nafi, H. Purwaningsih, R. Fajarin, and G. E. Kusuma, "The Preparation of Dye Sensitized Solar Cell (DSSC) from TiO2 and Tamarillo Extract," *Procedia Chem.*, vol. 9, pp. 3–10, Jan. 2014, doi: 10.1016/j.proche.2014.05.002.
[21] S. Prayogi, Y. Cahyono, I. Iqbalbudin, M. Stchakovsky, and D. Darminto, "The effect of adding an active layer to the structure of a-Si: H solar cells on the efficiency using RF-PECVD," *J. Mater. Sci. Mater. Electron.*, vol. 32, no. 6, pp. 7609–7618, Mar. 2021, doi: 10.1007/s10854-021-05477-6.
[22] D. Sridhar and N. Sriharan, "Structural, Morphological and Optical Features of SnO2 and CuO2 Doped TiO2 Nanocomposites Prepare by Sol-Gel Method," *India Science Tech*, vol. 2, pp. 94–98, Feb. 2014.
[23] S. Z. Mohamed Siddick, S. S. Suhaimi, M. M. Shahimin, M. H. Che Mat, and B. Man, "Performance of dye-sensitized solar cells based on varied dye thermal extraction," in *36th International Electronics Manufacturing Technology Conference*, Nov. 2014, pp. 1–4. doi: 10.1109/IEMT.2014.7123143.
[24] Y.-H. Nien *et al.*, "Preparation and Characterization of the Dye-Sensitized Solar Cell With Modified Photoanode by FePt/TiO2 Nanofibers," *IEEE Trans. Nanotechnol.*, vol. 20, pp. 507–511, 2021, doi: 10.1109/TNANO.2021.3088954.

Biographies of Authors

Dr. Soni Prayogi, M.Si is currently works as Electrical Engineering, Pertamina University, Indonesia. He does research in materials science, condensed matter physics, magnetic compounds and nano-/2D-materials. His group's current project is 'Development of carbon-based materials from 'green' sources of carbon and functional materials from natural resources' for electronic and magnetic applications

Dr. Marza Ihsan Marzuki, S.T., M.T. is a lecturer in Electrical Engineering at Pertamina University, Indonesia. He does research in applied science and engineering, modeling, and statistical learning.

Vol. 1, No. 1, August 2022, pp. 7-18
p-ISSN: 2963-8577
DOI: 10.57102/jescee.v1i1.2

ACID TREATMENT ON CARBONATE ROCK: AN EFFECT OF HCL CONCENTRATION ON ROCK PROPERTIES AND FLUID FLOWRATES

Agung Nugroho[1,2], Nur Layli Amanah[3], Hary Perdana Kamal[1], Syahreza Angkasa[4*]
[1]Department of Chemical Engineering, Faculty of Industrial Engineering, Universitas Pertamina
[2]Center for Advanced Materials, Universitas Pertamina, Jakarta, 12220 Indonesia
[3]Department of Material Science and Engineering, National Taiwan University of Science and Technology No.43, Sec. 4, Keelung Rd., Da'an Dist., Taipei City 106, Taiwan (R.O.C.)
[4]Center for Geological Resources; National Research and Innovation Agency

Abstract

A series of analyses techniques were performed to study the influence of different acid concentrations on the rock properties during the acidizing process. Based on the Thin section and Routine Core Analysis (RCA), the calcite content have effect on the reservoir quality from the aspect of rock-fluid properties. In this paper, the physical and mineralogical responses to rock acidizing of carbonate rock are evaluated. This study found that calcite content decreases approximately 25% from the total calcite content of rock samples after the addition of HCl. Scanning Electron Microscope (SEM) Analysis show that samples treated using HCl 15% provide a wider pore size distribution, resulting in the increasing permeability fluid flow rate.

Keywords:
HCl; carbonate; rock; fracturing; calcite

Article History:
Received: July 31st, 2022
Revised: August 7th, 2022
Accepted: August 25th, 2022
Published: August 31st, 2022

Corresponding Author:
Syahreza Angkasa
Center for Geological Resources; National Research and Innovation Agency
Email:
syahreza.s.angkasa@brin.go.id

1. Introduction

Oil and gas production still facing numerous challenges due to the different type of reservoir found around the globe. Common challenge that still attracted is the carbonate reservoirs, which have low capacity flow rate for hydrocarbon to pass through rock reservoir. They are commonly termed as low-permeability reservoirs with <10 millidarcy in permeability [1,2]. These made optimal oil production is hard to achieved, because of the limited flow hydrocarbon fluid that can be passed through [3]. Therefore, stimulation method become one of the best solutions to tackle the problem.

Stimulation method is one of the ways to increase the productivity of a reservoir by tuning the rock properties, such as porosity and permeability. Porosity is an important rocks properties which can be used to estimate the amount of hydrocarbons that can be stored inside the reservoir [4,5]. Another important rock properties is permeability, which is the ability of the rock to pass fluid through its pores [6]. Porosity and permeability can be used to determine the amount of fluid that can be produced to the surface of a reservoir, or to estimate Original-Gas-In-Place (OGIP) [7,8]. One of the reliable stimulation methods to stimulate the carbonate reservoir is acid treatment method [5].

Acid treatment is one of the most widely used acidification techniques to stimulate carbonate reservoir. The conventional acid treatment model is widely used to develop fracture in low – permeability - gas carbonate reservoir [9]. The acid stimulation methods are advantageous in carbonate formation, because of the presence of acid soluble minerals in form of calcite [3]. In this method, acid fluid were contacted into the rock formation at a certain temperature and pressure conditions [10]. However, acid treatment still has many challenges to be optimally done. Acid treatment method has been extensively researched in the laboratory. Because acid treatment experimental studies are commonly using outcrop samples deposited on the surface; therefore, the results obtained are not fully representative of the actual situation beneath the surface [11]. In those cases, it required further study to observe influencing factors of acid stimulation method.

Although an acid treatment model can provide some initial stimulation, it is still relatively difficult to achieve stable production rate result [12]. Variable condition such as acid volume and concentration, during the acid treatment method in carbonate reservoir, usually more difficult to control than in other reservoir type of

reservoir, like dolomite [11]. Ameri et al. reported that the higher HCl concentration which contact to rock will produce more significant effect on fracture damage [2]. However, Li et al shows the greater HCl concentration will provide more challenge in terms to control in micro scale damage, leading to weaken the rock structure and made it brittle [3]. They also suggested the acid system that should be chosen is the one that provide a wider range of fractures or pores distribution, not because based on its magnitude of fracture damage. Based on those facts, we used variations in HCl concentrations of 10%, and 15 % to observe the resulting impact on rock properties (e.g., porosity and permeability). In this study, we investigate the relationship of rock properties to the fluid flowrate through several analysis such as RCA (Routine Core Analysis), Thin Section 2D Analysis, and SEM Images. The permeability was calculated based on theoretical of Kozeny – Carman [13,14]. While Darcy equation was used to calculate the fluid flowrate of gas that passed through the rock [15,16]. Moreover, fracture is related to the rock-fluid properties that could influence on reservoir productivity because it could increase permeability of a reservoir [17]. Therefore, more research is needed to investigate the effect of acid concentration on rock properties and the resulting fluid flowrate, especially on changes in rock properties.

Samples were obtained from outcrop samples at Kutai Basin, East Kalimantan. The Kutai Basin carbonate platform (Oligocene Berai Limestone) covers a subsurface area measuring approximately 11 by 16 km in the westernmost Kutai Basin, Central Kalimantan. The Kutai Basin platform is approximately 1,000 m thick and comprises of three aggrading seismic sequences identified by the downlap of basinal strata at the platform margin and downlap of transgressive strata within the platform. The platform rim is characterized by interbedded bioclastic wackestones, packstones, grainstones and boundstones, with grainstones increasing toward the platform margin [18].

In this work, we correlated the effect of changes in crystallinity (e.g., calcite content) and diameter of the pore size distribution due to differences in HCl concentration. With the rock-fluid properties produced, the determination of a more suitable acid system can be considered to be applied to the reservoir by considering the crystallinity of calcite content so that the results obtained can be used to improve reservoir quality from the aspect of rock-fluid properties.

2. Experimental Method

A. Samples Preparation

We collected several carbonate samples (KR - 1 to – 14), which are crop out at the Kutai Basin, East Kalimantan. We prepared the samples for several analysis, 1) petrographic (thin section analysis), 2) Routine Core Analysis (RCA), 3) SEM Images Analysis, and 4) Acid Treatment. Prior to the analysis, acid treated samples undergo washing procedure using DI water to neutralize the sample.

First, samples were prepared for petrographic analysis and were sectioned into blue dyed thin section of rock at Obsidian Geo - Laboratory. The dimension of the thin sections is approximately 30 micrometers (μm) in thickness for 2D porosity analysis using an free software of ImageJ [19].

Second, sample was prepared as cylindrical cores for porosity and permeability measurement using RCA method at Geoservice, Ltd. The dimension of core samples is 2 x 2 cm in length and diameter. Then, sample KR-1 to 14 was crushed to smaller size and weighed about 2 grams before acid treatment. The same dimension was also used in SEM analysis.

In this study, thin sections were scanned using EPSON LV - 600 Film Scanner with polarized film. Scanned thin sections were used to observe the component of carbonate rocks (e.g., micrite, fossil) and were analyzed using an ImageJ software under 8-bit thin section images. We use JPOR feature on imageJ software to calculate the actual porosity of fresh and treated samples [20].

B. Routine Core Analysis

Before treatment, porosity of the sample was measured by Porosimeter - Permeameter instrument (AP – 608 Automated, Poretest System Inc.) using helium inert gas as fluid. Then, permeability before treatment was also measured using the same instrument but with nitrogen inert gas fluid. This analysis method is generally referred to RCA with the same principles as previous report [21].

C. SEM Images Analysis

We conducted SEM Images analysis to observe fracture in micrometer scale using Phenom ProX Dekstop SEM Image. The operation condition was 15-kV at the magnification at 500x. This method was similar to what has previously reported in the microstructure of shale [17].

D. Acid Treatment

Samples is heated in an oven with temperature of 120 ºC for 1 hour, to model the actual reservoir temperature [18]. The sample was immediately reacted with HCl solution at various concentration (10% and 15%) for the acid treatment process. In typical preparation 81.08 and 54.05 ml HCl (37%, SmartLab) was dissolved in 200 mL distillate water to make 15% and 10% HCl solution respectively. The rock sample then react with HCl solution at volume 25 ml for 30 seconds at ambient pressure of 1 atm.

E. Theoretical Approach in calculating Permeability and Fluid Flowrate

After acid treatment, we use theoretical approach using Darcy and Kozeny-Carman Equation to estimate permeability and fluid flowrate changes. Due to the limitation of the RCA and the availability of samples, permeability (K) of each samples was calculated using equation (1) and (2) [13,14].

$$K = c\emptyset^3/S^2 \tag{1}$$

$$c = \left(4\cos\left(\frac{1}{3}\arccos\left(\emptyset\frac{8^2}{\pi^3} - 1\right) + \frac{4}{3}\pi\right) + 4\right)^{-1} \tag{2}$$

Kozeny-Carman factor (c) was obtained from equation (2), while the surface area (S) was obtained from previous research about carbonate reservoir [14].

$$Q = \frac{KS}{\mu}\frac{(p_1 - p_2)}{L} \tag{3}$$

After permeability data is obtained, the fluid flowrate was calculated using the Darcy's Law as shown in equation (3) [15,16]. Where μ is the fluid viscosity and pressure gradient, (p1 – p2)/L, was obtained from the previous research at the Kutai Basin [22]. These reservoir scenarios and variable approach is used to calculate the permeability and rate of fluid produced after the acid treatment by using a reference paper that is close to the actual field conditions.

3. Results and Discussion

A. Sample Rock Properties Profile

Fig. 1. shows that sample has various range of permeability before acid treatment. We could observe that samples are divided into 3 regions of range, depict by region (a), region (b) and region (c). Region (a) indicates that there are some samples that has permeability far below than 1 millidarcy and the porosity below than 5 %, these samples are KR – 9, KR – 11 and KR – 14, so the region could classified as low – permeability reservoirs [2]. Region (b) shows where most of the samples are located, these region ranging 0.5 – 2 millidarcy in permeability and porosity 10% - 15%, this indicates that some of the samples has natural fracture that allows pore opening to be formed because geological circumstances [23]. Region (c) shows there is a sample (KR – 5) that overlapped from the rest region with permeability 4.7 % and porosity 23.5 %, that indicates in same type reservoir we could have very broad range of permeability and porosity, although the rock components is relatively the same, the amount of the contents are very depends on the location of sample obtained. But in common, we could classified that these samples can be categorized as low – permeability reservoir because the overall permeability of each sample doesn't exceed 10 millidarcy [22].

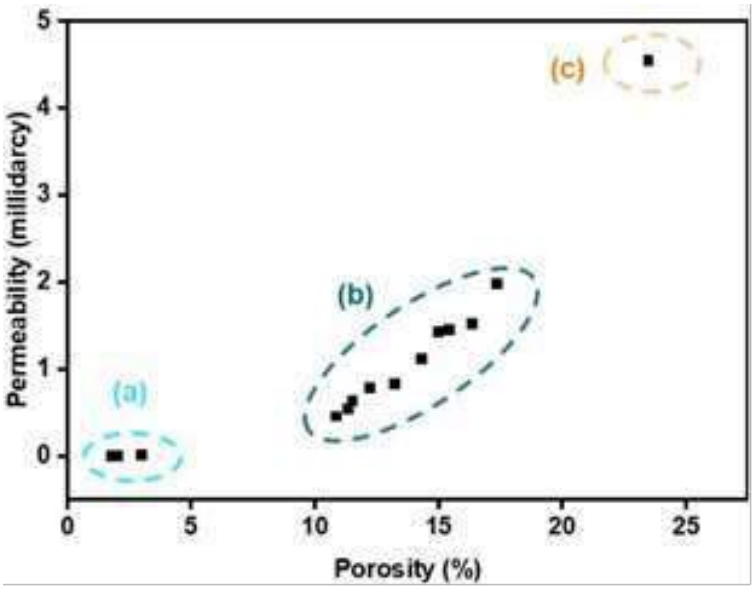

Figure 1. Porosity and permeability profile of the samples before acidizing treatment.

B. Thin section analysis

Based on Dunham's classification, three textural features fundamental in classifying carbonate rocks hold their depositional texture. (1) Presence of carbonate mud, which distinguishes muddy carbonate from grainstone; (2) Abundance of grains to subdivide muddy carbonate into *mudstone*, *wackestone*, and *packstone;* and (3) presence of signs of binding during deposition, which characterized boundstone. The distinction between packstone and wackestone can be seen in grain support and mud support. Packstone contains plenty of grain support, while wackestone contains mainly mud support. The packstone's depositional texture is related to crystalline carbonate content [24].

Fig. 2. shows the thin section of the KR – 1 and KR – 9 before treatment. The white area of KR-1 shows that the sample is dominated by fossil (1) and coral (5), which have turned into calcite after undergoing the rock recrystallization process. In contrast, the brown one (3) is a matrix structure commonly called micrite [24,25]. Thus, KR-1 is classified as packstone because it is dominated by calcite. It also can be observed from Fig. 2b that KR – 9 is dominated by brownish color, as indicated by number (2), which is called the micrite matrix. As suggested by number (4), KR - 9 still contains a small amount of calcite, then KR – 9 is categorized as wackestone by its dominated micrite matrix [26].

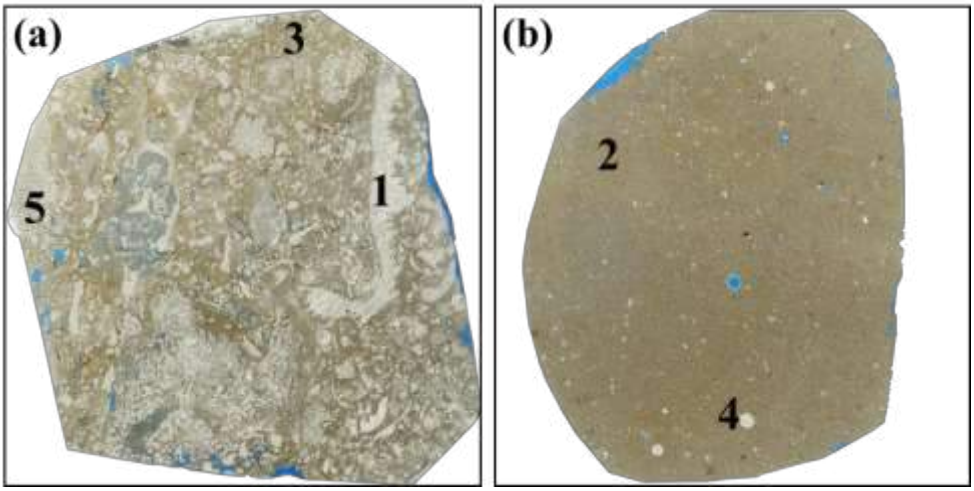

Figure 2. Thin section image of (a) KR - 1 before treatment; (b) Thin section image of KR – 9 before treatment.

Fig. 3. shows that the thin section of KR-1 component components is calculated using ImageJ software, by utilizing the difference in color thresholds displayed. The difference in color thresholds was clearly seen where the red one is part of KR - 1 which is dominated by the micrite matrix. While those that are not red are fossils

and corals that have become calcite [26]. Thus, based on the software, micrite matrix content in KR – 1 is 22.82%. The same procedure was applied to sample KR-2 to KR-14 and then micrite matrix content along with calcite content were summarized in Table 1. Based on Dunham classification KR - 1 and 2 are packstone with high calcite content (76.83 and 75.39 %, respectively). Meanwhile, KR-3 to 14 classifieds to wackestone with lower calcite content.

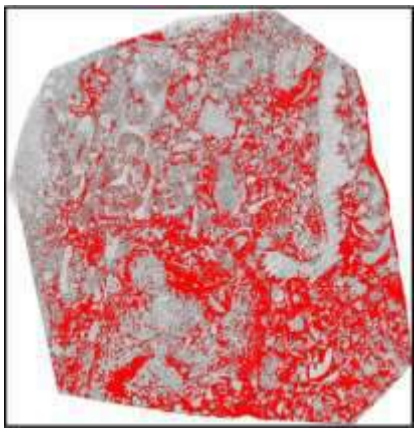

Figure 3. KR - 1 components analyzed by using ImageJ software.

Table 1. Summary of proportion of rock components before acidizing treatment

Sample Name	Component		Qualitative Description
	Matrix	Calcite	
KRC-1	22.82%	76.83%	Packstone
KRC-2	24.22%	75.39%	Packstone
KRC-3	37.68%	61.73%	Wackestone
KRC-4	34.47%	64.99%	Wackestone
KRC-5	33.31%	66.17%	Wackestone
KRC-6	32.27%	67.22%	Wackestone
KRC-7	31.35%	68.16%	Wackestone
KRC-8	38.29%	61.11%	Wackestone
KRC-9	37.84%	61.56%	Wackestone
KRC-10	34.33%	65.13%	Wackestone
KRC-11	38.08%	61.32%	Wackestone
KRC-12	32.82%	66.66%	Wackestone
KRC-13	39.68%	59.70%	Wackestone
KRC-14	37.94%	61.46%	Wackestone

Fig. 4. shows thin section of sample KR – 9 after 15% HCl treatment which has been given blue dye. As can be seen in Fig. 4a. the blue color fills the voids in the rock which show the porosity of the KR – 9. Meanwhile Fig. 4b. is a thin section that has been processed with ImageJ by using the difference in color threshold, the amount of porosity will be represented by the red area. By using this method, the calculated porosity in KR – 9 is 10%. Further analysis using same technique can be done to another sample and the result is presented in Table 2. All sample show increasing in porosity by HCl 10% treatment due to pore opening. This might be due to the decreasing calcite content as the result of carbonate reaction with HCl. Further increase in HCl concentration to 15% lead to the increase in porosity as corelated with calcite decreasing.

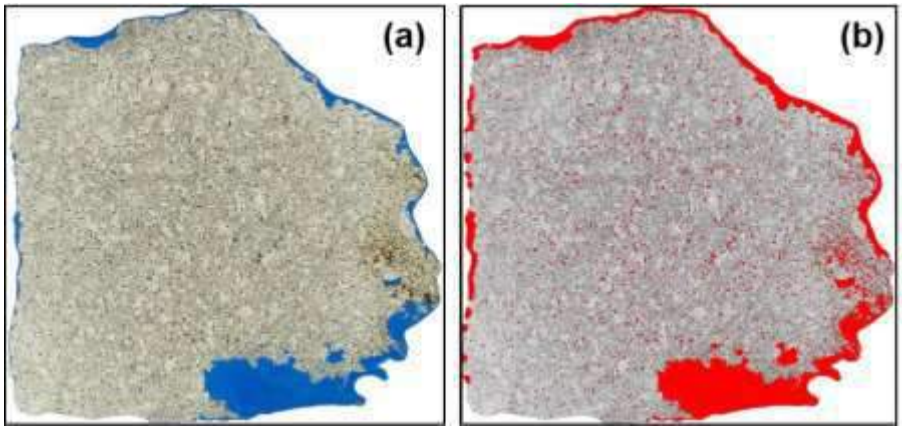

Figure 4. shows Porosity of KR - 9 after HCl 15 % treatment using ImageJ. (a) Thin section of KR – 9 after HCl 15 % treatment before color thresholding. (b) Thin section of KR – 9 after HCl 15 % treatment after color thresholding using ImageJ.

Table 2. Porosity and calcite contents after acidizing treatment

Sample Name	Porosity			Calcite		
	HCl 0 %	HCl 10 %	HCl 15 %	HCl 0 %	HCl 10 %	HCl 15 %
KRC-1	15.46%	24.52%	25.77 %	76.83%	51.07%	52.31%
KRC-2	10.86%	18.10%	37.34%	75.39%	57.29%	38.05%
KRC-3	15.02%	25.03%	43.83%	61.73%	36.69%	17.90%
KRC-4	17.36%	28.94%	44.08%	64.99%	36.05%	20.90%
KRC-5	23.49%	39.15%	40.56%	66.17%	27.01%	25.60%
KRC-6	14.33%	23.89%	38.67%	67.22%	43.33%	28.55%
KRC-7	13.24%	22.06%	27.54%	68.16%	46.09%	40.62%
KRC-8	12.23%	20.38%	30.63%	61.11%	40.73%	30.48%
KRC-9	3.00%	5.00%	10.00%	61.56%	56.56%	51.56%
KRC-10	11.54%	19.23%	33.25%	65.13%	45.90%	31.88%
KRC-11	1.79%	2.98%	4.92%	61.32%	58.34%	56.40%
KRC-12	10.41%	11.34%	18.90%	66.66%	56.25%	47.76%
KRC-13	16.37%	27.28%	51.60%	59.70%	32.42%	8.10%
KRC-14	2.07%	2.10%	2.54%	61.46%	58.49%	58.91%

C. Surface SEM – Analysis

Fig. 5a. shows KR-14 before HCl treatment which natural fractures has been observed (1). However open pores are still very small and far apart. After acidizing process Fig. 5b., we can see that the surface texture is damaged after adding HCl due to the dissolution of calcite. Moreover, after addition 10% HCl, the new cracks or pores began to form due to the dissolution of the calcite content by HCl. However, the distance between the pores was still relatively far apart as indicated by blue circle (2). At higher acid concentration Fig. 5c. and Fig. 5d., as indicated by number (3), the change in surface texture looks very significant compared to the sample that treated by 10% HCl. Moreover, the new pores are larger compared to 10% HCl treatment and have varying sizes with fairly close distances. From Fig. 5d. depicted by number (3) we could observe that elongated fracture was formed after acidizing treatment. This can happen because the dominance of soluble calcite is located between the elongated fossil grains, so that when the calcite is dissolved, elongated fractures are formed.

Also, we could observe that SEM observation indicate that 15% HCl gave a significant change to sample texture compared to 10% HCl. HCl 15% tends to form more pores, relatively larger in size and the distance between pores is closer than the samples treated with HCl 10% which form pores that are relatively smaller and spaced apart. This can be explained because the sample by treating with 15% HCl have higher dissolution of calcite compared to sample treated by 10% HCl. From the reaction stoichiometry, 15% HCl will have a higher dissolving power than 10% HCl in higher temperature than 100 ^{o}C and pressure 1 atm where more calcite with

CO2 gas is formed [5]. The presence of calcite will cause the cementation effect which closing the pores that lead to poor productivity of the reservoir.

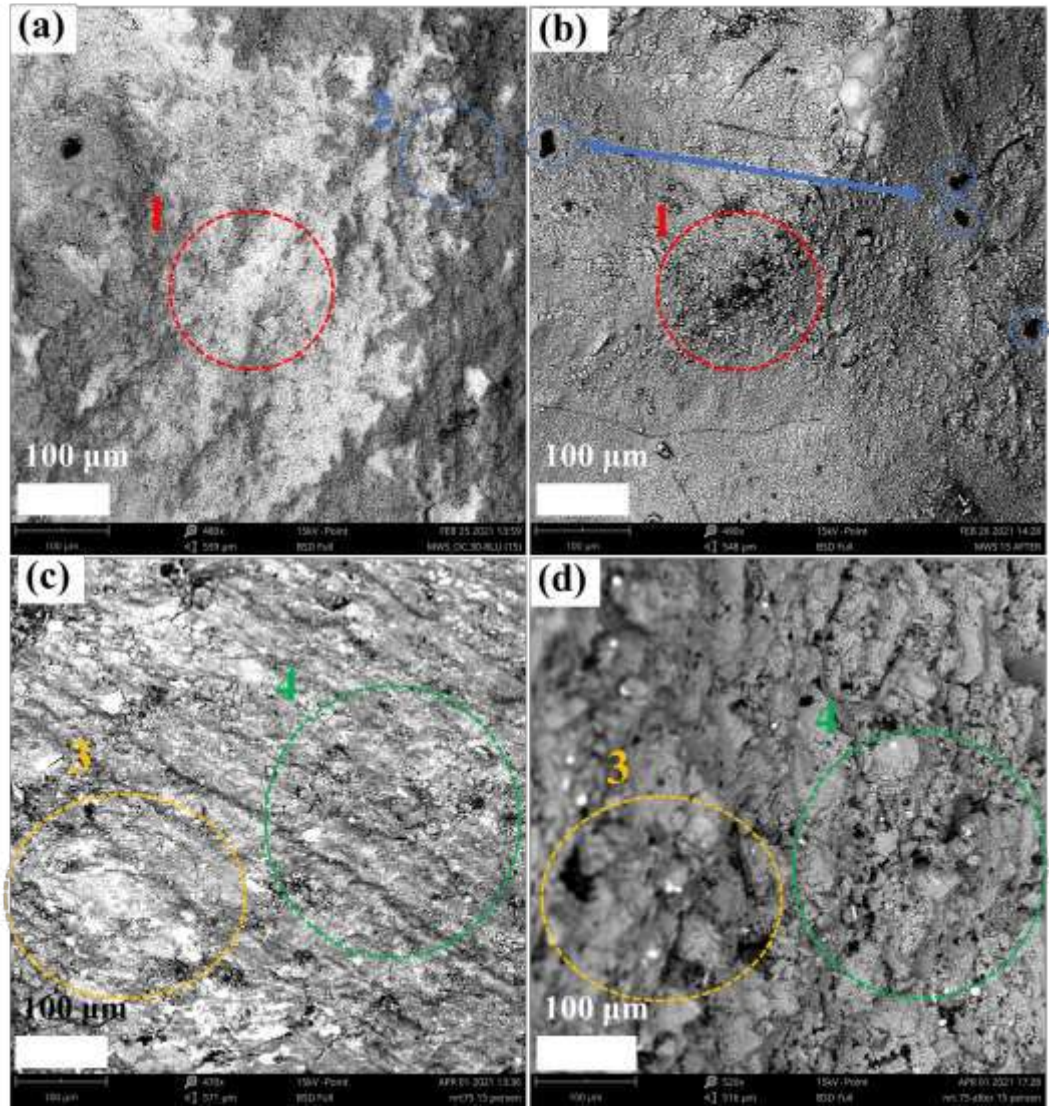

Figure 5. SEM Images of (a) KR-14 before acidizing, (b) KR – 14 after acidizing by HCl 10 %, (c) KR – 14 before acidizing, (d) KR – 14 after acidizing by HCl 15 %.

D. HCl Concentration effect on permeability

Fig. 6. shows the effect of HCl concentration on rock permeability. The rock sample before HCl treatment has high calcite content, which is above 50%. While the permeability is relatively low, which is around 0.1 - 5 millidarcy. The high calcite content in the rock will have a cementation effect, where the result of this cementation is the closing of the pores in the rock thereby reducing its permeability. The data in red color shows the rock samples that have been treated with 10% HCl. The calcite content begins to decrease because it is dissolved in HCl, thereby increasing the permeability due to the presence of new open pores as confirmed by the SEM analysis result. Meanwhile, the data in green color represent samples that have been treated with 15% HCl. The permeability has increased higher than the samples treated with 10% HCl. This is because the amount of calcite that decreases in the rock is getting bigger. The higher the concentration of HCl for acidizing, the higher the permeability of the rock, so that 15% HCl is recommended to increase the permeability of the rock. The SEM result also suggest that there is certain increase in the permeability of the rock because the porosity cavities formed are interconnected. These indicate that an increase in permeability as a result of the acid treatment process [3].

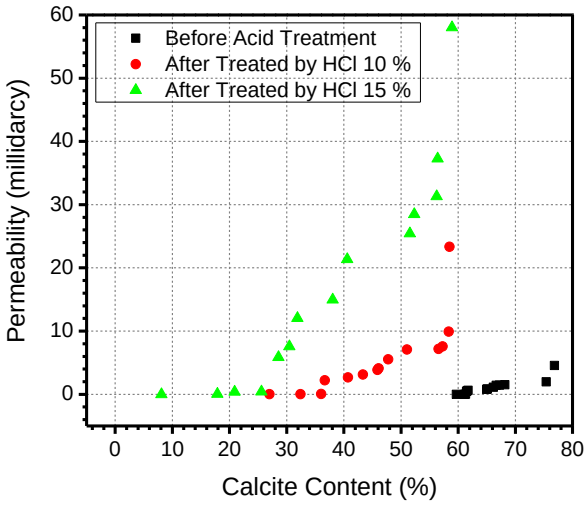

Figure 6. Effect treatment using HCl on various concentration on permeability.

E. HCl concentration on Fluid Flowrate Reservoir

The fluid flowrate is calculated using a theoretical approach such as the Darcy equation [16] as shown in equation (1) which was mentioned in the experimental section. The calculated fluid flowrate data is presented in Fig. 7. This study uses several variables from previous studies that are relevant to the Kutai Basin and other carbonate reservoirs to calculate the fluid flowrate. The surface area data was obtained using the data presented by Fabricius on the typical carbonate reservoir [14]. The fluid flowrate calculation was done using the assumptions that fluid pass to the rock is inert nitrogen gas, which was also used in RCA to measure permeability [21]. The platform temperature at Kutai Basin is approximately 120 ^{o}C with pressure of 1 atm [18]. The viscosity of nitrogen gas is 0.000021681 Pa.s calculated from equation (4) which was used by Johannson using similar operating conditions [15].

$$\mu = \mu_{ref} \left(\frac{T}{T_{ref}}\right)^{\omega} \quad (4)$$

Where μ is viscosity in this cases is nitrogen, T is temperature that used in this study (120 ^{o}C), Tref is Temperature reference at 273.15 K and ω is viscosity index as well as explained by Johansson [15], where they studied the microporous flow on low - gas reservoir.

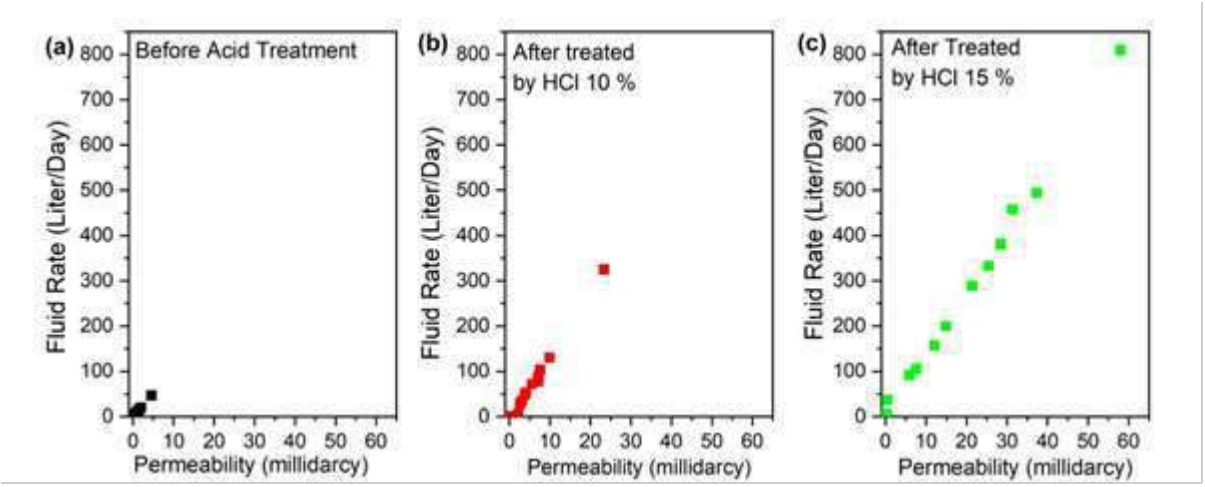

Figure 7. HCl Concentration effect on fluid flowrate of the rock sample. The data in black color shows the fluid flowrate of the sample before being

The data in black color shows the fluid flowrate of the sample before being treated with HCl. From this data, the rate of fluid that can be passed by rocks is still relatively small below 100 Liter/Day, this is due to the small permeability of the sample because the pores of the rock are still closed by calcite. After acidizing treatment with 10% HCl (red color), the fluid flowrate begins to increase with increasing permeability due to dissolution of calcite. The addition of 10% HCl formed a population of fluid flowrates that gathered in the range of 0.07 – 325 Liters/ Day as shown by red data with an average increase in permeability below 10%. The data also shows that the fluid flowrate increases significantly as the permeability increases sharply. After treatment in 15% HCl (green color), the variation of the fluid flowrate and permeability range in each sample, namely 0.09 - 809 Liters/Day as shown by green data. The difference in the range of fluid flowrate produced by 10% and 15% HCl treatment, may occur due to the difference in pore size diameter resulting from the two acid concentrations as well. After treatment in 15% HCl (green color data), the variation of the fluid flowrate and permeability range is longer in each sample than after treatment HCl 10 %This is because sample treated by 15% HCl gives wider distribution range of pore size diameter compared to rocks treated with 10% HCl as show on Fig. 7.

Fig. 8. shows pore size diameter distribution of 100 point taken from samples treated with HCl 10 % and 15 %. These porosity data was measured using ImageJ to calculated pore size diameter from SEM Images as similarly suggested by Rishi [27]. The samples treated with HCl 10 % has pore size diameter with the range of 3.93 – 45.97 μm, where most of the pore size diameter are in 3 – 10 μm. While samples treated with HCl 15 % has pore size diameter within range at 6.5 – 144.1 μm, where the most of pore size diameter are in 20 – 40 μm.

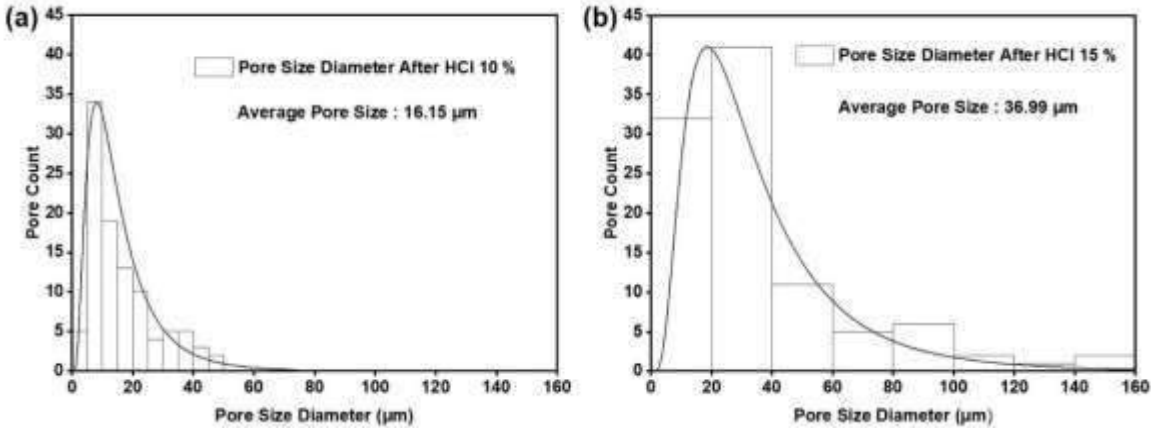

Figure 8. Graphs shows (a) pore size diameter distribution of HCl 10 % treated samples, and (b) pore size diameter distribution of HCl 15 % treated samples.

Further data analysis revealed that the samples treated with HCl 15 % has average pore size 36.99 μm which was higher than samples treated with HCl 10 % (16.15 μm). These tell us that there is difference on the pore size distribution after different acid treatment. Pore size diameter distribution data shows that sample treated with HCl 15 % gives wider fluid flowrate distribution range compared to sample treated with HCl 10%. The comparison between green and red color data show that even with low - permeability, fluid rate can be significantly increase with the wider pore size distribution. This might be due to the changes of surface texture or pore size of the samples treated with higher HCl concentrations. The wider range of pore diameter distribution will allow a larger amount of fluid to pass through it without having to experience a significant increase in permeability [10]. The effect of the pore size on fluid flowrate is also explained by the Poiseuille equation that relates permeability to pore size in general:

$$Q = \frac{\pi P r^4}{8 \mu L} \tag{5}$$

Where Q is fluid flowrate, P/L is pressure gradient along the area, r is pore radius and μ represents the fluid viscosity. The equation (5) tells us that amount of fluid passed through a material will affect the size of the open pores in the material [28]. This is in agreement with SEM showing 15% HCl will provide larger pores which then have higher fluid flowrate compared to the 10% HCl treated sample.

4. Conclusions

Based on this study, we conclude that HCl treatment give significant impact on carbonate reservoir microscale damage and rock properties. We suggested that high HCl concentration will provide better increase in permeability. In this case, HCl 15 % give permeability increase better than HCl 10 %. From rock-fluid aspects, HCl 15 % shows better results than HCl 10 % in increasing the fluid flowrate in reservoir samples. These phenomena are caused by the dissolution of the calcite content of the reservoir which can reduce the reservoir quality. Moreover, the study results shows that the pore size diameter also has significant effect on increasing fluid flowrate. Where HCl 15 % provides a wider pore size distribution in rocks compared to HCl 10 %. These lead to the higher gas fluid flow rate that can be passed on the sample after 15% HCl treatment than 10% HCl. The findings of this study indicate that 15% HCl will provide good stimulation results in terms of changes in rock-fluid properties. However, further studies are still required related to other variables that can be optimized such as volume of HCl and acidizing treatment reaction time.

Acknowledgements.

We would like to gratefully acknowledge all staff of the Chemical Engineering Laboratory and Geology Laboratory of Universitas Pertamina.

References:

[1] H. Alam, D.W. Paterson, N. Syarifuddin, I. Busono, S.G. Corbin, Reservoir potential of carbonate rocks in the Kutai Basin region, East Kalimantan, Indonesia, J. Asian Earth Sci. 17 (1999) 203–214. https://doi.org/10.1016/S0743-9547(98)00047-6.

[2] A. Al-Ameri, T. Gamadi, Optimization of acid fracturing for a tight carbonate reservoir, Petroleum. 6 (2020) 70–79. https://doi.org/10.1016/j.petlm.2019.01.003.

[3] N. Li, J. Dai, C. Liu, P. Liu, Y. Zhang, Z. Luo, L. Zhao, Feasibility study on application of volume acid fracturing technology to tight gas carbonate reservoir development, Petroleum. 1 (2015) 206–216. https://doi.org/10.1016/j.petlm.2015.06.002.

[4] T.A.A.O. Ganat, Fundamentals of reservoir rock properties, Springer International Publishing, Cham, 2019. https://doi.org/10.1007/978-3-030-28140-3.

[5] M.J. Economides, K.G. Nolte, Reservoir stimulation, 3rd ed., Wiley, Chichester, England; New York, 2000.

[6] W. Wu, M.M. Sharma, Acid fracturing in shales: Effect of dilute acid on properties and pore structure of shale, in: SPE Prod. Oper., Texas, 2017: pp. 51–63. https://doi.org/10.2118/173390-pa.

[7] H. Sun, Advanced Production Decline Analysis and Application, Elsevier Science, Texas, 2015.

[8] K. Ling, X. Wu, H. Zhang, J. He, More Accurate Method to Estimate the Original Gas in Place and Recoverable Gas in Overpressure Gas Reservoir, in: SPE Prod. Oper. Symp., SPE, Oklaho, 2013: pp. 382–397. https://doi.org/10.2118/164502-MS.

[9] B.E. Bekbauov, Acidizing Process in Acid Fracturing, Eurasian Chem. J. 11 (2016) 159. https://doi.org/10.18321/ectj310.

[10] R. Zhang, B. Hou, B. Zhou, Y. Liu, Y. Xiao, K. Zhang, Effect of acid fracturing on carbonate formation in southwest China based on experimental investigations, J. Nat. Gas Sci. Eng. 73 (2020) 103057. https://doi.org/10.1016/j.jngse.2019.103057.

[11] N. Li, J. Dai, P. Liu, Z. Luo, L. Zhao, Experimental study on influencing factors of acid-fracturing effect for carbonate reservoirs, Petroleum. 1 (2015) 146–153. https://doi.org/10.1016/j.petlm.2015.06.001.

[12] B.B. Williams, D.E. Nierode, Design of Acid Fracturing Treatments, J. Pet. Technol. 24 (1972) 849–859. https://doi.org/10.2118/3720-PA.

[13] P.C. Carman, Flow of Gases Through Porous Media, Academic Press Incorporated, New York, 1956.

[14] I.L. Fabricius, G. Baechle, G.P. Eberli, R. Weger, Estimating permeability of carbonate rocks from porosity and vp/vs, Geophysics. 72 (2007) E185–E191. https://doi.org/10.1190/1.2756081.

[15] M.V. Johansson, F. Testa, I. Zaier, P. Perrier, J.P. Bonnet, P. Moulin, I. Graur, Mass flow rate and permeability measurements in microporous media, Vacuum. 158 (2018) 75–85. https://doi.org/10.1016/j.vacuum.2018.09.030.

[16] C. McPhee, J. Reed, I. Zubizarreta, Routine Core Analysis, in: C. McPhee, J. Reed, I.B.T.-D. in P.S.

Zubizarreta (Eds.), Core Anal., 1st ed., Elsevier, Amsterdam, 2015: pp. 181–268. https://doi.org/10.1016/B978-0-444-63533-4.00005-6.

[17] C. Lu, L. Ma, J. Guo, S. Xiao, Y. Zheng, C. Yin, Effect of acidizing treatment on microstructures and mechanical properties of shale, Nat. Gas Ind. B. 7 (2020) 254–261. https://doi.org/10.1016/j.ngib.2019.10.007.

[18] A.H. Saller, S. Vijaya, Depositional and diagenetic history of the Kerendan carbonate platform, Oligocene, Central Kalimantan, Indonesia, J. Pet. Geol. 25 (2002) 123–149. https://doi.org/10.1111/j.1747-5457.2002.tb00001.x.

[19] C.A. Schneider, W.S. Rasband, K.W. Eliceiri, NIH Image to ImageJ: 25 years of image analysis, Nat. Methods. 9 (2012) 671–675. https://doi.org/10.1038/nmeth.2089.

[20] C. Grove, D.A. Jerram, jPOR: An ImageJ macro to quantify total optical porosity from blue-stained thin sections, Comput. Geosci. 37 (2011) 1850–1859. https://doi.org/10.1016/j.cageo.2011.03.002.

[21] J.H. Stiles, J.M. Hutfilz, The Use of Routine and Special Core Analysis in Characterizing Brent Group Reservoirs, U.K. North Sea, J. Pet. Technol. 44 (1992) 704–713. https://doi.org/10.2118/18386-PA.

[22] H. Safrizal, Success Story of Flow Channel Fracturing for Weathered Basement Reservoir at Jabung Block, in: Proc Indones. Pet. Assoc. 42nd Annu. Conv., Jakarta, 2019: p. E349. https://doi.org/10.29118/ipa19.e.349.

[23] T.D.V. Golf-Racht, Chapter 7 Naturally-fractured carbonate reservoirs, in: Dev. Pet. Sci., Elsevier, New York, 1996: pp. 683–771. https://doi.org/10.1016/S0376-7361(96)80029-X.

[24] R.J. Dunham, Classification of Carbonate Rocks According to Depositional Texture, in: W.E. Ham (Ed.), Classif. Carbonate Rocks, American Association of Petroleum Geologists, Tulsa, 1962: pp. 108–121.

[25] H.T. Janjuhah, J.S. Girbau, M.K. Salah, An Overview of the Porosity Classification in Carbonate Reservoirs and Their Challenges: An Example of Macro-Microporosity Classification from Offshore Miocene Carbonate in Central Luconia, Malaysia, Int. J. Geol. Environ. Eng. 13 (2019) 308–316. https://doi.org/10.5281/zenodo.2702789.

[26] E. Flügel, Classifications of Carbonate Rocks, in: Microfacies Anal. Limestones, Springer Berlin Heidelberg, Berlin, Heidelberg, 1982: pp. 366–382. https://doi.org/10.1007/978-3-642-68423-4_6.

[27] Rishi Kumari, Narinder Rana, Particle Size and Shape Analysis using Imagej with Customized Tools for Segmentation of Particles, Int. J. Eng. Res. Technol. V4 (2015) 247–250. https://doi.org/10.17577/ijertv4is110211.

[28] J. Bryan, P. Eng, Fundamentals of Fluid Flow, in: Treat. Syst. Hydraul., American Society of Civil Engineers, Reston, VA, 2008: pp. 53–79. https://doi.org/10.1061/9780784409190.ch04.

Biographies of Authors

Agung Nugroho is lecturer at Chemical Engineering Universitas Pertamina.

Nur Layli Amanah is a master student at the Department of Material Science and Engineering National Taiwan University of Science and Technology

Hary Perdana Kamal is an alumnus of the Universitas Pertamina class, 2021

Syahreza Angkasa is researcher in Research Center Geological Resources National Research and Innovation Agency

Vol. 1, No. 1, August 2022, pp. 19-34
p-ISSN: 2963-8577
DOI: 10.57102/jescee.v1i1.7

PURESHARE METHOD IN DASHBOARD DEVELOPMENT TO MONITOR WAREHOUSE PERFORMANCE AT PT XYZ USING THE COST PER CASE (CPC) PERSPECTIVE

Millenia Shinta Anggraeni[1], Harummi Sekar Amarilies[2*]
[1, 2]Department of Logistics Engineering, Faculty of Industrial Engineering, Universitas Pertamina

Abstract
Warehouse costs contribute about 22% of the company's total logistics costs. Thus, a warehouse manager must have comprehensive knowledge of costs and cost triggers in the warehouse to be able to minimize costs while keeping customer satisfaction. One effective way to minimize warehouse costs is by conducting the cost analysis. Although PT XYZ is one of the biggest Fast Moving Consumer Goods (FMCG) companies in Indonesia applying one of the most comprehensive Enterprise Resource Planning software, its existing warehouse management support system occupies only standard Microsoft Excel. One of its warehouses, located in West Java, is responsible for more than 147,000 pallets each day, and the warehouse manager still uses Microsoft Excel with limitations in displaying the required information, especially the information related to the Cost Per Case (CPC) in every activity. Therefore, a template or dashboard that can provide information related to CPC in the warehouse is urgently needed. Given the importance of cost monitoring in the warehouse of PT XYZ, this research aims to create a dashboard that can make it easier for companies to monitor warehouse performance from a CPC perspective. The methods used in data collection consist of several processes, namely interviews, observations, and literature studies. While analyzing the needs of dashboard creation, this research uses the PureShare method. Thus, the results are obtained in the form of a proposed warehouse dashboard that can be used by the company to conduct cost analysis by providing information related to CPC of every activity in the warehouse, where the information presented on the dashboard is in accordance with the company's needs.

Keywords:
Dashboard; cost per case; warehouse; cost analysis; PureShare

Article History:
Received: July 31st, 2022
Revised: August 7th, 2022
Accepted: August 25th, 2022
Published: August 31st, 2022

Corresponding Author:
Harummi Sekar Amarilies
Department of Logistics Engineering, Universitas Pertamina, Indonesia
Email: harummi.sa@universitaspertamina.ac.id

1. Introduction

Business competition in the current era of globalization is getting tougher. As a result of globalization, the development of the business world will continue to experience socio-economic changes that are increasingly broad, competitive, and complex, both in the company's internal and external environment. This results in obstacles and challenges that must be overcome by every company, thus requiring them to develop strategies in order to be able to compete with other companies. Of the various competitions conducted by the company, the goal is to create an effective and efficient process in producing goods or services for distribution to consumers. However, in reality, companies can't do all that to overcome them, so they choose shortcuts and conveniences to compete with their competitors through supply chain management [1]. Supply chain management is the integration of activities into three main streams, the first is sourcing, procurement, and supply management, the second is material management, and the last is logistics and distribution. Successful supply chain management requires many decisions related to the flow of information, products, and money. Every decision must be made to increase supply chain surplus or maximize value [2]. In this study, the authors focus on material management, especially warehouse management system that also includes the functions of forecasting, inventory management, store management, stock storage, and the production planning and control.

Warehousing plays a major role in the supply chain. The role of the supply chain is to deliver the right product, at the right condition, in the right quantity, to the right customer, at the right place, at the right time, and

at the right price. Providing the right amount of product to customers depends on the warehouse's accuracy in picking and dispatching a product. In order to be able to deliver to the right customer at the right place and time, products should be properly labeled or coded and loaded on the correct vehicle in sufficient time not to exceed the delivery time limit. In the right condition means that the product is ensured to leave the warehouse clean and free of damage [3]. The importance of the role of the warehouse in the supply chain urges companies to continuously improve their systems so that operational activities in the warehouse are more effective and efficient. Thus, it is necessary to find out what improvements will be made in order to increase productivity and accuracy in the warehouse and reduce costs and inventory along with improving service to customers. This was done because the warehouse cost contributed about 22% of the total logistics costs incurred by the company [3]. Thus, a warehouse manager requires comprehensive knowledge of all costs and cost drivers in the warehouse to be able to reduce costs but still produce optimal customer service.

Decision making for every manager in the warehouse certainly requires accurate data in a that can be obtained shortly while maintaining minimum business risk. Therefore, it is important for every manager to have all the information in a fast, intuitive, and fluent reading. One of the opportunities that companies can take advantage of to support managers in decision making is the development of technology. This technology is needed for the development of the company so that managers can see and analyze the handling costs in the warehouse for each box. For that we need a system that can integrate all supporting elements in order to be able to produce performance monitoring that allows management to be more effective and efficient [4].

Dashboard is a data visualization tool that provides information by displaying the latest conditions related to organizational performance in the form of key indicators or Key Performance Indicators, widely known as KPI [5]. The dashboard created will assist companies in cost analysis by providing accurate information related to Cost Per Case (CPC). CPC can be used to monitor the operational activities in the warehouse so that they are in accordance with what has been planned and when there are processes that are not according to plan, it is immediately known which areas and activities are seen from the cost side. In addition, the purpose of cost analysis is to be able to see opportunities to increase productivity and accuracy in the warehouse and reduce production and distribution costs along with improving service to customers through improvements in the warehouse such as changes of warehouse layout, improvement of order management, application of automation or systems, sophisticated software in operational activities in the warehouse as well as other improvements that can increase the company's gross margin. When the gross margin increases, the company will be able to invest more in advertisement and marketing or to improve warehouse performance to handle more product effectively to increase sales.

Traditionally, there are two techniques to maintain a company healthy: increasing sales and reducing costs. Cost reduction can be done after a comprehensive cost analysis is completed. The case study in this paper is the West Java warehouse of PT XYZ, one of the biggest Fast Moving Consumer Goods (FMCG) companies in Indonesia. Although it already implemented the comprehensive Enterprise Resource Planning software, for the supporting warehouse management system, PT XYZ uses only standard Microsoft Excel application. It is quite effective in recording and computing costs, but it cannot meet the needs of managers to perform cost analysis at the warehouse, especially the Cost per Case (CPC) in each activity. It happens due to the limitations the existing system has in displaying the required costs information. Considering the scale of PT XYZ West Java warehouse, which handles more than 147,000 pallets, not less than 650 truckloads and dispatch volume of more than 480,000 cases per day, a simple but effective Microsoft Excel template in a form of dashboard is urgently needed.

This research focuses on the preparation of the dashboard which aims to determine the Cost Per Case (CPC) of each activity in the warehouse. This dashboard is also expected to make it easier for companies to monitor warehouse performance from a Cost Per Case (CPC) perspective. This research also explains the flow of using the dashboard to display the required information for the activities of West Java Warehouse that supplies the demand of greater areas in Jakarta.

2. Methodology

This research was conducted using the following method:

A. Data Collection.

This method was carried out through several processes, namely [6]:

- Interview: A Question-and-Answer session with warehouse supervisor was done to obtain crucial information related to the data needed to create a dashboard.
- Observation: Observations were carried out by analyzing data provided by the company, such as product inbound and outbound volume data, fixed and variable costs data for each area and activity, direct and indirect cost data, productivity data, and overtime data.

- Literature study: This activity was done by exploring various research to obtain information related to the dashboard and PureShare method as described in Table 1.

Table 1. Previous Research

Characteristics	Previous Research					This Research (2022)
	Ilyas and Setiaji (2021)	Lavrador and Laureano (2019)	Utomo and Sungkar (2014)	Saputra, Hendrawan and Priand (2013)	Sungkar, Mustafid and Widyanto (2011)	
Research Purpose						
Productivity and Performance Measurements	√			√		
Customers data visualization			√			
Management Control System					√	
Cost Monitoring		√				√
Research Object						
Students and faculty members at a university	√					
Hospitality service at a hotel		√				
Medical record and healthcare service at a hospital			√		√	
Government institution				√		
Private, profit-oriented organization						√
Method						
PureShare	√		√	√		√
Noetix					√	
Qualitative, Explorative Interviews		√				√

From Table 1, it can be concluded that PureShare is a method commonly used to build a dashboard for various purposes. It was applied to design the attendance monitoring system of students and faculty members at a university, to keep the in-patient record as well as to measure the healthcare service at a hospital, to evaluate employees' performance at a government institution, and to compute the cost per case at a warehouse. PureShare method uses top-down approach in the planning stage and bottom-up approach during implementation, but a combination between PureShare and Qualitative, Explorative Interviews for cost monitoring at a private, profit-oriented organization dashboard was applied in this research. The focus of this research is to prepare the dashboard to determine the Cost Per Case (CPC) of each activity at the warehouse. This dashboard is also expected to make it easier for PT XYZ to monitor the performance of a warehouse in West Java that supplied the demand of greater areas in Jakarta from a CPC perspective.

B. The analysis method is carried out using the PureShare method, where this method consists of several stages which can be seen in Table 2 [7]:

Table 2. Stages of Research Work Based on PureShare Method

PureShare Method	Research Work Stages
Planning and Design	1. Data Collection 2. Needs Analysis a. Identify the Purpose of Making the Dashboard b. Dashboard User Identification c. Identify Dashboard Type d. Determination of KPIs in the Dashboard e. Identify Dashboard Design Needs f. Making Dashboard Layout Design
System and Data Review	3. Identification of Data Needs and Sources

PureShare Method	Research Work Stages
Dashboard Prototype	4. Dashboard Prototype Making
Prototype Improvement	5. *Testing or Trial Using Dashboard*
Release	6. Company Use of Dashboard
Continuous Improvement	7. Dashboard Updates and Modifications

3. Theoretical Foundation

This research raises several theoretical foundations as a theoretical framework, namely:

A. Supply Chain Management

The supply chain includes all parties involved directly or indirectly in meeting customer needs, not only manufacturers and suppliers, but also transportation companies, warehouses, retailers, and even consumers. In each of these organizations, for example in manufacturing, the supply chain includes all the functions involved in receiving and meeting the needs of consumers. These functions include, among others, the production process, new product development, marketing, distribution, finance, and customer service. While supply chain management is integration and coordination across departments and across companies related to the flow of material, information, and money to transform and use supply chain resources in a rational way along the value chain where there are activities on three main streams, including as follows [2]:

1. Sourcing, procurement, and supply management

These functions are part of the purchasing sector which has a fairly dominant role because of its impact on cash flow and its contribution to company profitability. The company realized that efforts to increase profits through increased sales were far greater than generating equivalent revenue through reducing procurement costs. Purchasing responsibilities relate to procurement and material management functions. Usually better known as a series of activities, functions, and processes related to the procurement or flow of inputs into the company as well as efficient control over the flow of funds out of the company. In the context of supply chain management, this process includes sourcing, supply side management, inbound logistics, and supplier relationship management related to material, information, and money flows that are interconnected with each other.

2. Material management

Classical material management includes functions of forecasting, inventory management, storage management, warehousing, stock keeping, scheduling to production planning and control, then expanded and developed into material management. Furthermore, it is better known as integrated material management because of the ordering process. Efficient material management is being implemented by companies as a way to reduce expenses and increase profits, this is because 60% of the production cost of a product is material costs. Merging purchases provides an opportunity to reduce material input costs. Several techniques in materials management focus on reducing the total cost of inventory at the lowest possible level but not neglecting the service level. In relation to supply chain management, it is considered the management of the flow of materials out, throughout, and for the company.

3. Logistics and distribution

Logistics is part of the supply chain management process from planning, implementing, and controlling the effective and efficient storage and flow of goods or services, money, and information from the point of origin to the point of destination to meet customer needs. The distribution function that Peter Drucker identified as "today's frontier" is synonymous with logistics. Meanwhile, transportation is the backbone of logistics because it contributes up to 50% of the total logistics costs. This makes the company pay special attention to creating efficient transportation management by developing practices related to transportation that involve all modes (multimodal). This can be evidenced by the development and growth of the handling and movement of containerized cargo around the world. The existence of a tradeoff between the choice of transportation mode and inventory policy causes integration and logistics to appear as cross-functional. An approach that integrates all materials, purchasing functions, purchasing management, production control, inbound movement, warehousing, and quality control with the aim of ensuring efficient operations. In this case, logistics is considered as an early avatar of supply chain management.

In the context of supply chain management, logistics is the end of a network of flow of goods or processes from raw materials to finished products to the hands of consumers, which is commonly referred to as inbound and outbound logistics. In manufacturing logistics, the flow of materials between companies gives this discipline a wide range of material movement from end (producer) to end (consumer) at every stage of industry and business in the distribution of value to customers. Thus, supply chain management has emerged as a strategic integration and business practice covering the flow of goods/services, money, and information across networks that provide value to customers.

Based on the description of the three main activities, it can be concluded that supply chain is the physical network, while supply chain management is a tool, method, or approach to manage it. [8]

B. Warehouse

The role of the supply chain is to deliver the right product, in the right quantity, to the right customer, at the right place, time, condition and price. Warehouse has an important role in the supply chain. Delivering the right product with the right quantity highly depends on the accuracy of the picking and dispatching processes in the warehouse. Delivering the product to the right customer at the right place and time means that the product must be properly labeled and loaded on to the right vehicle in sufficient time span to meet delivery deadlines. While in the right condition means that the warehouse must ensure the product is delivered in good condition or without damage. Finally, at the right cost means that operational activities must be efficient so that they are able to provide value to the product at the appropriate cost.

According to Meyers and Stephens (2002), the warehouse is a place to store products, both raw materials and finished goods. Meanwhile, according to the Warehousing Management Institute (2008), a warehouse is a storage place that has a function to store inventory before further processing is carried out. [9]. In the book Warehouse Management by Gwyne Richards (2011) it is explained that the warehouse is a place for storing stock by adjusting between supply and demand or acting as a buffer between producers and consumers. So, it can be concluded that the warehouse is a temporary place to store raw materials for use in the manufacturing process as well as finished goods that are ready to be distributed.

There are several activities carried out in the warehouse, ranging from inbound to outbound processes, where the processes in the warehouse can be seen in Fig. 1 and the following are some of the main activities in it. [3]

1. Receiving. This is the most important activity in the warehouse. This activity consists of receiving goods, checking the suitability and condition of goods (checking), to determining the quality of goods (accepted or rejected).
2. Putaway. This activity covers distributing goods from the receiving area to storage or racking locations.
3. Storage. This is an area at a warehouse that is divided into storage for raw materials and finished goods.
4. Picking. This activity involves taking goods according to consumer demand from the storage area to be collected in the dispatch area.
5. Dispatch. It is an activity of consolidating goods according to customer requests and then carrying out the loading process on the transport vehicle complete with the preparation of documents for delivery of goods.

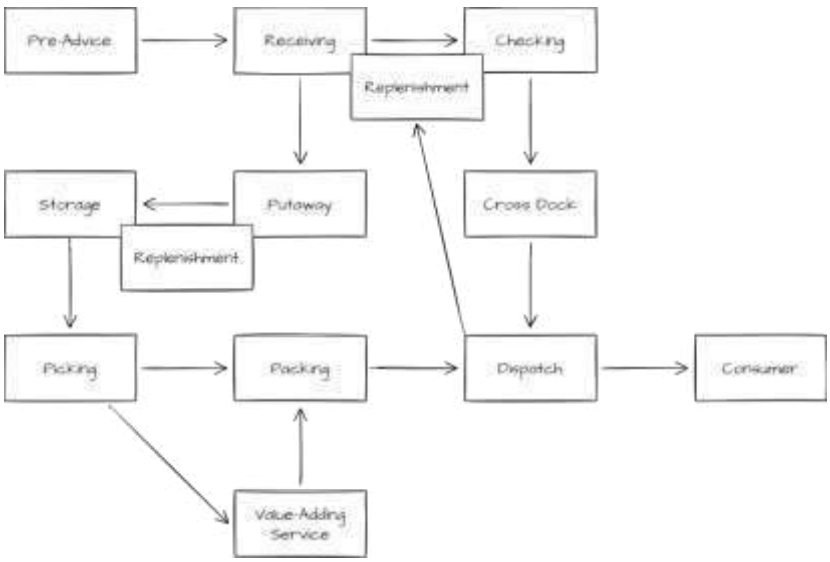

Figure 1. Warehouse Processes

Operational activities in the warehouse cost an average of 1% - 5% of the total cost of sales depending on the type of company and the value of the goods. Meanwhile, costs for warehousing activities account for up to 22% of the company's total logistics costs. [3]. The costs included in warehouse operations can be seen in Fig. 2. The existence of various types of costs ranging from storage, handling, to overhead costs exposes a warehouse manager to comprehensive knowledge regarding all costs that trigger expenses in the warehouse in order to perform cost analysis and minimize cost without reducing the quality of services.

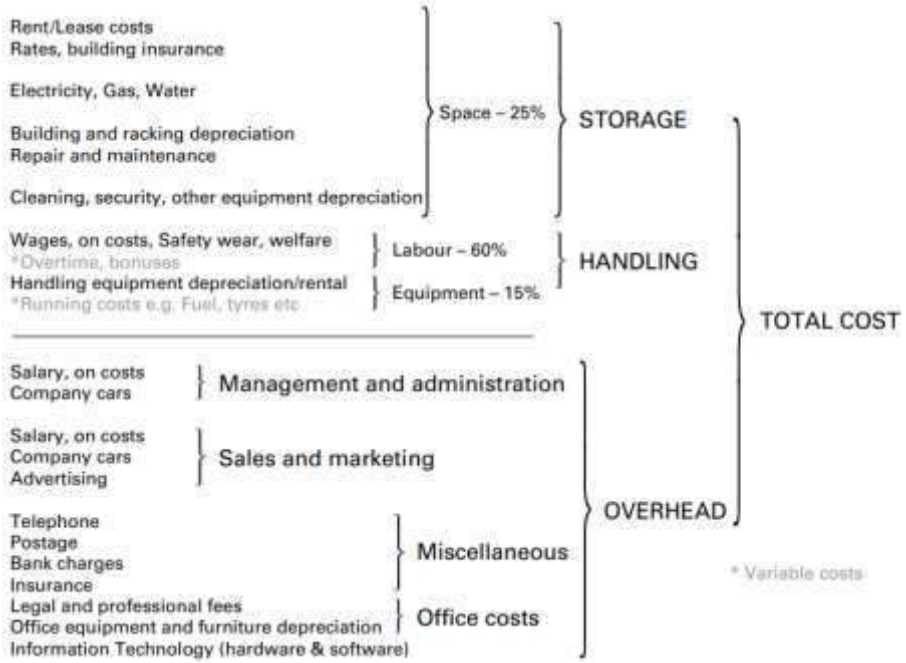

Figure 2. Simple Warehouse Cost Tree

C. Cost Analysis

Cost analysis according to Stock and Lambert is the basis of integrated logistics management to minimize the costs of transportation, warehousing, storage, ordering processes, and information systems by achieving the appropriate level of customer service. The purpose of cost analysis is to examine the effect of each alternative improvement on the company's total logistics costs [10]. By knowing the effect of alternative improvements based on cost analysis, the results of the analysis can be used for decision making by managers through cost comparisons or other cost components.

D. Activity Based Costing (ABC)

Activity Based Costing (ABC) is an approach to allocate additional costs or other costs that often appear outside of the previous plan to several sets of activity costs and then assign these costs to products and services through cost drivers or factors that have an impact on changes in the total cost level. For example, companies can track the costs of setting up or setting up machines for each batch of a production process. Then the company can allocate a portion of the total set-up cost to a particular product based on the number of set up required by the product. [11]

E. Dashboard

Dashboard is basically a new name for an executive information system which was first developed around 1980. After going through a series of studies and having experienced a hibernation phase due to the support method for providing data, namely data has not evolved to provide a data handling methodology, Few (2006) defines dashboards as a visual display of important information the company needs to achieve a goal. These displays are consolidated and arranged into one screen so that the information to be conveyed can be monitored in one view [12]. There are four main criteria that must be owned by a dashboard, including the following [13]:

1. Combine relevant business information and present it in a unified view.
2. Information submitted must be accurate and timely.
3. Provide secure access to sensitive information. The dashboard must have a security mechanism so that data or information cannot be accessed by unauthorized parties.
4. Dashboard is able to provide comprehensive solutions to the main problems that need to be addressed.

According to Few (2006), there are 6 categories of presentation forms in the dashboard, including:

1. Graphics
   In general, the type of data on the dashboard is quantitative data, so most dashboard presentation media use graphical form. Several types of graphs that can be used in the dashboard are bullet graph, stacked graph, bar

chart, line graph, combination bar and line graph, sparklines, box plots, scatter plots, treemaps. All types of graphs, except treemaps, are two-dimensional with the x and y axes.

2. Figures
   Images on the dashboard can be used to display things that need to be displayed in the form of images, such as faces, room conditions, and others. The use of images such as illustrations, photos, and diagrams are sometimes useful in the dashboard, but in practice this type of image is still very rarely used.
3. Icon
   An icon is a simple image that can be used to describe a simple function.
4. Drawing objects
   Drawing objects is a combination of several types of dashboard presentation to present information in a structured manner so that it can provide information properly. One example of drawing objects is a combination of graphic and text types.
5. Text
   Each type of dashboard must have information that can only be displayed in text form. Text can be placed somewhere as a caption or information or used to provide a label that identifies the item in the image.
6. Organizer
   There are three types of organizers on the dashboard, namely spatial data, tables, and small multiples. Where the information presented by the table is information arranged in rows or columns, either in the form of images, icons, or text. Spatial maps are used to provide information in the form of geographic maps. While small multiples present information consisting of one row or column with a graph, or several rows and columns arranged in a matrix.

According to Eckerson (2006), based on the level of management it supports, dashboards can be grouped into three parts, namely, operational dashboards, tactical dashboards, and strategic dashboards. The explanation of each dashboard can be seen in Table 3.

Table 3. Types of Dashboards Based on Management Level

Criteria	***Operational Dashboard***	***Tactical Dashboard***	***Strategic Dashboard***
Function	Provides direct information related to several matters that need to be responded to quickly	Provide information needed to find out the reasons for an event	Provide information to make business decisions, predict opportunities, and provide direction for achieving strategic goals
Focus	Monitoring activities and events that change constantly	Determine the cause of a certain condition or event from an analysis	Measurement of high-level performance and achievement of the organization's strategic goals
Presentation of Information	The information presented is very specific and detailed through simple, easy-to-understand media, and there are alert facilities	Designed to interact with data such as drilldowns that allow users to analyze data	The information presented is not too detailed, so the mechanism is simple, easy to understand, and graphical display
Data Requirements	Dynamic and real time	Does not require real time data	Does not require real time data

F. Key Performance Indicator (KPI)

Monitoring activities can be carried out properly if the information displayed on the dashboard is in accordance with the solution to the problems faced by the company. Therefore, Key Performance Indicators are used to formulate key indicators for the problems encountered, so that the information displayed is effective and can overcome company problems. [14]. By definition, KPIs are financial and non-financial metrics that can help an organization, or a company determine and measure progress towards the organization's or company's targets [15]. In simple terms, KPIs are quantitative indicators that can be used to analyze and evaluate the effectiveness and efficiency of the current and future performance of an organization or company. Performance evaluation is carried out to measure and determine the performance of various levels (organization, process, and people) so that it can be seen the comparison of expected and observed performance to align tasks with the strategy and

goals of the organization or company. The monitoring process also aims to maximize the chances of success in achieving the commitments set out in the strategic plan of activities and the company's annual budget. The selection of indicators that will be used as performance measurements must consider several requirements, including selectivity, representation, simplicity, cost reduction, stability, experimental approach, external comparison, accessibility, and continuous improvement. There are several indicators that can be used in management, generally divided into main types, namely financial and non-financial, which are used to define each objective, calculation formula, result, goal, deviation, performance, evaluation. [4]

G. PureShare

The PureShare method was developed by the PureShare vendor to facilitate projects related to the management and measurement of organizational performance, including the construction of dashboards. [16]. The following Fig. 3 describes the stages of the PureShare method [17]:

Figure 3. Stages of PureShare method

During the planning and design step, the dashboard developer must gather information regarding users' needs to determine the key features that will be displayed on the dashboard. After key features are firm, the system and data review stage are carried out with a bottom-up implementation approach, ensuring the indicators of data quality, data source and how to access the data.

Creating a prototype design involves both top-down and bottom-up approaches simultaneously. This stage is done to prove an overview of the final appearance and interface of the dashboard. The prototype is then reviewed by the developer and users. Feedbacks are treated as references to dashboard further development.

When the dashboard is complete, a release is mandatory to ensure that every user of the dashboard get enough exposure regarding the new dashboard and eventually uses it effectively.

A continuous improvement of the dashboard is mandatory since it needs to be adjusted as what the users need.

4. Results and Analysis

This dashboard development research was completed during three-month internship and the company found it useful to compute and monitor CPC at the West Java Warehouse. This chapter describes the stages of creating a dashboard using PureShare method that also involves in-depth interviews with the users. After the dashboard was completed, it was released to the users, and it got various suggestions for improvement, especially in terms of integrating the executed data to the existing ERP module.

Following PureShare method, the dashboard development was as follows.

A. Planning and Design

At the planning and design stage, the developer must understand the user's needs and be able to determine the key features that will be displayed on the dashboard. Therefore, data collection was carried out using several methods to determine user needs. In conducting a needs analysis, it is necessary to identify the purpose of manufacture, users, types, and needs of the dashboard design, as well as determine the KPIs in the dashboard.

1. Data Collection
   Data was collected using interviews, observations, and literature studies as a source for the authors in identifying relevant indicators to be displayed on the dashboard as a source of information for users. In addition, data collection is needed to find out the data needed in making the dashboard.
2. Needs Analysis
   At the planning and design stage, there are several activities to analyze dashboard needs, including:
   a. Identify the Creation Purpose, User and Dashboard Type
      The purpose of making this dashboard is to assist companies in obtaining important information related to handling costs per box for each activity in the warehouse in an attractive and easy-to-understand visual form. This dashboard is used by warehouse managers to conduct cost analysis on warehouse operations to find out the cost of handling each box for each month. So that the dashboard used is included in the type of operational dashboard.
   b. Identification of Business Processes and Calculation of Cost Per Case (CPC)

The company's business processes start from production carried out at the factory, then the products are stored in the warehouse for further distribution to customers. The business process of the company can be seen in a simpler way in Fig. 2. In carrying out its business processes, there are costs incurred by the company. One of the cost components incurred by the company is the handling cost per box or CPC obtained from the quotient between the costs incurred by the company for activities in the warehouse and the volume handled on the activity. The following is an example of calculating CPC for putaway activity in April in WH 1.

CPC = Cost/Volume
= IDR 400,000,000.00/16,000,000 cardboards
= IDR 25.00 per box

3. Identify Relevant KPIs for Users (Warehouse Manager)
Based on the results of interviews, observations, and literature studies that have been carried out by the author, the KPIs can be grouped into two dimensions to make it easier for users to understand the information displayed on the dashboard. The following are KPIs used to display information related to Cost Per Case (CPC).
   a. Warehouse Volume
      It is an indicator obtained from the volume of inbound and outbound products in the warehouse.
   b. Cost Per Case
      It is an indicator that is obtained from the calculation of cost per activity data divided by inbound or outbound volume.
4. Identify Design Needs and Create Dashboard Layout Designs
After carrying out the previous stages, identification of design needs and the creation of a dashboard layout design are carried out by identifying the form of visualization that you want to display from each information. The form of dashboard visualization can be seen in Table 4 below.

Table 4. Dashboard Visualization Forms

No.	Information	Form Visualization
1	Warehouse Volume	Bar Chart
2	CPC per Activity	Bar Chart
3	CPC Comparison	Bar Chart
4	Quartal	Table

B. System and Data Review

The next stage is a system and data review to identify the data sources used. The data must be in accordance with the needs in making the dashboard.

After identifying the relevant KPI requirements for users at an early stage, the next step is to determine the needs and data sources as input on the dashboard. Identification of data sources for each KPI can be seen in Table 5.

Table 5. Identification of Data Sources

No.	Key Performance Indicator (KPI)	Data Source
1.	Warehouse Volume	Inbound/Outbound Volume Data
2.	Cost Per Case	Data Resume CPC Warehouse

C. Prototype Design

In the third stage, prototype design was carried out using Microsoft Excel software.

1. Data Cleaning
   This step is mandatory since not all the data obtained from the company is needed and not all data is in the right format of table, so it should be organized and sorted following the arrangement that has already planned for the dashboard.
2. Data Processing (Dashboard Creation)
   This process was carried out to process data so that the information presented on the dashboard is in accordance with the company's needs. There were several stages in creating a dashboard, including:
   a. Creating Sheets in Microsoft Excel and Data Input
      The first step in creating a dashboard in Microsoft Excel is to create a sheet according to what the user needs. In this warehouse dashboard, 20 sheets were made, ranging from dashboard display

sheets, instruction sheets, to sheets for data that need to be inputted. The display of the instruction sheet and several sheet names on the warehouse dashboard can be seen in Fig. 4.

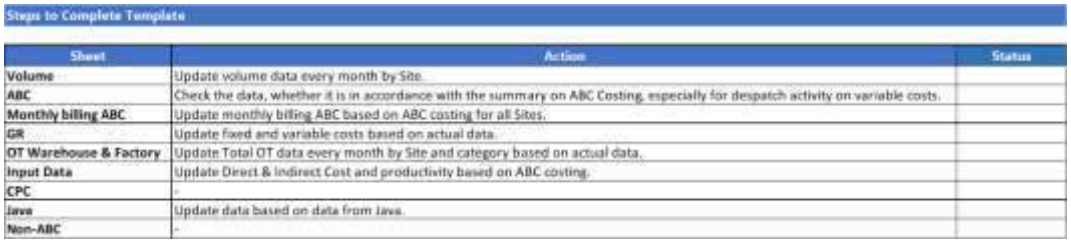

Steps to Complete Template

Sheet	Action	Status
Volume	Update volume data every month by Site	
ABC	Check the data, whether it is in accordance with the summary on ABC Costing, especially for despatch activity on variable costs.	
Monthly billing ABC	Update monthly billing ABC based on ABC costing for all Sites.	
GR	Update fixed and variable costs based on actual data.	
OT Warehouse & Factory	Update Total OT data every month by Site and category based on actual data.	
Input Data	Update Direct & Indirect Cost and productivity based on ABC costing.	
CPC	-	
Java	Update data based on data from Java.	
Non-ABC	-	

Figure 4. Instruction Sheet Display

The required input data were incoming and outgoing goods volume data, fixed and variable costs in each area of the warehouse, ABC monthly invoices, actual costs for fixed and variable costs, total costs and overtime hours, direct and indirect costs, productivity of handling equipment. materials, and monthly bills for non-ABC expense groups.

b. Calculation Process

After all the required data were met, the next step was to carry out the calculation process to present the required information. The first calculation was to determine the percentage of fixed and variable costs in each area of the warehouse. The second was to determine the volume of inbound and outbound that could be handled during overtime for each month. The third was to determine the percentage of direct and indirect costs incurred by the company for handling cardboard and pallets in each area. Fourth was to determine the percentage of costs incurred by the company for the use of material handling equipment based on its productivity. The last was to calculate the handling cost per box for each activity, both fixed costs and variable costs for the ABC group, such as direct costs which were divided based on expenses in each area of the warehouse and indirect costs such as administration, management, and others. Meanwhile, for the non-ABC group, the handling fee per box was calculated for each group of expenses such as rental fees, minimizing the risk of Covid-19 transmission, electricity, water, employees' meals, and others. The following is an example of a calculation to determine the percentage of fixed and variable costs in each area of the warehouse with the percentage of other areas can be seen in Fig. 5.

% Picking (fixed cost) = Picking (fixed cost)/Total fixed cost × 100%
= Rp 25,968,872.164/Rp 195,517,891,074 × 100%
= 13,282 %

Area	Core Activity	Activity	Warehouse					
			Total	%	Fixed	%	Variable	%
1	Receiving	Unloading	9.625.744.034	6,328%	6.763.980.369	7,991%	2.861.763.666	4,241%
1	Receiving	Checking	1.738.895.700	1,143%	-	0,000%	1.738.895.700	2,577%
2	Put In / Out & Storage	Putaway	17.171.299.223	11,288%	6.296.597.294	7,438%	10.874.701.930	16,117%
3	Picking	Picking	41.809.442.566	27,484%	10.186.359.128	12,034%	31.623.083.438	46,866%
4	Despatch	Loading	21.612.894.713	14,207%	18.137.830.599	21,427%	3.475.064.114	5,150%
4	Despatch	Checking	4.958.821.635	3,260%	-	0,000%	4.958.821.635	7,349%
5	Returns	Returns & Other	6.987.939.951	4,594%	2.893.809.846	3,419%	4.094.130.104	6,068%
6	Administration & General	Administration & General	12.835.350.393	8,437%	12.835.350.393	15,163%	-	0,000%
7	Site Costs	Site Costs	12.126.116.189	7,971%	12.126.116.189	14,325%	-	0,000%
8	Management	Management	14.657.046.294	9,635%	14.657.046.294	17,315%	-	0,000%
9	Miscellaneous Other	Miscellaneous Other	8.601.756.266	5,654%	752.749.213	0,889%	7.849.007.053	11,632%
Total			152.125.306.965	100%	84.649.839.324	100,000%	67.475.467.641	100,000%

Figure 5. Percentage Display of Fixed and Variable Costs for Each Area in the Warehouse

c. Creating Graphics

After the required data was collected and data processing had been carried out, the last step in making the dashboard was to create a graph. The graphing was adjusted to the results of the analysis of the company's needs. The results of the dashboard design that have been made can be seen in Fig. 6.

Figure 6. Warehouse Dashboard

d. Prototype Repair

At this stage, improvements were made to the dashboard obtained from the results of testing or trials by users. The trial phase was carried out to ensure whether the dashboard made was in accordance with the company's needs or there were things that need to be improved. The initial display on the dashboard only presents information on handling costs per box or CPC for each activity in the form of simple tables and graphs for the ABC group as shown in Fig. 7, while for the non-ABC group only information on handling costs per box for each expenditure group such as covid19, depreciation, fixed costs, maintenance, and others as shown in Fig. 8. Therefore, a prototype improvement for the ABC group was made to make it more user friendly and make it easier for users to analyze the results of data processing presented. Improvements for non-ABC groups were not possible if done at this time because the existing data was not able to accommodate for dashboard creation.

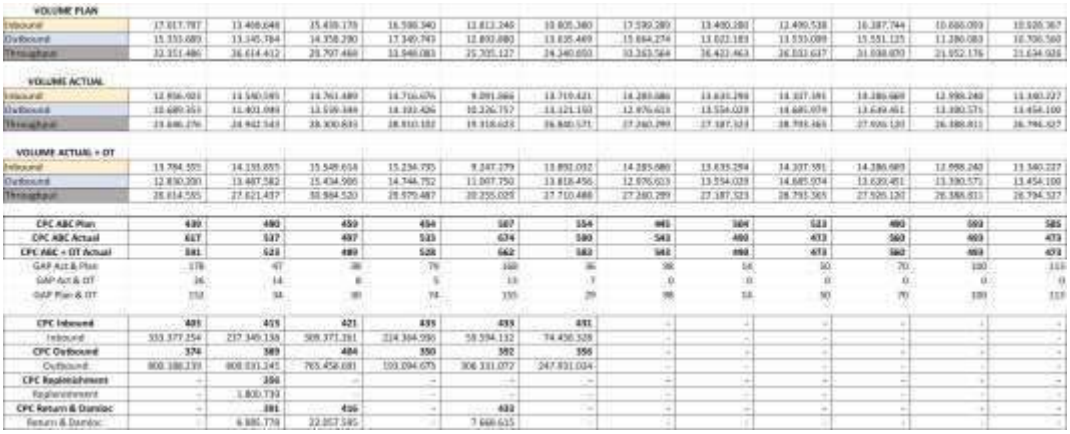

Figure 7. CPC Display Before Repair

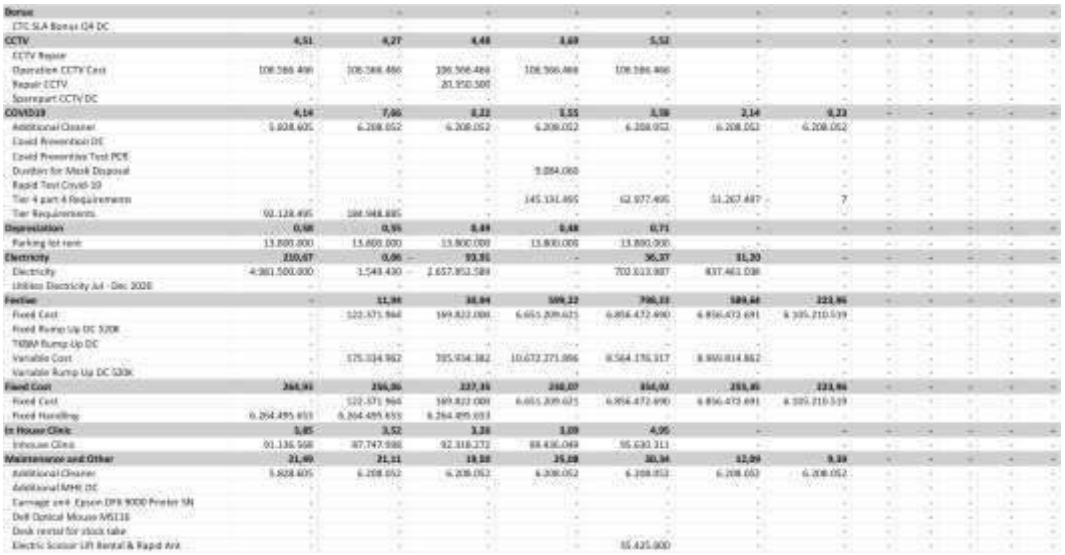

Figure 8. Display of CPC in the Non-ABC Group

e. Release
When the dashboard had passed the testing phase and improvements have been made, the users could start using the finished dashboard after several simple training following the manual (process flow) as shown in Table 6.

Table 6. Steps to Complete the Dashboard

Sheet	*Action*	Status
Volume	Update volume data every month by Site.	
ABC	Check the data, whether it is in accordance with the summary on ABC costing, especially for dispatch activity on variable costs, the cost is split into loading and checking.	
Monthly billing ABC	Update monthly billing ABC based on ABC costing for all Sites.	
Good Receipt	Update fixed and variable costs based on actual data from finance team.	
Overtime Warehouse	Update Total overtime (Hour and Value) data every month by Site and category based on actual data from 3rd party logistics.	
Input Data	Update direct & indirect cost and productivity based on ABC costing to find out the percentage of cost usage by area.	
CPC	-	
Java	Update data based on data from Java YTD (Year to Date).	
Non-ABC	-	

Users must complete all sheets in Microsoft Excel so that they can see the required information on the dashboard. The 'Status' column is a description of filling out the sheet required by the user.

f. Continuous Improvement
Several updates and modifications were carried out to adjust the dashboard as needed by the users, such as the expense identification for the non-ABC section. It was added to enable the identification and calculation of expenses that were not included in the non-Activity Based Costing group.

g. Results and Analysis
Based on the results, after several adjustment, the dashboard can be effectively used by PT XYZ to compute the Cost per Case (CPC), so the company can do a cost analysis and monitor the operational activities in the warehouse. This CPC is crucial, since it checks whether the activities are

done in accordance with what has been planned and to see opportunities in an effort to increase productivity and accuracy in the warehouse along with improving service to customers through improvements in the warehouse, such as layout changes, order management repair, application of automation or sophisticated software systems in operational activities in the warehouse as well as other improvements that can increase the company's gross margin. The increase in gross margin can be used by the company to invest in product development or to improve the warehouse so that more products are handled and in parallel can increase sales.
In order to perform a cost analysis, the company must know the description of each chart on the warehouse dashboard. The following is a chart description based on the warehouse dashboard to monitor CPC:

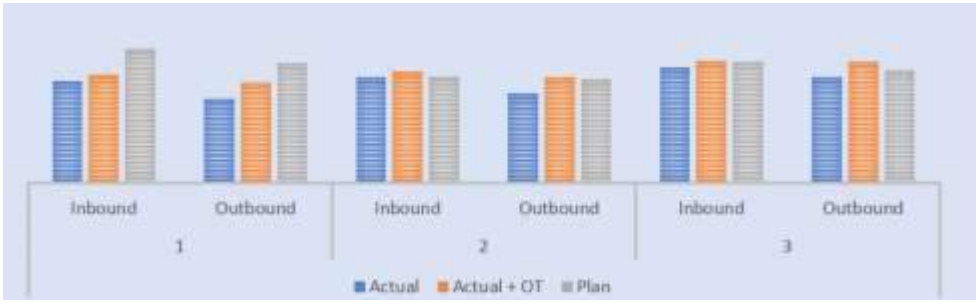

Figure 9. Warehouse Volume

The diagram in Fig. 9 is a comparison of inbound and outbound volumes in the warehouse for planning volume, actual volume, and actual volume in the presence of overtime. The display on the dashboard can be set for each month or every quarter.

Figure 10. CPC per Activity Each Month

The diagram in Fig. 10 shows the cost per case for each activity in the warehouse, from inbound to outbound activities. The display on the dashboard can be set for each month or every quarter.

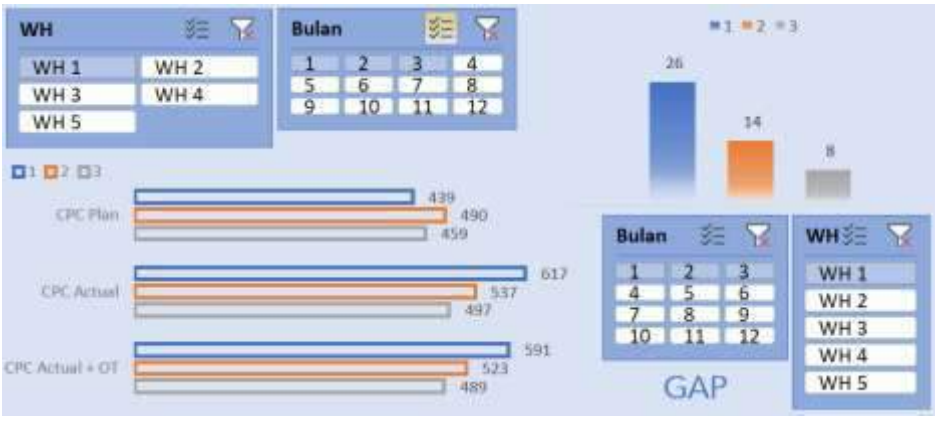

Figure 11. Comparison of CPC

The diagram in Fig. 11 is a comparison of Cost Per Case (CPC) in the warehouse for several categories including, CPC plan, actual CPC, and actual CPC with overtime. The display on the dashboard can be set for each month or every quarter as described in the following Table 7. In

addition, there is also a display of the difference in CPC for each category each month which can be adjusted by setting the month panel and warehouse information.

Table 7. Quarter

The information is displayed Quarterly (Q)	
Quarter	Remarks
Q1	January to March
Q2	April to June
Q3	July to September
Q4	October to December

Figure 12 is a panel for tracking what data users want to display. There are descriptions of volume, month, cost, and warehouse.

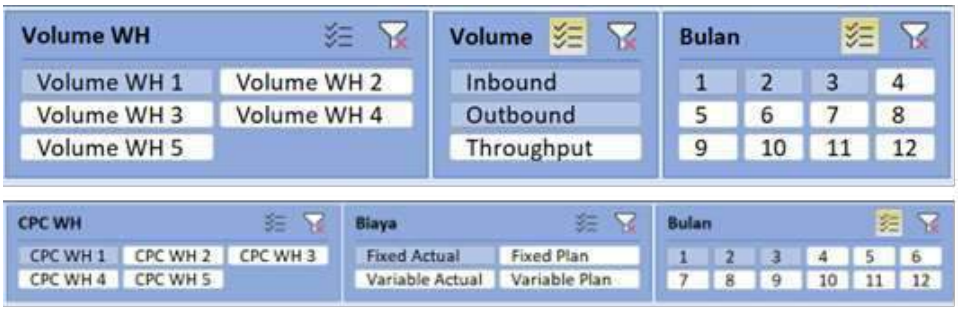

Figure 12. Tracking

When the dashboard was presented to all users, they found it very useful and came up with several improvement ideas. This dashboard is effectively used by PT XYZ to compute CPC as the basis for cost optimization as well as to provide the input data for the existing ERP module.

5. Conclusions and Suggestions

In this chapter, conclusions are drawn on the research that has been carried out and suggestions for the development of further research related to dashboard design are carried out.

A. Conclusion

Since warehouse is really important in the whole supply chain, continuous improvements in warehouse operational activities should be done more effectively and efficiently. Given the importance of monitoring costs in the warehouse of PT XYZ, this study aims to create a dashboard that can make it easier for companies to monitor warehouse performance from a Cost Per Case (CPC) perspective. Based on the results and analysis that has been done, conclusions can be drawn from this practical work research, namely:

1. The business process at PT XYZ starts from production to distribution with the CPC calculation obtained from the quotient between the costs incurred by the company for activities in the warehouse and the volume handled for these activities.
2. The process of creating a dashboard to find out the Cost Per Case (CPC) of each activity in the warehouse so that the information presented on the dashboard is in accordance with the company's needs is through three stages, namely making Microsoft worksheet creating and data input, performing the calculation process, and lastly is creating graphs.
3. Before using, the dashboard must pass the testing phase and be repaired. After passing this stage, the dashboard can be used by following the process flow of using the dashboard so that it can display information according to company needs. The process flow or steps can be carried out by completing the required input data as shown in Table 6.
4. Based on the results of data collection and processing, the results obtained in the form of a proposed warehouse dashboard that can be used by companies to perform cost analysis by providing information related to Cost Per Case (CPC). The purpose of conducting a cost analysis from CPC is to monitor the operational activities in the warehouse so that they are in accordance with what has been planned and to see opportunities in an effort to increase productivity and accuracy in the warehouse along with improving service to customers through improvements in the warehouse.

B. Suggestion

Suggestions for further research on similar topics in the future are as follows:

1. Developers can consider other dashboard design methods such as the Noetix method, Brightpoint, or other new methods such as the Dashboard Development Methodology.
2. There is a need for development in terms of graphics and appearance on the dashboard to make it more user friendly and easy to understand.
3. Dashboard not only displays information related to CPC for ABC group but also for non-ABC group.
4. Adding filter data such as time and location on the dashboard so that the presentation of information can be more dynamic and tailored to user needs.
5. A module can be designed that contains a guide for users to follow up on every possible output generated by the dashboard. For example, when an error occurs in the output or when producing a number on a certain indicator, it can be explained what the purpose of the output is and what follow-up should be done.

References

[1]. Binus Online Learning, "Pentingnya Supply Chain Management bagi suatu Perusahaan," 10 April 2020. [Online]. Available: https://onlinelearning.binus.ac.id/2020/04/10/seminar-online-supply-chain-4-0/.
[2]. S. Chopra, P. Meindl and D. V. Kalra, Supply Chain Management (Strategy, Planning, and Operation), Delhi: Pearson, 2016.
[3]. G. Richards, Warehouse management: a complete guide to improving efficiency and minimizing costs in the modern warehouse, London: Kogan Page, 2011.
[4]. A. M. S. Lavrador and R. M. S. Laureano, "Dashboard to monitor performance of an hotel in the financial perspective," in 2019 14th Iberian Conference on Information Systems and Technologies (CISTI), Coimbra, 2019.
[5]. O. Rud, Business Intillegince Success Factors: Tools for Aligning Your Business in the Global, New Jersey: Wiley Publishing, Inc, 2009.
[6]. S. Alfeno, Sutrisno and M. D. Soleman, "Implementasi Dashboard Informasi Sistem Sebagai Model Alat Ukur Tingkat Penjualan PT Sumber Sekar Sejahtera," Jurnal Sisfotek Global, pp. 8-12, 2020.
[7]. Manajemen pergudangan logistik, "Memahami Definisi Gudang dan Manajemen Pergudangan Logistik," 29 Oktober 2019. [Online]. Available: https://www.3pl.co.id/manajemen-pergudangan-logistik/.
[8]. I. U. Ilyas and H. Setiaji, "Pengembangan Dashboard Untuk Monitoring Sistem Informasi Manajemen Presensi (Studi Kasus di Fakultas Teknologi Industri Universitas Islam Indonesia)," AUTOMATA, pp. Vol. 2, No.1, 2021.
[9]. M. Tuominen and J. Korpela, "A decision aid in warehouse site selection," Elsevier, pp. 169-180, 1996
[10]. J. J. Weygandt, P. D. Kimmel and D. E. Kieso, Accounting Principles, Wiley, 2008.
[11]. D. Anggoro and M. L. Aksani, "Dashboard Information System sebagai Pendukung Keputusan dalam Penjualan Tiket Pesawat Studi Kasus: PT. Nurindo Tour," Jurnal Sistem Informasi, pp. 218-228, 2015
[12]. Novell, "Secure Enterprise Dashboards: a Key to Business Agility," White Paper, 2004.
[13]. A. S. Gunawan, H. Maharani and Y. B. Oktavianus, "Perancangan dan Implementasi Dashboard System pada Bagian Pergudangan Perusahaan Distributor Farmasi (Studi Kasus: PT Y)," Telematika, pp. 111-118, 2018.
[14]. H. Murti and V. A. Srimulyan, "Pengaruh Motivasi Terhadap Kinerja Pegawai Dengan Variabel Pemediasi Kepuasaan Kerja Pada PDAM Kota Madiun," Jurnal Riset Manajemen dan Akuntansi, pp. 10-17, 2013.
[15]. B. Santosa, Data Mining : Teknik Pemanfaatan Data Untuk Keperluan Bisnis Teori & Aplikasi, Jakarta: Graha Ilmu, 2007.
[16]. Gie, "Mengenal Manajemen Rantai Pasokan Untuk Kemudahan Pemantauan Stok Pada Bisnis," 24 Februari 2020. [Online]. Available: https://accurate.id/marketing-manajemen/mengenal-manajemen-rantai-pasokan/.
[17]. Kusnawi, "Tinjauan Umum Metode Pendekatan Dashboard pada Proses Business Inteligence," DASI, pp. 43-48, 2011.

Biographies of Authors

Millenia Shinta Anggraeni is a final student of Logistics Engineering Department, Universitas Pertamina, Indonesia. Born in Kediri, East Java, in the year 2000, Millenia was selected to be one of Universitas Pertamina students under the full scholarship scheme in 2018. She has great interest in Route Optimization and Warehouse Management System.

Harummi Sekar Amarilies is a lecturer in Logistics Engineering Department, Universitas Pertamina. She has been a lecturer for six years, covering mostly the oil and gas logistics, packaging, project management, procurement system, and sustainability subjects. Her research interest includes oil and gas logistics, warehouse and inventory system, as well as sustainable packaging.

Vol. 1, No. 1, August 2022, pp. 35-40
p-ISSN: 2963-8577
DOI: 10.57102/jescee.v1i1.14

SYNTHESIS AND CHARACTERIZATION OF ANTIBACTERIAL POLYSULFONE MIXED MATRIX MEMBRANE BY ADDITION OF ZnO

Ribka Rumintang[1], Rinaldi Medali Rachman[1,2*]
[1]Department of Chemical Engineering, Faculty of Industrial Technology, Universitas Pertamina
[2]Center for Downstream Chemical Industry, Universitas Pertamina

Abstract

Membrane technology is an emerging alternative in water treatment. This study aims to synthesize a filtration membrane made of polysulfone polymer with the addition of ZnO in order to enhanced the membrane antibacterial/antibiofouling property. The membrane was manufactured via Non-Induced Phase Separation (NIPS) phase inversion of the polymer casting solution. The composition of ZnO was varied into 0%, 0.5%, 1%, 2%, and 3%. The results of the membrane synthesis were characterized using Fourier Transform Infrared Spectroscopy (FTIR), Scanning Electron Microscope (SEM), pure water permeability test, and selectivity test with a turbid meter. The hydrophilic properties of the membrane were analysed by measuring the contact angle, and the antibacterial characteristics were analyzed by the disc diffusion test. Analysis by FTIR showed the presence of a sulfone functional group (S=O) derived from polysulfone polymer and a methyl functional group (C-H) derived from PEG. SEM analysis showed that each variation of the polysulfone membrane had an upper surface structure that was close to the honeycomb structure. The pure air permeability test shows that the membrane is porous and able to pass through pure air. Selectivity test with a turbid meter showed that the membrane is selective to the feed stream that passes through it. Analysis of contact angle measurements showed that the polysulfone membrane surface was hydrophilic. Antibacterial activity analysis showed that polysulfone membrane had antibacterial ability with the largest zone of inhibition with a value 1.8 mm n the membrane with the largest concentration of ZnO.

Keywords:

Antibacterial; membrane; phase inversion; polysulfone

Article History:
Received: July 31st, 2022
Revised: August 7th, 2022
Accepted: August 25th, 2022
Published: August 31st, 2022

Corresponding Author:
Rinaldi Medali Rachman
Faculty of Industrial Technology,
Universitas Pertamina
Email:
rinaldi.rachman@universitaspertamina.ac.id

1. Introduction

Every year the need for clean water increases in line with the increasing population and industry growth. But in some circumstances, meeting the need for clean water is a problem that cannot be overcome in several parts of Indonesia, especially during the current pandemic. As in Bolangi Hamlet, Timbuseng Village, Pattallassang District, which has problems with the need for clean water every dry season. Residents in these areas still use well water and rainwater that does not meet clean water standards in meeting their daily needs. Residents admitted that it was difficult because clean water assistance only came once a week and not every resident received the clean water assistance.

In its development to meet the need for clean water, further studies on water resources and processing methods are needed as an alternative. Membranes are an alternative technology that can be used to treat various water resources. Membranes are used for the separation of dissolved organic and inorganic substances, suspended solids, microorganisms, and can be applied to desalination, sewage treatment, and gas separation. In the operation of membranes for water treatment processes, membranes generally will experience fouling events.

Fouling is the deposition of particles, macromolecules, salts, colloids, which are retained on the membrane surface or membrane pore walls, which causes a continuous decrease in flux [1].

Fouling can be classified into three types, namely inorganic fouling, organic fouling, and biological fouling. Biological fouling (biofouling) is formed because of the accumulation and growth of biological species in the form of biofilms on the membrane surface which affects membrane permeability which causes a loss of membrane productivity. Microorganisms are the main cause of biofouling [1].

Biofouling on the membrane can interfere with the operation and even damage the membrane, causing a decrease in the performance of the membrane. However, the process of biofouling formation on the membrane surface can be slowed down. The increasing resistance of biofilms to antibacterial compounds encourages the development of new alternatives to remove these biofilms [2]. One alternative antibacterial agent that can be used is ZnO. ZnO compounds show an antibacterial effect on gram-positive and gram-negative bacteria that are resistant to high pressure and temperature [3]. In this study, the synthesis of polysulfone membranes was chosen with the addition of ZnO as an antibacterial agent to be applied in water treatment.

2. Experimental Method

A. Materials

PSF purchased from Solvay Advanced Polymer, N-Methyl-2-pyrrolidone (NMP) obtained from Merck Milipore, and PEG400 obtained from local supplier were used for membrane casting solution preparation. Zinc oxide (ZnO) obtained from Loba Chemie were used as additives. Nutrient Agar and Nutrient Broth was purchased from local supplier.

B. Membrane Fabrication

PSF membranes were synthesized by additive blending methods and casted via phase inversion method. The detailed composition of the membrane solution is summarized in Table 1. Briefly, membrane preparation consists of dissolving PSF and PEG400 in NMP, blending additives in PSF solution, casting the membrane solution, and immersing the cast solution in a coagulation water bath.

Table 1. Casting solutions composition

Variation	Polymer Solution			Nanoparticle
	PSF (gram)	NMP (gram)	PEG (gram)	ZnO (gram)
Control	18	82	10	0
Sample 1	18	82	10	0.5
Sample 2	18	82	10	1
Sample 3	18	82	10	2
Sample 4	18	82	10	3

C. Membrane Characterization

The membrane surface was analysed by scanning electron microscope (SEM, Phenom Pro X). Membrane chemical structures were analyzed by FTIR (Nicolet™ iS50 FTIR Spectrometer with NIR). Pure water permeability and selectivity tested using syringe filter and turbid meter. Water contact angle (WCA) was determined by the sessile drop technique.

D. Antibacterial Activity Studies

Antibacterial tests were carried out on Gram negative bacteria *E. coli*, using Kirby-Bauer disk diffusion method. The bacterial cultures were sub cultured on Nutrient broth medium. The culture was inoculated on Nutrient agar plates. PSF membrane disks were placed aseptically on the Nutrient agar medium which was already swabbed with the test organism. The experiment was carried out for both PSF membranes, with and without ZnO nanoparticles. The plates were incubated at 37 ^{0}C for 48 h to observe the inhibition zone.

3. Results and Discussion

A. Membrane Morphology

The morphological characteristics of the top surface of the polysulfone membrane were analyzed by Scanning Electron Microscope (SEM) using Desktop Phenom ProX. Each image was taken at 200x magnification. This membrane morphological observation was carried out only on the upper surface of the membrane due to limited

equipment in observing the cross-sectional surface of the membrane which required liquid nitrogen. In this study the analysis focused on the pores of the membrane surface, not on the effective pores of the membrane itself.

Fig. 1 shows the results of the surface SEM micrographs on the five membrane variations. Based on the micrograph below, each membrane has an expected surface pores with a honeycomb structure [4]. This honeycomb structure is formed due to changes in the diffusion rate of solvent and non-solvent caused by changes in polymer viscosity when ZnO nanoparticles are added [4].

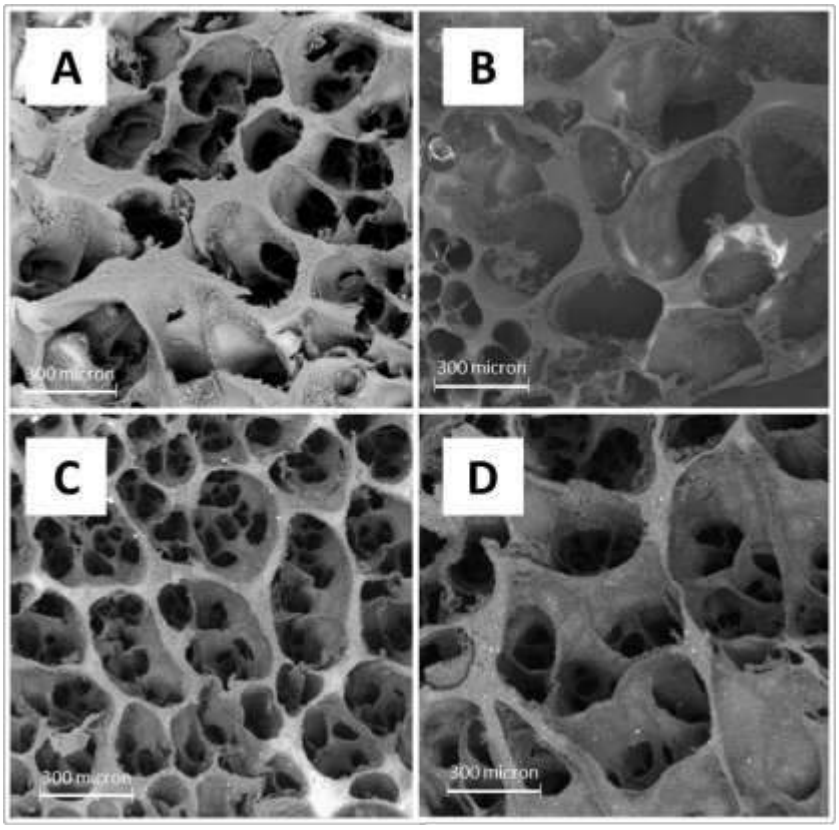

Figure 1. Micrograph of Surface Morphology Polysulfone Membrane
(A: Control, B:Sample 1, C:Sample 2, D:Sample 3)

B. Membrane Chemical Structure

To demonstrate the successful introduction of ZnO, in PSF membrane, all variation membranes were characterized via FTIR analysis (Fig. 2). All membranes showed absorption peaks at around 1,450-1,230 cm^{-1} indicating S=O stretching vibration [4]. The S=O represents the sulfonic groups of PSF. Absorption peaks at around 1,560-1,650 cm^{-1} were found which represent the functional group of C=C of the benzene ring [5]. The stretching vibrations of O-H were represented by the strong, broad band at around 3,650–3,450 cm^{-1}.

Absorption peaks at around 1,200-950 cm-1 were found which represent the functional group of C-O of the ether group [6]. Absorption peaks at around 2,980-2,800 cm^{-1} were found which represent the functional group of C-H represents methyl group of PEG [7]. Thus, the use of zinc oxide in the PSF membrane into the dope formulation does not result in any reaction and new phases or new bonding formation. This was revealed by the FTIR results in this study, which determines that all the PSF bonding patterns in all the PSF and mixed matrix PSF membranes show the existence of the same peaks.

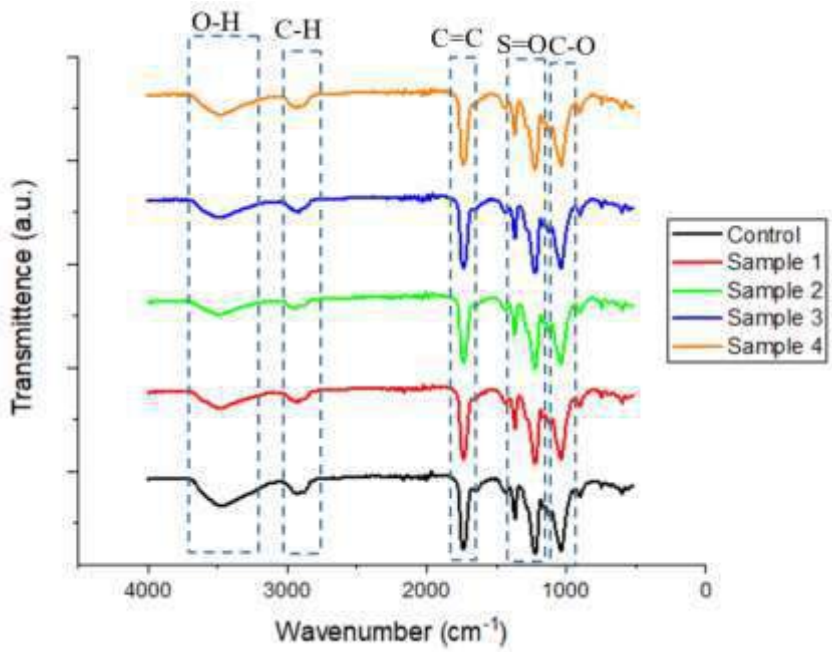

Figure 2. FTIR Spectra of the synthesized polysulfone membrane.

C. Pure Water Permeability & Membrane Selectivity

Pure water permeability tested using syringe filter & syringe filter holder. The result shows all variation of PSF membrane had pore and passed by pure water. Membrane selectivity tested using turbidity meter. The result shows removal percentage value increase as nanoparticle ZnO added as shown in Table 2. The addition of nanoparticle ZnO change surface pore characteristic of the membrane thus poses a different selectivity towards turbidity.

Table 2. Percent removal of suspended solid

Variation	Starch Water
	%Removal
Control	24.71
Sample 1	15.89
Sample 2	27.43
Sample 3	30.23
Sample 4	56.95

D. Membrane Hydrophilicity

Contact angle measurement was carried out to evaluate hydrophilicity of membrane surface. The contact angle values obtained in the measurement of all variations of polysulfone membranes are in the range of less than 90^{o} which categorized as hydrophilic as shown in Fig. 3. The value of the surface contact angle of the polysulfone membrane decreased with the addition of ZnO nanoparticles, but this decrease was not significant between sample 3 and sample 4. This was due to the formation of ZnO aggregates on the membrane surface which caused pore blocking.

Pore blocking causes the feed stream to pass through the membrane. The decrease in the value of the contact angle of the membrane surface indicates that the level of hydrophilicity of the membrane surface also increases. The level of hydrophilicity of the membrane affects the permeability of the membrane, so that the increasing level of hydrophilicity of the membrane, the more permeable the membrane.

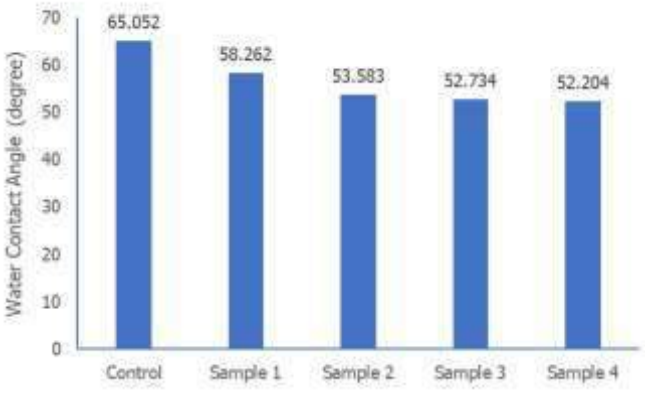

Figure 3. Water Contact Angle of Polysulfone Membrane.

E. Antibacterial Properties

The antibacterial properties of polysulfone membranes were evaluated against E. coli. Here, Kirby Bauer technique was adopted to evaluate the antimicrobial activity. The results are shown in Fig. 4. The pure PSF membrane was used as a control. According to the results obtained, no detectable inhibition Zones were seen for the bare PSF membrane. Conversely, the Zones were observed for ZnO embedded PSF. The diameters of the zone of inhibition around the membranes after one day were measured to be 1 mm, 1.5 mm, 1.7 mm, and 1.8 mm. The inhibition zone formed increases with the increase in the concentration of ZnO nanoparticles. The largest inhibition zone formed was in the sample membrane 4 (addition of 3 grams of ZnO) with a value of 1.8 mm.

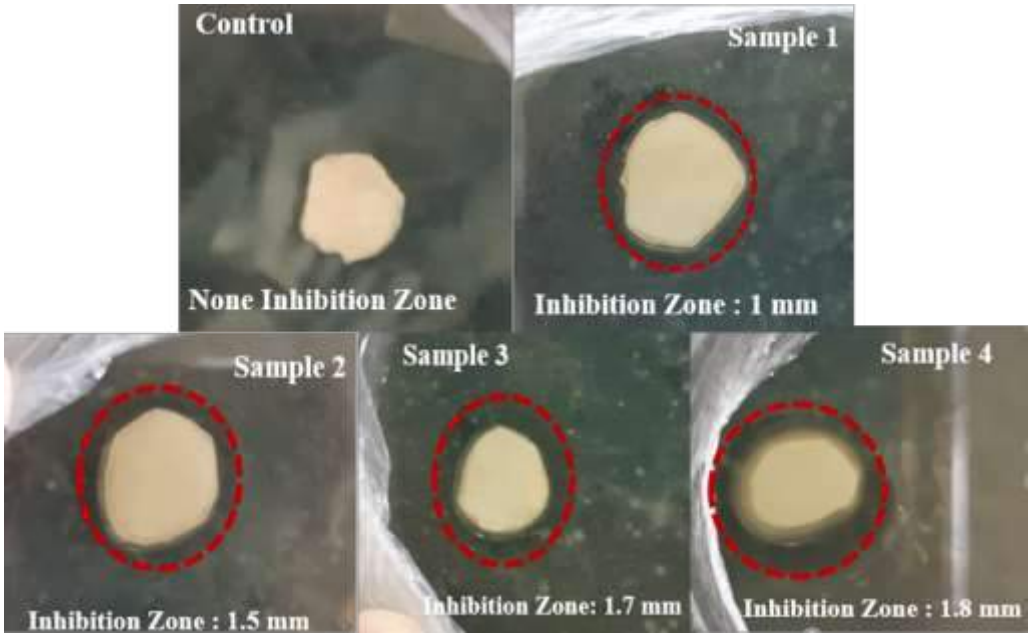

Figure 4. Antibacterial inhibition zone of the synthesized polysulfone membrane

The zone of inhibition was caused by the release of Zn^{2+} ions from ZnO nanoparticles contained in the membrane. The release of Zn^{2+} ions damage the bacterial cell wall and causes protein denaturation. When bound to bacterial cells, Zn^{2+} ions from ZnO nanoparticles damage the bacterial cell membrane and cause leakage in the interior of the cell so that ZnO nanoparticles can enter the cell membrane, disrupting cell metabolism, proteins, and DNA. Then the bacterial cells are damaged, and their development is hampered [8].

4. Conclusions

This research proves that polysulfone mixed-matrix membrane with the addition of ZnO nanoparticles is permeable to pure water and semi-permeable (selective) to turbidity. The addition of ZnO nanoparticles influences the pore characteristics of the membrane surface and affects the level of turbidity selectivity. The addition of ZnO nanoparticles increased the antibacterial activity of the polysulfone membrane which was characterized by the appearance of an inhibition zone. The membrane that produced the best antibacterial activity was sample 4 with an inhibition zone of 1.8 mm against *Escherichia coli* bacteria.

Acknowledgements.

We would like to gratefully acknowledge all staff of the Chemical Engineering Laboratory and Integrated Laboratory of Universitas Pertamina.

References:

[1] Nguyen, T., Roddick, F., & Fan, L. Biofouling of water treatment membranes: A review of the underlying causes, monitoring techniques and control measures. Membranes, 2(4), 804-840. 2012.

[2] LeChevallier, M. W., Cawthon, C. D. and Lee, R. G. Mechanisms of bacterial survival in chlorinated drinking water. Wat. Sci. Tech.• 20(11/12),145-151. 1988.

[3] Azam, Ameer; Ahmed, ; Oves, ; Khan, ; Habib, ; Memic, Adnan. Antimicrobial activity of metal oxide nanoparticles against Gram-positive and Gram-negative bacteria: a comparative study. International Journal of Nanomedicine, (), 6003–. 2012.

[4] Mushtaq, Asim; Bin Mukhtar, Hilmi; Mohd Shariff, Azmi. FTIR Study of Enhanced Polymeric Blend Membrane with Amines. Research Journal of Applied Sciences, Engineering and Technology, 7(9), 1811–1820. 2014.

[5] Zhang W.F., Wang Q.H., Fang M.X., Luo Z.Y. and Cen K.F. Progress of separation of CO2 from flue gas by membrane absorption, Chemical Industry and Engineering Progress, 27, 635-639.2008.

[6] Abdelrasoul, A., Doan, H., Lohi, A., & Cheng, C.-H. Morphology Control of Polisulfon Membranes in Filtration Processes: a Critical Review. ChemBioEng Reviews, 2(1), 22–43. 2015.

[7] Nasirian, Danial; Salahshoori, Iman; Sadeghi, Morteza; Rashidi, Niloufar; Hassanzadeganroudsari, Majid. Investigation of the gas permeability properties from polysulfone/polyethylene glycol composite membrane. Polymer Bulletin, 2019.

[8] Sirelkhatim, A., Mahmud, S., Seeni, A. et al. Review on Zinc Oxide Nanoparticles: Antibacterial Activity and Toxicity Mechanism. Nano-Micro Lett. 7, 219–242. 2015.

Biographies of Authors

Rinaldi Medali Rachman, S.T., M.S. is currently a Lecturer in Chemical Engineering at the Universitas Pertamina, Jakarta, Indonesia. Some courses that he teaches are Intro to Chemical Engineering, Thermodynamics, Process Synthesis and Simulation, Oil Refinery, Oil dan Gas Upstream Facilities, and Membrane Technology. Before joining the university, he was a process engineer at Saudi Basic Industries Cooperation in the Kingdom of Saudi Arabia. He dealt with process improvement of ethylene plants owned by SABIC throughout the Kingdom and in correspondence with SABIC India and Europe. He received his Masters' Degree from King Abdullah University of Science and Technology where he gained research interest in water and wastewater treatment, membrane synthesis, and membrane-based desalination. His Bachelor of Engineering Degree is from the Institut Teknologi Bandung, Indonesia.

Ribka Rumintang graduated from Universitas Pertamina in July 2021. Her research interests are membrane synthesis and membrane-based chemical processes.

Vol. 1, No. 1, August 2022, pp. 41-54
p-ISSN: 2963-8577
DOI: 10.57102/jescee.v1i1.10

EFFECTS OF FLOW RATE AND INLET TEMPERATURE ON PERFORMANCE OF ANNULUS TYPE LOW-TEMPERATURE LATENT HEAT THERMAL ENERGY STORAGES

Rifki Yusup[1*] and Byan Wahyu Riyandwita[1]
[1]Department of Mechanical Engineering, Faculty of Industrial Technology, Universitas Pertamina, Indonesia

Abstract
Solar energy is one of the largest energy potentials which can be utilized in solar heater and integrated with the latent heat energy storage (LHTES). This research aims to investigate the effects of the operating conditions of flow rate and inlet temperature on the performance of the annulus type Low-Temperature LHTES using Computational Fluid Dynamics method in which the enthalpy-porosity is used as the solidification model. The results indicated that better performance can be obtained by increasing the flow rate and inlet temperature. The increase in flow rate resulted in a higher heat transfer, producing better performance up to 11.91% and 24.91% during the charging and discharging, respectively. Meanwhile, increasing the inlet temperature in the Low-Temperature LHTES system enhanced the performance up to 192.72% during the charging and 13.07% during the discharging.

Keywords:
Thermal storage; low-temperature LHTES; heat transfer performance; enthalpy-porosity; numerical simulation

Article History:
Received: July 31st, 2022
Revised: August 7th, 2022
Accepted: August 25th, 2022
Published: August 31st, 2022

Corresponding Author:
Rifki Yusup
Department of Mechanical Engineering, Universitas Pertamina, Indonesia
Email:
rifki.yusup@outlook.com

1. Introduction

The need of global energy has been increasing exponentially since the 1900s as depicted in Fig. 1 [1]. Considering the Paris Agreement in 2015, the world has started to see the potential of renewable energy to reduce fossil fuel emissions [2]. The largest renewable energy potential in Indonesia is solar with 207.8 GWp [3]. However, for harvesting solar energy, one of the biggest challenges is the intermittent characteristics of solar energy or only can be harvested in a limited period and in a fluctuated nature, as shown in Fig. 2 [4]. The use of the renewable energy worldwide is still low due to the imbalance of energy supply and demand period. Currently, the technology of energy storages such as sensible heat energy storages, latent heat energy storages, and chemical energy storages have been developed to solve the problem in the most effective, efficient, and safest way [5, 6].

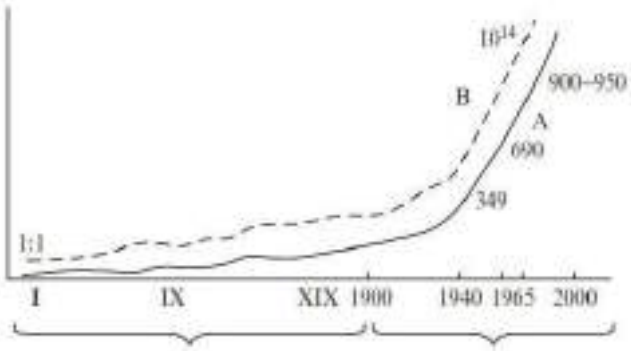

Figure 1. Global Energy Consumption [1]

Scapino, et. al. [7] reviewed that the latent heat thermal energy storages (LHTES) is one of the technologies that could achieve the three indicators explained before. LHTES is more effective in cost, has a high efficiency, and has a minimum response time [7]. Almost all LHTES applications have the same phase change material (PCM) geometry configuration of doughnut-shape, where the PCM will cover the tube in which heat transfer fluid is flowing inside the tube, as shown in Fig. 3 a) [5, 8–10]. One of methods to improve the thermal performance can be done by extending the heat transfer area and by making the fluid flows more turbulent [11, 12], by changing

the geometry configuration of the PCM, where the heat transfer fluid covers the annulus tube that contains the PCM.

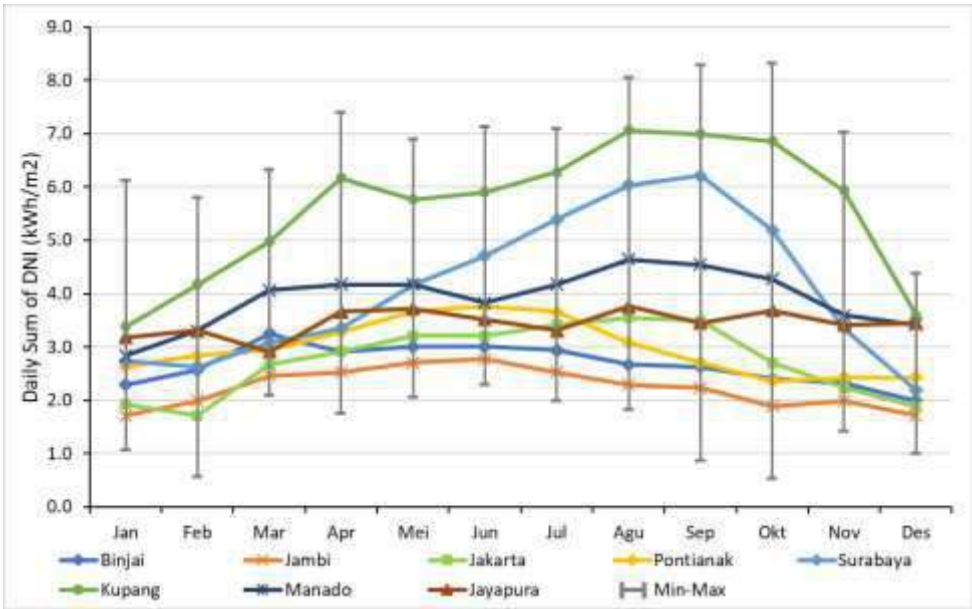

Figure 2. The Average of Daily Direct Normal Irradiance in a Few Cities in Indonesia [4].

Based on the applications, LHTES relies on the PCM or material for absorption of the thermal energy (heat storage) and classified as Low-Temperature (below 150°C, like for solar heater), Medium-Temperature (between 150°C-400°C), and High-Temperature (above 400°C, for Concentrated Solar Power, Steam Power Plant, etc.) applications [6, 13]. In this study, low temperature LHTES is selected for solar applications by using paraffin wax like *n*-octadecane for the PCM and evaluated in charging and discharging region because the properties of paraffin wax have a high density, stability of termal properties, unreactive, and the most important is the cycle resistance up to 2000 cycles [14, 15].

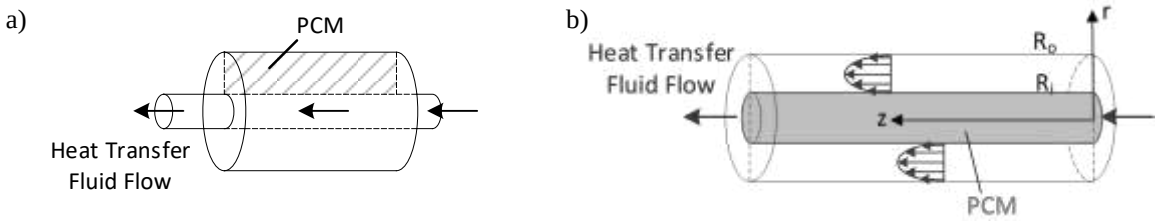

Figure 3. The Schematic Diagram of LHTES in a Geometry of
a) Doughnut Type (Shell-and-tube); and b) Annulus-tube.

2. Model Formulation

Here, the PCM is placed in the inner tube and the heat transfer fluid (HTF) flows through a pipe in the outer side of tube and cover the PCM tube (shell-side) with adiabatic wall as depicted in Fig. 3 b). Various configuration of inlet temperature and flow rate of HTF are considered in this research. The evaluation of performance of charging and discharging is evaluated by enthalpy of the process.

A. Governing Equations

The governing equations are employed for two components, water and PCM. During charging, the water, which flows in the outer side tube, transferred the heat to melt the PCM and stored the thermal energy in a liquid phase. While during discharging, the heat that stored in PCM is then taken by the cold water and thus solidified the PCM. In this research, a three-dimensional model is simplified into two-dimensional to reduce the cost of computation.

In the HTF, the convection of heat and fluid flow will be considered by using the Navier-Stokes equations. These equations focused on conservation of mass, momentum, and energy [5, 9].

$$\frac{\partial \rho}{\partial t} + \nabla.(\rho \boldsymbol{u}) = 0 \tag{1}$$

$$\frac{\partial(\rho \boldsymbol{u})}{\partial t} + \nabla.(\rho \boldsymbol{u_r} \boldsymbol{u}) + \rho[\omega \times (\boldsymbol{u} - \boldsymbol{u_t})] = -\nabla p \boldsymbol{I} + \nabla.[\mu(\nabla \boldsymbol{u} + (\nabla \boldsymbol{u})^T)] + \rho \boldsymbol{g} \tag{2}$$

$$\frac{\partial(\rho\, c_p\, T)}{\partial t} + \nabla.\left(\rho\, \boldsymbol{u_r}\, c_p\, T\right) = \nabla.(k\, \nabla T) \tag{3}$$

During the process of melting and solidification, the molten PCM will form a mushy zone where it will decrease the value of porosity. To evaluate solidification process, the enthalpy-porosity formulation is represented as a source term, $\boldsymbol{S}_{mom}$, and it is added to the conservation momentum Equation (2) with the value defined as:

$$\boldsymbol{S}_{mom} = \frac{(1-\beta)^2}{(\beta^3 + 1 \times 10^{-3})} \times \zeta\, \boldsymbol{u} \tag{4}$$

where, ζ is mushy zone constant that has value of $1{\times}10^{5}$` for *n*-octadecane.

Then, the enthalpy is added on energy conservation Equation (3) and defined as

$$H_{pcm} = \widetilde{h_{pcm}} + \widetilde{\Delta H_{pcm}} \tag{5}$$

where, $\widetilde{h_{pcm}}$ is sensible heat of PCM and defined as:

$$\widetilde{h_{pcm}} = \widetilde{h_{pcm,ref}} + \int_{Tref}^{T} C_{p,pcm} \tag{6}$$

where, $\widetilde{h_{pcm,ref}}$ is reference enthalpy on reference temperature and ΔH_{pcm} is latent heat of PCM which is a function of liquid fraction, β of the PCM.

$$\widetilde{\Delta H_{pcm}} = \beta.L \tag{7}$$

B. Constitutive Relations

The water liquid defines as HTF that has temperature dependent polynomial functions for the thermophysical properties. The density, viscosity, and thermal conductivity of water are defined in (8-10) respectively. The other thermophysical properties are presented in Table 1.

$$\rho_w = -3.570 \times 10^{-3}\, T^2 + 1.88\, T + 753.2 \tag{8}$$

$$k_w = -8.354 \times 10^{-6}\, T^2 + 6.53 \times 10^{-3}\, T - 0.5981 \tag{9}$$

$$\mu_w = 2.591 \times 10^{-5} \times 10^{\frac{238.3}{T-143.2}} \tag{10}$$

The PCM (*n*-octadecane) also has temperature dependent polynomial functions for the thermophysical properties that are defined in (11-13) and the other properties are presented in Table 1.

$$\rho_{pcm} = \frac{774}{9 \times 10^{-4}(T - 300.65) + 1} \tag{11}$$

$$k_{pcm} = \begin{cases} 0.358, & T < T_s \\ 126.421 - 0.42T, & T_s \le T \le T_l \\ 0.148, & T > T_l \end{cases} \tag{12}$$

$$\mu_{pcm} = 0.001 \times \exp\left(-4.649 + \frac{1.79 \times 10^3}{T}\right) \tag{13}$$

To evaluate the heat transfer rate, $\dot{Q}$ on charging and discharging condition can be evaluated by

$$\dot{Q}_{transfer,} = \frac{H_{pcm}}{t_{transfer}} \tag{14}$$

So, the efficiency of thermal enhancement ratio of heat transfer, *TER* can be determined by

$$TER = \frac{\dot{Q}_{transfer} - \dot{Q}_{transfer,base}}{\dot{Q}_{transfer,base}} \times 100\% \quad (15)$$

Table 1. Thermophysical Properties of Water Liquid and *n*-octadecane [9, 16].

Parameters	Value	Unit
Water Liquid		
Melting Temperature, $T_{m,w}$	273.15	K
Latent Heat, L_w	2100	J • kg^{-1}
Specific Sensible Heat, $C_{p,w}$	4200	J • kg^{-1} • K^{-1}
PCM (*n*-octadecane)		
Melting Temperature		
• Solidus Temperature, T_s	300.15	K
• Liquidus Temperature, T_l	300.65	K
Latent Heat, L_w	2.43×10^5	J • kg^{-1}
Specific Sensible Heat, $C_{p,pcm}$	2160	J • kg^{-1} • K^{-1}
Coefficient of Thermal Expansion	9.00×10^{-4}	K^{-1}

C. Boundary Conditions

In this research, these following boundary conditions are employed on the model.

- Inlet: at the inlet, a various inlet mass flow rate and inlet temperature is specified as shown in Table 2.
- Outlet: at the outlet, stream-wise gradient of temperature and gauge pressure are set to be zero.
- PCM wall is set to be no-slip condition, zero roughness height, and coupled
- HTF wall is set to be insulated wall (no heat flux), no-slip condition, and zero roughness height.

Table 2. Inlet Conditions.

Various Mass Flow Rate						**Various Inlet Temperature**					
Charging			***Discharging***			***Charging***			***Discharging***		
No	**$\dot{m}$ (kg/s)**	**T_c (K)**	**No**	**$\dot{m}$ (kg/s)**	**T_d (K)**	**No**	**$\dot{m}$ (kg/s)**	**T_c (K)**	**No**	**$\dot{m}$ (kg/s)**	**T_d (K)**
CF1	0.01575	310.65	DF1	0.01575	295.65	CT1	0.03150	305.65	DT1	0.03150	295.65
CF2	0.03150	310.65	DF2	0.03150	295.65	CT2	0.03150	310.65	DT2	0.03150	295.65
CF3	0.15750	310.65	DF3	0.15750	295.65	CT3	0.03150	320.65	DT3	0.03150	295.65

3. Numerical Methodology

In this research, the LHTES model and grid generation are conducted in ANSYS Workbench 2019 R2 in which simplified symmetrical 2D model is used as depicted in Fig. 4. Then, the mathematical model formulation (governing equations, constitutive relations, and boundary conditions) is implemented and solved. For several thermo-physical properties of HTF and PCM, the C-Language is coded and compiled for user-defined functions in the model.

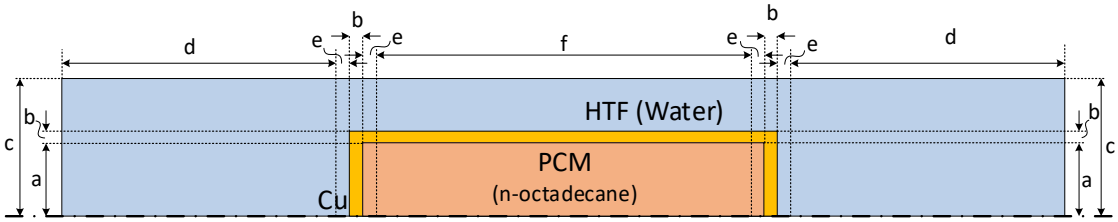

Figure 4. The Schematic Diagram of 2D Symmetrical Annulus-tube LHTES System.

To ensure the grid generation is independence, the grid independent study was conducted by dividing the domain into areas and set the number of divisions in c-side to increase the number of fluid elements (cells), the summary of the test shown in Table 3 and the results is presented in Fig. 5. It is seen that, there is no significant differences on the average liquid fraction of PCM due to the time which means the number of cells is not affecting the value significantly. Hence, the grid size of 71,568 cells was chosen for all cases of this study. The results of this grid is shows in Fig. 6 with the orthogonal quality is 0.9998 which means the setting of grid is good.

Semi-Implicit Pressure Linked Equation (SIMPLE) algorithm is chosen for solving the numerical model of this research. The momentum and energy equations are solved by the second order upwind discretization and pressure correction equation is adopted in the PRESTO! scheme. A time step of 0.1 second is taken with the number of maximum iterations of 20 times for each time step. Convergence criterion of 1×10^{-3} is selected for the momentum and turbulent equations and 1×10^{-5} is set for the energy.

Table 3. Grid Generation for Grid Independent Study.

No	Number of Partition*			Size of c-side* (mm)	Number of Elements (Cells)
	Area b	Area d	Area f		
1	6	80	800	1.00	57,960
2	6	100	1000	1.00	71,568
3	8	100	1300	1.00	88,368
4	8	150	1500	0.75	116,436
5	8	200	2000	0.75	153,760

Note: *Check the area *x* in Figure 4

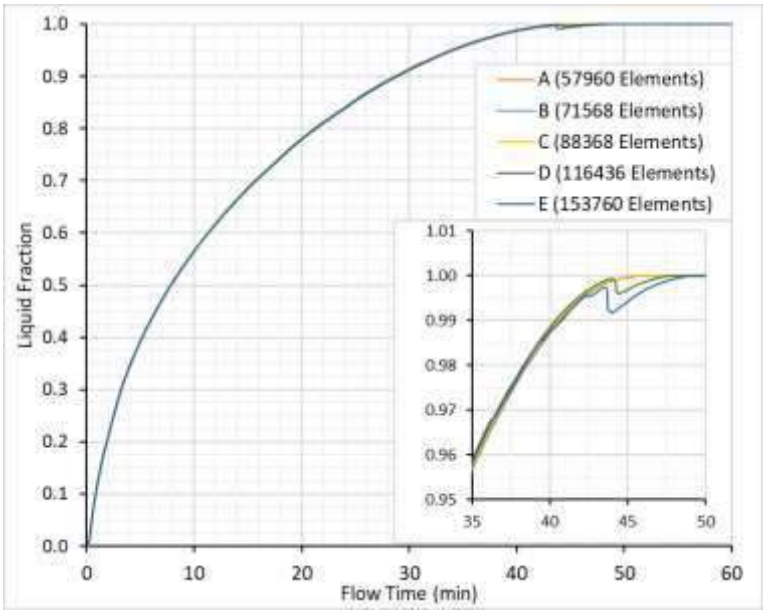

Figure 5. Comparison of Grid Independent Study.

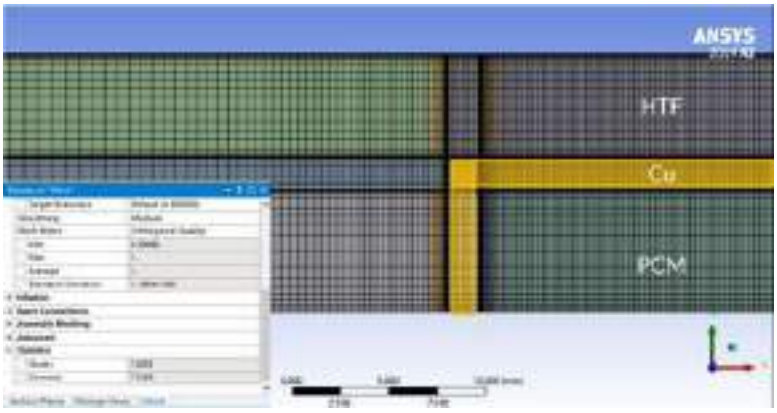

Figure 6. Detail Grid Result (71,568 cells in Total: Orthogonal Quality of 0.9998).

4. Results and Discussion

A. Model Validation

To ensure correct selection and settings of the mathematical model, the validation is made by comparing the results of the simulation with the results of previous experiment [8]. The comparison is focusing on two temperature locations (T_1 and T_2) and the results are shown in Fig. 7. As can be seen from Fig. 7, a relatively good behavior is shown with small relative error of 0.357% for T_1 and 0.152% for T_2. This explain that the settings and parameters of this research are valid and thus the simulation results sufficiently describe the behavior of the LHTES.

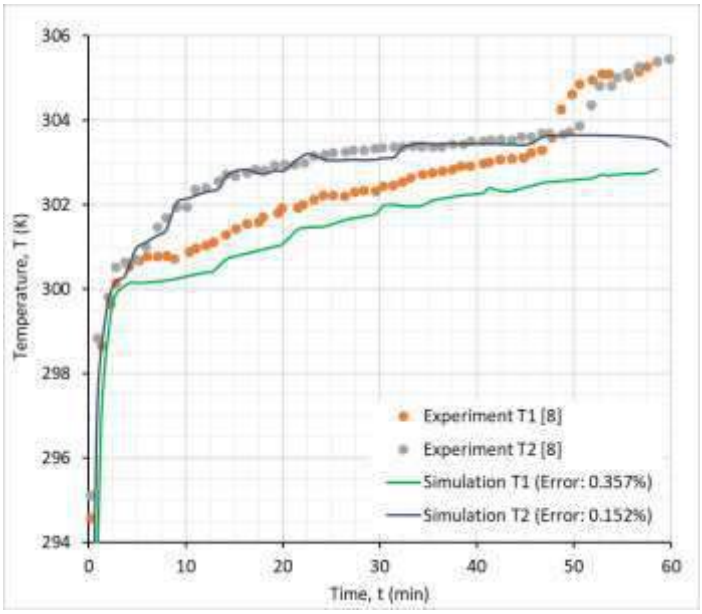

Figure 7. Comparison of Simulation and Experiment Results [8].

B. Effect of Mass Flow Rate

The heat transfer in LHTES is affected by the flow condition, especially flow rate. Hence, this research is carried out to prove and find the behavior of heat transfer of PCM in three variation flow rates of 0.01575 kg/s; 0.03150 kg/s; and 0.15750 kg/s. The simulation is evaluated by flowing the hot water with 310.65 K (10 K above the melting temperature of PCM, *n*-octadecane) in the inlet.

Fig. 8 presents the average PCM liquid fraction during charging-discharging process for the flow rate variation. This figure shown that from the initial until charging process ended, the increase of flow rate will increase the heat transfer rate. This is also implied that at higher flow rate the liquid fraction of PCM is faster to reach value of 1.0 which means the PCM has melted completely into the liquid phase. Higher flow rate creates more turbulence eddies. These eddies will mix the fluid elements and speed up the convection rate in the heat transfer process, thus give faster melting process in the PCM [17].

Fig. 8 also shows that the rate of liquid fraction is slower towards the end of charging cycle because the heat transfer in PCM is started to be dominated by convection process. This phenomenon also depicted in Figs. 9 and 10 where the melting process in the center region of the PCM is reduced due to the change of conduction process into a convection process near the wall. Figs. 9 and 10 also shows that towards the end of the charging cycle, the temperature of PCM will approach the hot water temperature and in the higher flow rate and the melted area in the PCM tends to be larger.

The behavior of flow rate effect on the discharging process is similar to the charging process. When the flow rate is increased, the solidification of PCM is increased because turbulence effect on heat transfer. Fig. 11 and 12 show that at higher flow rate, the area of solidification near the wall in PCM is larger and accompanied with lower temperature distribution.

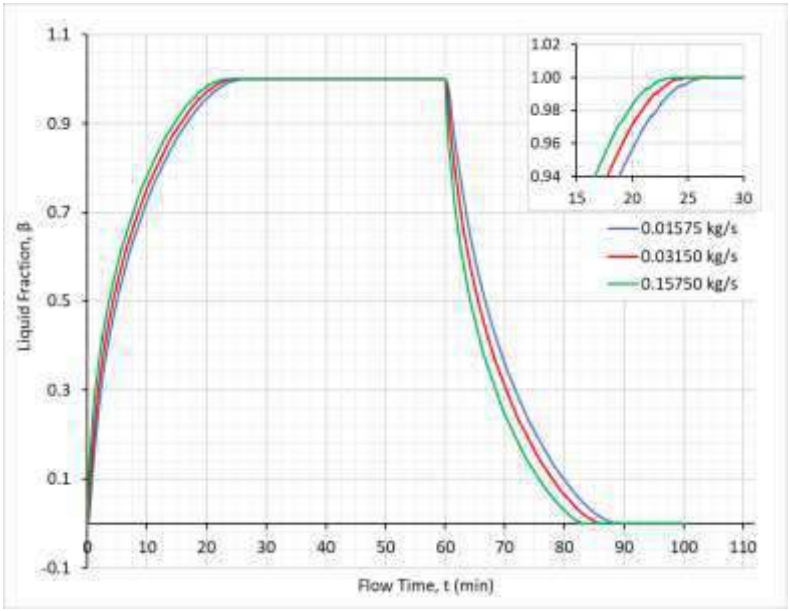

Figure 8. Average PCM Liquid Fraction during Charging and Discharging for Different Flow Rates.

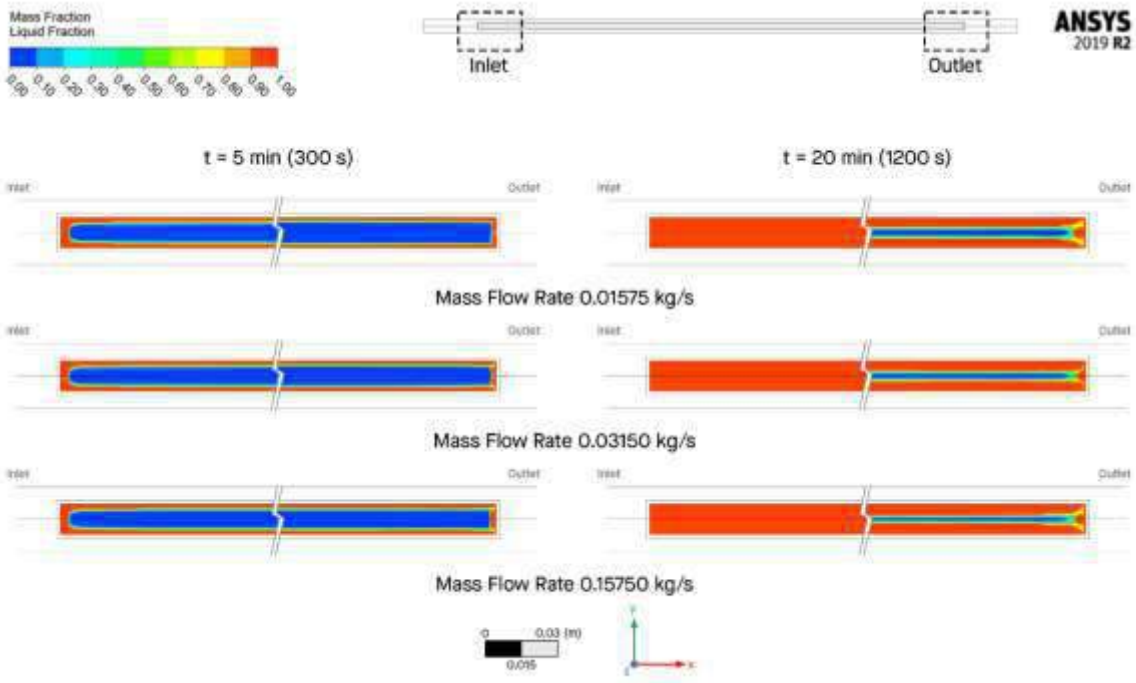

Figure 9. Comparison of Average PCM Liquid Fraction for Different Flow Rates at 5 mins and 20 mins (Charging).

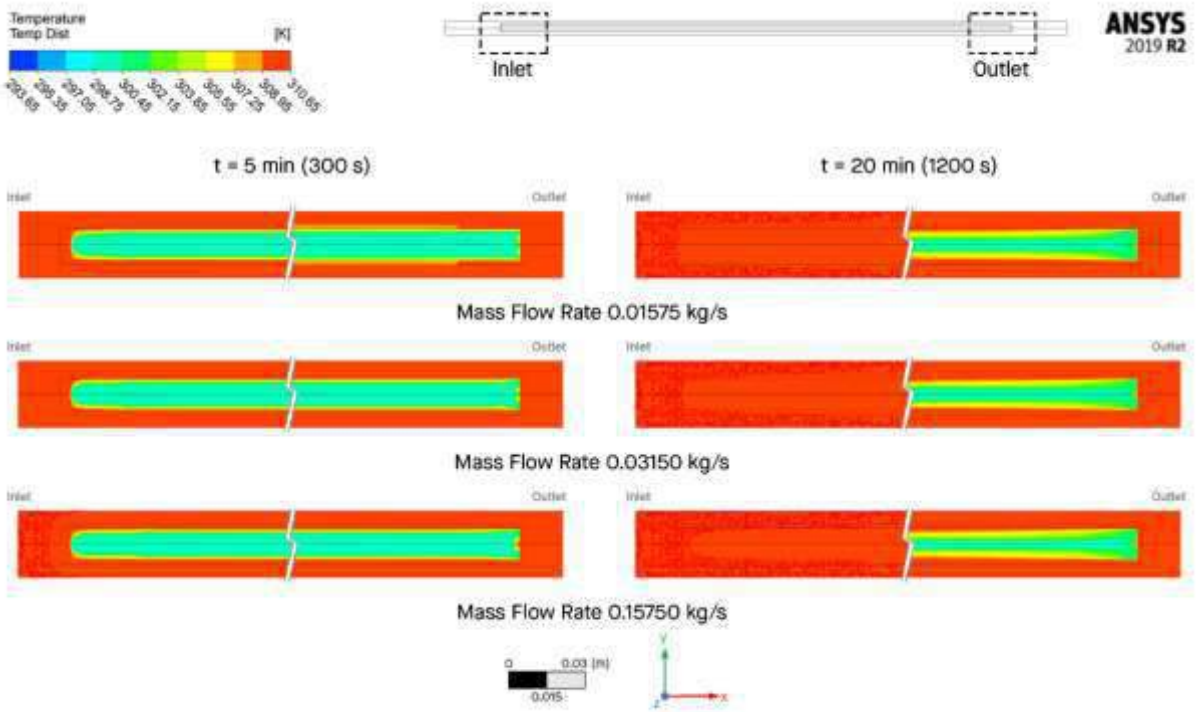

Figure 10. Comparison of Temperature Distribution for Different Flow Rates at 5 mins and 20 mins (Charging).

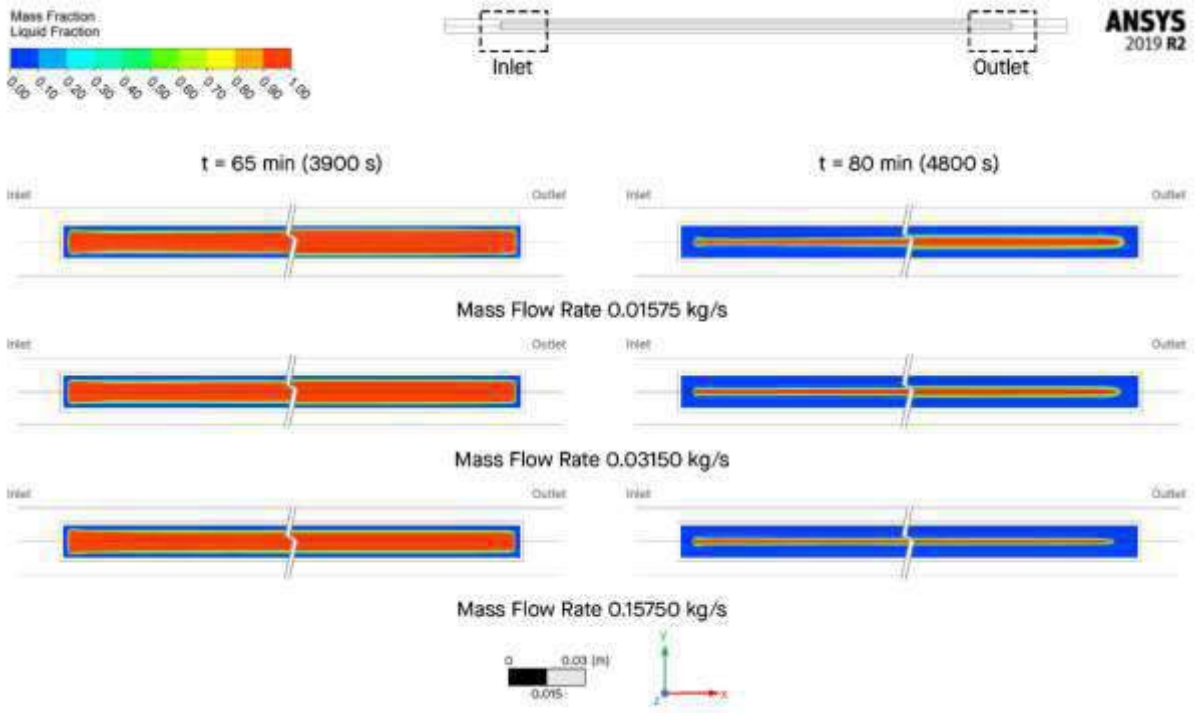

Figure 11. Comparison of Average PCM Liquid Fraction for Different Flow Rates at 65 mins and 80 mins (Discharging).

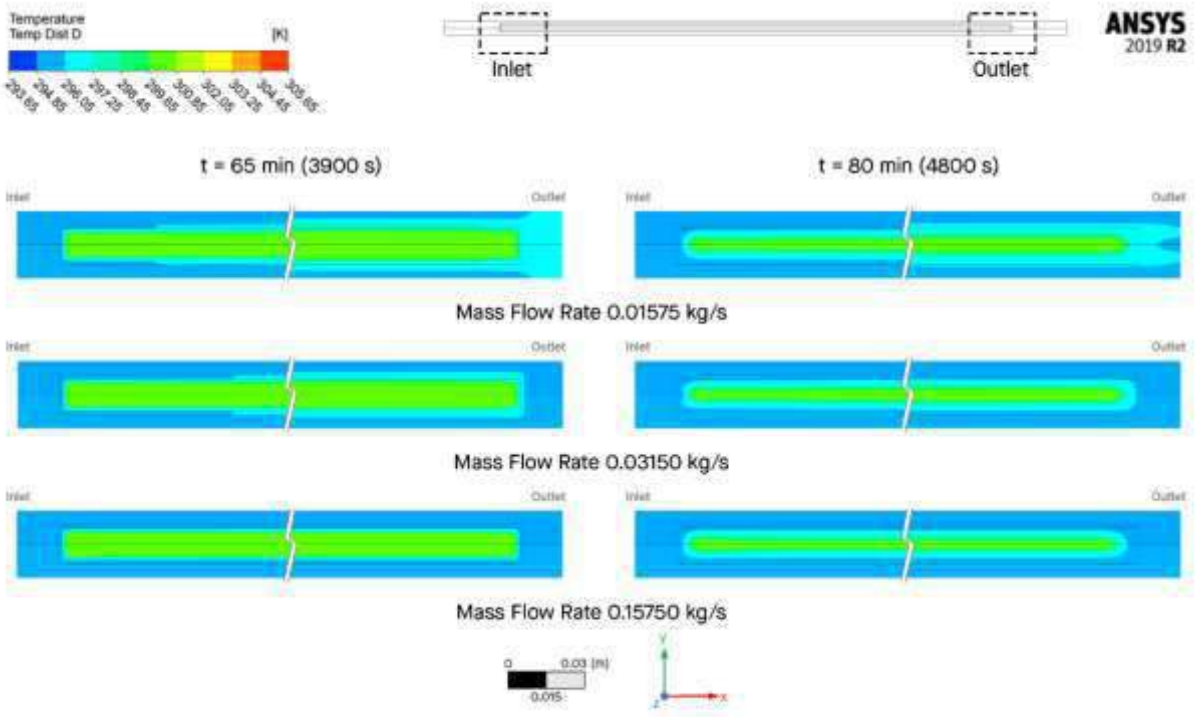

Figure 12. Comparison of Temperature Distribution for Different Flow Rates at 65 mins and 80 mins (Discharging).

Table 4 is the summary for the evaluation of the overall heat transfer performance (Thermal Enhancement Ratio, TER) for each case. The value shows that by increasing the flow rate the heat transfer process will be faster. Increasing 2 times the flow rate will give 6.17% and 10.90% higher efficiency of heat transfer on charging and discharging, respectively. Meanwhile, increasing 10 times of the flow rate will improve the efficiency by 11.91% in charging and 24.91% in discharging.

Table 4. Heat Transfer Enhancement due to Flow Rate.

Mass Flow Rate, (kg/s)	Heat Transfer Rate (W)		Thermal Enhancement Ratio (%)	
	Charging	Discharging	Charging	Discharging
0.01575 (*base*)	15.251	-14.662	0.00	0.00
0.03150	16.193	-16.260	6.17	10.90
0.15750	17.068	-18.314	11.91	24.91

C. Effect of Inlet Temperature

The inlet temperature gives more significant effect towards the average PCM liquid fraction as depicted in Fig. 13, especially during the charging process. As can be seen from Fig. 13, the heat transfer rate increases as the inlet temperature of the HTF increases and promotes faster melting processes of the PCM. Figs. 14 and 15 shows supporting evidence for this tendency that in the fifth minute of charging, the PCM is melted in the area near wall and the area of liquid PCM is larger at the higher temperature water. The similar behavior also depicted at the 20th minute of charging. Thus, with increasing of the inlet temperature of HTF, the temperature difference will also increase and will drives the heat transfer process both by conduction (in the solid state) and convection (in the liquid state) faster [8, 18] and gives higher trend of the curve gradient.

During discharging process, it shows slightly different behavior from the charging one. Fig. 13 shows the rate of the average PCM liquid fraction during discharging is almost similar or looks like there is no effect by the temperature variation. The temperature and liquid fraction distribution that shown in Figs. 16 and 17 respectively also shows almost no differences due to the inlet temperature. However, if the graphs in Fig. 13 are enlarged in Fig. 13, the curve with 320.65 K was reaching the zero liquid fraction which slightly faster than the other two which indicate that the heat transfer process for 320.65 K slightly faster than the others.

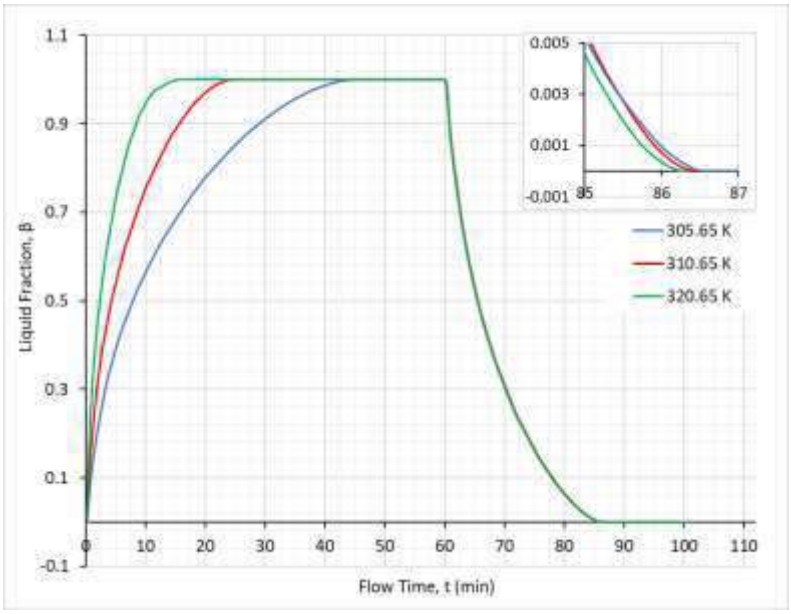

Figure 13. Average PCM Liquid Fraction during Charging and Discharging for Different Inlet Temperature.

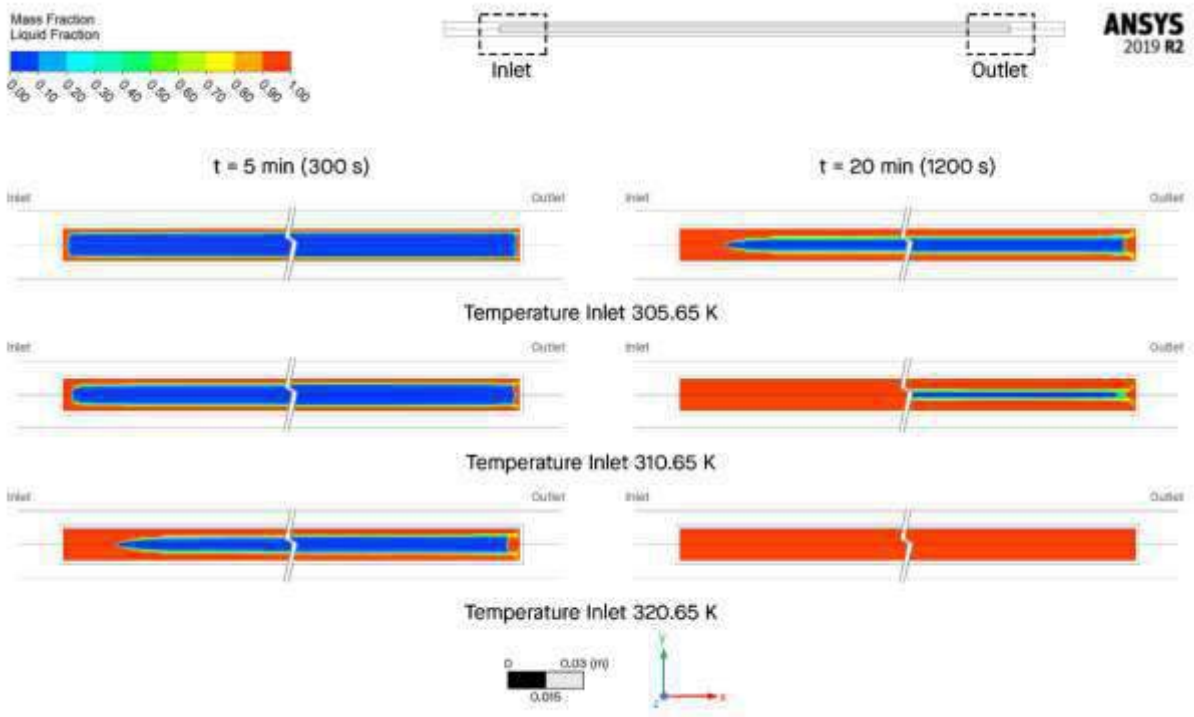

Figure 14. Comparison of Average PCM Liquid Fraction for Different Inlet Temperature at 5 mins and 20 mins (Charging).

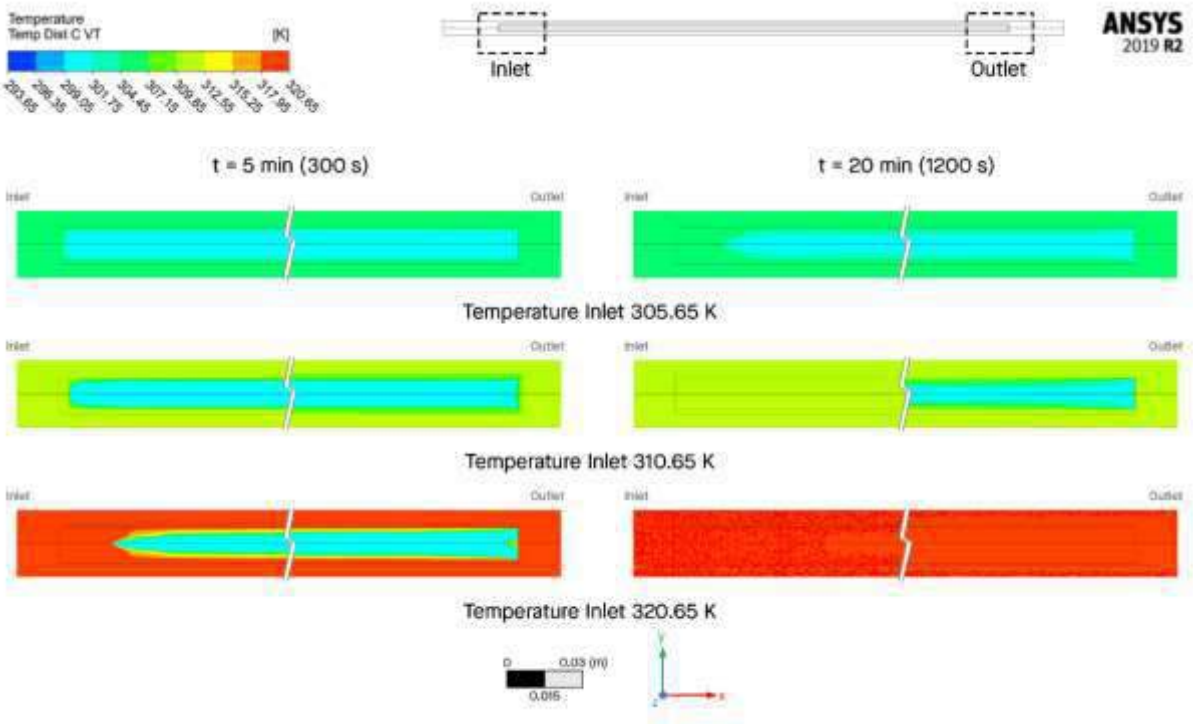

Figure 15. Comparison of Temperature Distribution for Different Inlet Temperature at 5 mins and 20 mins (Charging).

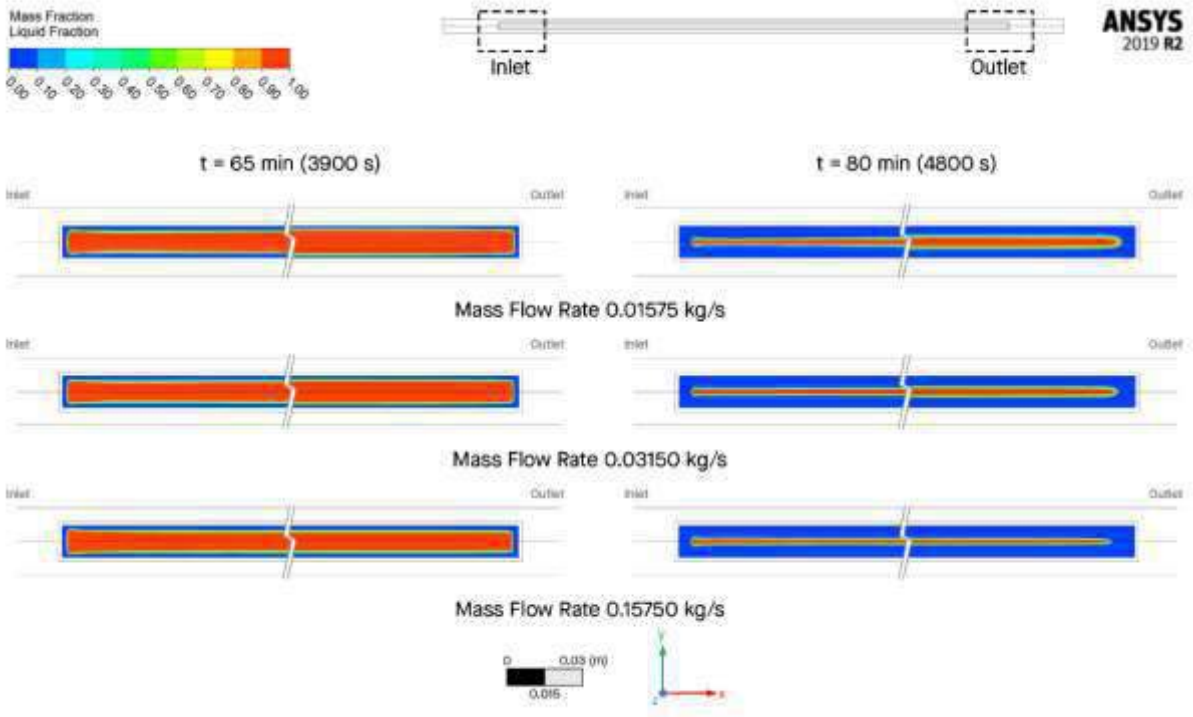

Figure 16. Comparison of Average PCM Liquid Fraction for Different Inlet Temperature at 65 mins and 80 mins (Discharging).

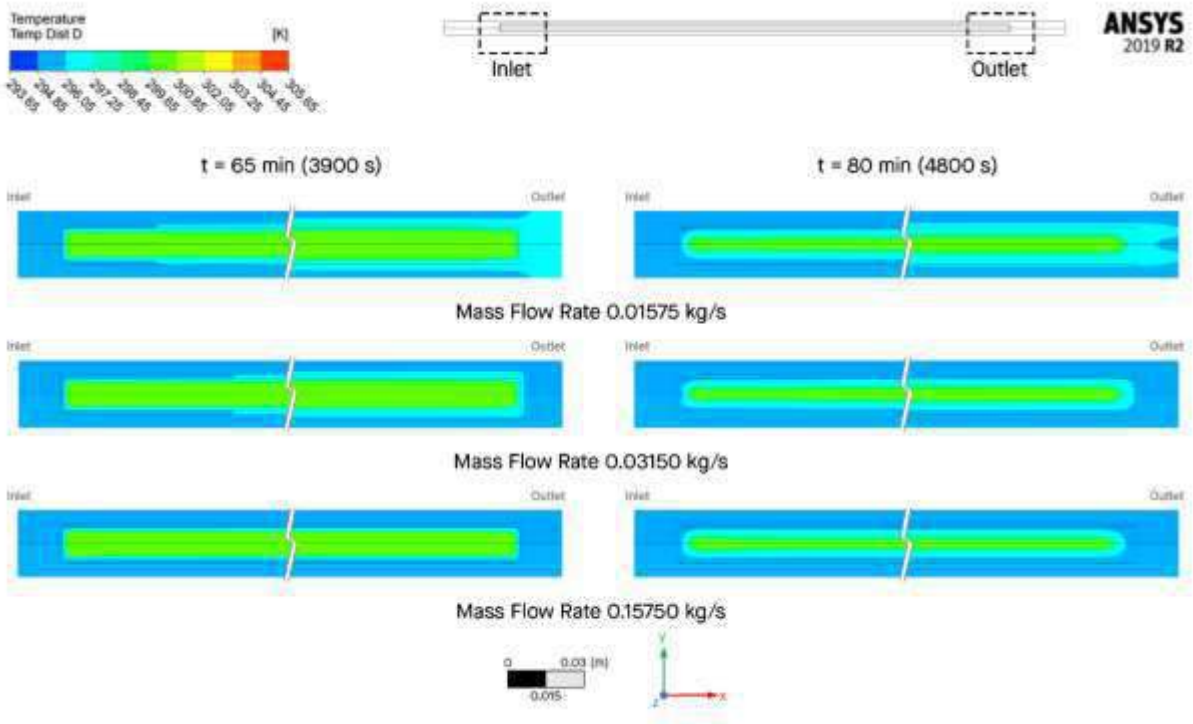

Figure 17. Comparison of Temperature Distribution for Different Inlet Temperature at 65 mins and 80 mins (Discharging).

Looking at the heat transfer performance for different inlet temperatures, as summarized in Table 5, it is found that the inlet temperature will gives relatively a higher effect on the heat transfer performance (thermal enhancement ratio, TER) especially during charging cycle. The highest temperature (adding 20 K above the melting point of PCM) will give relatively a higher heat transfer performance up to 192.72% during the charging and 13.07% during the discharging.

Table 5. Heat Transfer Enhancement due to Inlet Temperature.

Inlet Temperature (K)	Heat Transfer Rate (W)		Thermal Enhancement Ratio (%)	
	Charging	Discharging	Charging	Discharging
305.65 (*base*)	8.898	-15.573	0.00	0.00
310.65	16.193	-16.260	81.98	4.41
320.65	26.047	-17.609	192.72	13.07

5. Conclusions

Based on this numerical simulation, the behavior of flow rate and inlet temperature on annulus type LHTES with *n*-octadecane as PCM could give significant effect in the heat transfer performance, both during charging and discharging process.

- Maximizing the flow rate could give more turbulence effect on LHTES system so it could speed up the heat transfer process. In this research, increasing the flow rate 10 times will give 11.91% and 24.91% efficiency during charging and discharging respectively.
- Rising the inlet temperature will give more significant temperature difference and drives the heat transfer process. By setting the temperature 10 K above melting point of PCM could give the efficiency of heat transfer up to 192.72% during charging and 13.07% during discharging.
- Based on the characteristics above, preferred thermal performance could be designed by carefully at first evaluate the operating condition of the inlet temperature and then followed by the flow rate.
- This research also imply that the annulus-type could be applied on Low-Temperature LHTES system.

References

[1] A. Ter-Gazarian, "Energy Storage for Power Systems," *The Institution of Engineering and Technology*, 2011.
[2] C. Strinati and R. Ferroukhi, Renewable Energy and Climate Pledges: Five Years After the Paris Agreement, Abu Dhabi: International Renewable Energy Agency, 2020.
[3] D. Siswanto, Outlook Energi Indonesia 2019, Jakarta: Sekretariat Jenderal Dewan Energi Nasional, 2019.
[4] Solargis, Solar Resource and Photovoltaic Potential of Indonesia, Washington DC: The World Bank, 2017.
[5] J. C. Kurnia, A. P. Sasmito, J. S. V. and A. S. Mujumdar, "Improved Design for Heat Transfer Performance of a Novel Phase Change Material (PCM) Thermal Energy Storage (TES)," Applied Thermal Energy, pp. 896-907, 2013.
[6] A. Crespo, C. Barreneche, M. Ibarra and W. Platzer, "Latent Thermal Energy Storage for Solar Process Heat Appliacations at Medium-High Temperature - A Review," Solar Energy, pp. 1-32, 2018.
[7] L. Scapino, H. A. Zondag, J. V. Bael, J. Diriken and C. C. Rindt, "Sorption Heat Storage for Long-term Low-temperature Applications: A Review on The Advancements at Material and Prototype Scale," Applied Energy, pp. 920-948, 2017.
[8] M. Lacroix, "Numerical Simulation of a Shell-and-Tube Latent Heat Thermal Energy Storage Unit," Solar Energy, pp. 357-367, 1993.
[9] J. C. Kurnia and A. P. Sasmito, "Numerical Investigastion of Heat Transfer Performance of Rotating Latent Heat Thermal Energy Storage," Applied Energy, pp. 1-13, 2017.
[10] D. Li, Y. Hu, D. Li and J. Wang, "Combined-Cycle Gas Turbine Power Plant Integration with Cascaded Latent Heat Thermal Storage for Fast Dynamic Responses," Energy Conversion and Management, pp. 1-13, 2019.
[11] F. Yuan, M.-J. Li, Z. Ma, B. Jin and Z. Liu, "Experimental Study on Thermal Performance of High-Temperature Molten Salt Cascaded Latent Heat Thermal Energy Storage System," International Journal of Heat and Mass Transfer, pp. 997-1011, 2018.
[12] T. Istanto and W. E. Juwana, "Pengujian Karakteristik Perpindahan Panas dan Faktor Gesekan pada Penukar Kalor Pipa Kosentrik dengan Sisipan Pita Terpilin Berlubang," Mekanika, pp. 7-14, 2011.
[13] A. Shukla, D. Buddhi and R. Sawhney, "Solar Water Heaters with Phase Change Material Thermal Energy Storage: A Review," Renewable and Suistanable Energy Reviews, no. 13, pp. 2119-2125, 2009.
[14] S. P. Jesumathy, M. Udayakumar and S. Suresh, "Heat Transfer Characteristics in Latent Heat Storage System Using Paraffin Wax," Journal of Mechanical Science and Technology, no. 3, pp. 959-965, 2012.
[15] P. J. S. Siagian, Desain Thermal Energy Storage Tipe Shell-and-Tube pada Thermal Heat Energy Storage dengan Material Parafin Wax RT-55 sebagai Phase Change Material, Yogyakarta: Universitas Gadjah Mada, 2019.
[16] "PubChem Compound Summary for CID 11635, Octadecane," 2020. [Online]. Available: https://pubchem.ncbi.nlm.nih.gov/compound/Octadecane. [Accessed 1 August 2020].
[17] R. Winterton, "Fusion Reactors," in Thermal Design of Nuclear Reactors, Oxford, Pergamon, 1981, pp. 163-172.
[18] T. L. Bergman, A. S. Lavine, F. P. Icropera and D. P. Dewit, Fundamentals of Heat and Mass Transfer, Jefferson City: John Wiley & Sons, 2011.

Biographies of Authors

Rifki Yusup, S.T. is currently an engineer at one of oil and gas company and has graduated his bachelor's degree from Department of Mechanical Engineering, Universitas Pertamina, Jakarta, Indonesia in 2020.

Byan Wahyu Riyandwita, S.T., M.Eng., Ph.D. is currently a lecturer who focus on thermal-fluid modeling at Departement of Mechanical Engineering, Universitas Pertamina, Jakarta, Indonesia and has finished his doctoral degree program from Gyeongsang National University in 2011.

Vol. 1, No. 1, August 2022, pp. 55-62
p-ISSN: 2963-8577
DOI: 10.57102/jescee.v1i1.6

ANALYSIS INVENTORY OF CONSUMABLE GOODS USING MIN-MAX METHOD AT UNIVERSITAS PERTAMINA

Nurma Irfan Romadhon[1], Iwan Sukarno[2*], Mirna Lusiani[3]
[1,2,3]Department of Logistics Engineering, Faculty of Industrial Engineering, Universitas Pertamina

Abstract
Inventory control is one of the problems faced by Universitas Pertamina. In the management of inventory, especially office Stationery Stock, Universitas Pertamina does not determine the limited value of inventory that must be stored. There are 138 type of office stationery items managed by Universitas Pertamina. Thus, this causes asset management difficult to determine the ordering quantity for each item and how many items should be stored in the warehouse. As a result, the overall cost of Office Stationery at Universitas Pertamina and shown to increase almost 50% every year. The Therefore, it is necessary to analyze the inventory policies that used by Universitas Pertamina. The purpose of this study is to recommend policies related to the value of safety stock, minimum stock, and maximum stock for each consumable item. In addition, a comparison of inventory cost between the existing policy and Proposed policy is carried out. The method used is the Min-Max Stock method. In addition, the ABC classification method is also used to classify items based on the level of usage. The results of this study show from 138 items of office stationery, 19% are A class, 30% are B class and 51% are C class. The classification can be used to prioritize the number of ordered and reduce the overall inventory. Based on the calculation results, it is found that ordering cost whit existing method is Rp.100,898,604 and with Proposed method is Rp. 71,595,499 and form this result by using the min-max method, Universitas Pertamina can save up to 30% of inventory costs compared to the current policy.

Keywords:
Inventory control; min-max method; ABC classification, consumable goods; office stationery

Article History:
Received: July 31st, 2022
Revised: August 7th, 2022
Accepted: August 25th, 2022
Published: August 31st, 2022

Corresponding Author:
Iwan Sukarno
Department of Logistics Engineering, Universitas Pertamina, Indonesia
Email: iwansukarno@universitaspertamina.ac.id

1. Introduction

Facilities and infrastructure are one of the most influential factors in the quality of education, which has a contribution of 40.38% [1]. Facilities and infrastructure are defined as requirements that are used in the process of teaching and learning activities, both moving and immobile so that educational goals can run smoothly, regularly, effectively, and efficiently [2]. According to Matin and Fuad (2018), facilities and infrastructure are divided into several types of groups including books, tools, furniture, buildings, and land [3].

As an educational institution, Universitas Pertamina has several facilities and infrastructure to support its students. Some of the facilities include a library, classrooms, laboratory, indoor field, swimming pool, auditorium room, etc. In addition, Universitas Pertamina also provides consumable goods used to lecture activities and administration processes such as Office Stationery (ATK). Management control of goods in teaching and learning activities must be carried out optimally, where the amount must be adjusted to the level of user needs but also do not make large purchases because they require storage [4]. Fig.1 is the overall cost of Office Stationery at Universitas Pertamina and shown to increase every year due to an increase of student, educational activities, and laboratories.

One of the methods that is widely used in the inventory control process is the min-max method. Min-Max is the method of controlling inventory by determining the minimum and maximum amount of inventory that can be stored, and the safety stock. In other studies, this method is able to save inventory costs for each period [5], this method is also able to produce a smaller value than the company's final inventory [6]. Therefore, this paper aims to calculate the value of safety stock, minimum stock, and maximum stock for each stationery item.

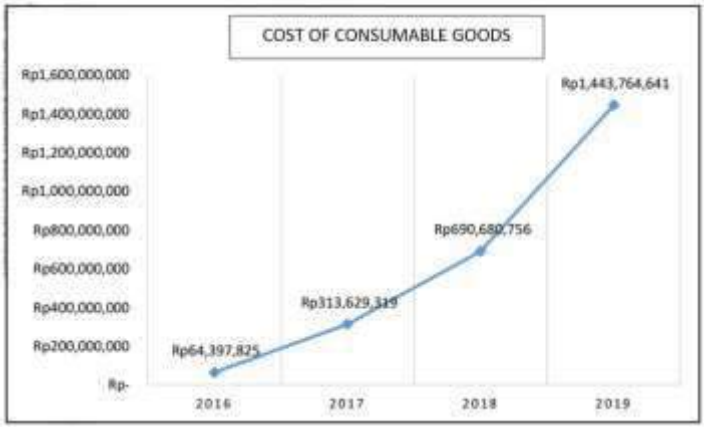

Figure 1. Cost of Office Stationery

2. Methods

In this study, the ABC analysis methods was used to classify the office stationery into 3 groups, Group A, B and C. ABC Analysis is a methods of inventory control based on the pareto principles [7]. ABC analysis method, the small portion of items represent the high value or amount of the total inventory. Technically, Class A is 15-20% of the total goods, but represents 75–80% of the total value. Class B is 20-25% of the total number of items but represents 10-15% of the total value and Class C is 60–65% of the total goods but represents 5–10% of the total value [7-11]. Determination of the class of goods is carried out based on the ordering frequency that occur from 2017 to 2019.

The Min-Max Stock method is a method of controlling inventory by determining the minimum and maximum stock values that must be stored, as well as the value of safety stock. The stages and calculation formulas are as follows [5]:

1. Determine the safety stock (ss)

   Safety Stock is a security stock to prevent the inventory from running out [4, 8]. The following is an equation used to calculate the value of safety stock:

$$ss = (Maximum\ Usage - T) \times \frac{C}{period\ of\ time} \quad (1)$$

   Where:
   T = Average usage of goods per period
   C = Lead time per period
   SS = Safety Stock

2. Determine the minimum stock

   The following is an equation used in calculating the value of minimum stock:

$$Minimum\ stock = \frac{(T \times C)}{Period\ of\ time} + SS \quad (2)$$

3. Determine the maximum stock

   The following is an equation used in calculating the maximum stock value:

$$Maximum\ stock = \frac{2(T \times C)}{period\ of\ time} + SS \quad (3)$$

Other stages that are also carried out in inventory control are calculation of the quantity or number of orders of goods (Q) to replenishment of supplies [11]. Reorder or order quantity is the order quantity for each period, as follows is the calculation formula [12].

$$Ordering\ Quantity\ (Q) = \frac{2\ x\ T\ x\ C}{period\ of\ time} \quad (4)$$

3. Results and Discussions

A. Stock Classification

This process is carried out by classifying the stock of Office Stationery to ABC class based on the number of ordering frequencies from 2017 to 2019. From inventory data, there are 138 type of stock that included in the Office Stationery. The example stock of Office Stationery was showed in Table 1 below.

Table 1. Demand Data During the 2017 - 2019 Period (Sample data)

No	Items	Atribute	2017		2018		2019		Total
			Even	Odd	Even	Odd	Even	Odd	
1	Amplop Coklat Custom	Pack	0	0	2200	0	4,003	2,500	8703
2	Amplop Putih PaperLine/ 110x230	Box	8	1	23	7	83	10	132
3	Amplop Universitas	pcs	0	2700	1350	0	1,520	1,507	7077
4	Bantex Box File 4011/ 100mm	pcs	67	221	530	243	721	351	2133
5	Bantex ordner	pcs	111	138	177	1156	1,006	284	2872
6	Bantex Pocket Transparant/ A4	pcs	520	440	5100	21519	677	125	28381
7	Bantex Pocket Transparant/ A4	pcs	640	100	780	1900	723	149	4292
8	Binder Clip No.105/ 15mm	Pack	69	52	41	85	5	42	294
9	Binder Clip No.107/ 19mm	Pack	64	98	56	70	534	231	1053
10	Binder Clip No.111/ 25mm	Pack	83	86	76	22	465	184	916
11	Binder Clip No.155/ 32mm	Pack	41	66	78	131	112	51	479
12	Binder Clip No.200/ 41mm	Pack	15	29	48	18	453	74	637
13	Binder Clip No.260/ 51mm	Pack	9	7	53	75	411	67	622
14	Buku Hard Cover	pcs	0	2	28	17	17	2	66
. .	. .	. .	. .	. .	. .	. .	. .	. .	. .
134	Tipe-X Liquid	pcs	73	24	75	53	287	132	644
135	Tisu Kering	Box	8	5	0	4	30	-	47
136	Trigonal Clip No.1	Pack	90	94	125	242	724	240	1515
137	Trigonal Clip No.5	Pack	28	2	9	5	202	85	331
138	Zipper Bag/ A5	Pcs	105	0	9	128	70	48	360

By using data from Table 1, the percentage of goods usage was calculated to determine the ABC classification based on the ordering frequency as shown in Table 2 below.

Table 2. ABC Classification of Office Stationery Stock

No	Items	Atribute	Total Usage (2017-2019)	% Usage	% Commulative	ABC Class
1	Bantex Pocket Transparat	pcs	28381	22.628%	22.628%	A
2	Amplop Coklat Custom	Pack	8703	6.939%	29.567%	A
3	clear sleeve Map/ A4	Pack	7735	6.167%	35.734%	A
4	Map Coklat perperekat	Pcs	7179	5.724%	41.458%	A
5	Amplop Universitas	Pcs	7067	5.635%	47.093%	A
. .	. .	. .	. .	. .	. .	. .
24	Kertas Sinar Dunia 70gr	Rim	930	0.741%	78.410%	A
25	Binder Clip No. 111/25mm	Pack	916	0.730%	79.140%	A
26	Pena Standard	Pcs	900	0.718%	79.858%	A
27	Pena Pilot	Pcs	796	0.635%	80.493%	B
28	Penghapus white board	Pcs	683	0.545%	81.038%	B
29	Double Tap 1/2"x72	Roll	679	0.541%	81.579%	B
. .	. .	. .	. .	. .	. .	. .
66	Isi Spidol Snowman Board Marker	pcs	255	0.20%	94.55%	B
67	Spidol WB Marker ABG-12	pcs	234	0.19%	94.73%	B
68	Clear Sleeve Map/ A4	Pack	212	0.17%	94.90%	B
69	Spidol WB Marker ABG-12	pcs	212	0.17%	95.07%	C
70	Lem Stick/ 8gr	pcs	193	0.15%	95.22%	C
. .	. .	. .	. .	. .	. .	. .
134	Stapler Heavy Duty	Pcs	16	0.013%	99.95%	C
135	Buku Name Card Holder/ A5	Pcs	14	0.011%	99.97%	C
136	Map Diamond / Biola / Stop Map	Pack	14	0.011%	99.98%	C
137	Spidol Gambar Snowman PW-12A	Set	14	0.011%	99.99%	C
138	Map Diamond / Biola / Stop Map	Pack	13	0.010%	100%	C

Based on stock data, there are 138 types of items stored as Office Stationery. Fig. 2 below shows the percentage of ABC stock classification.

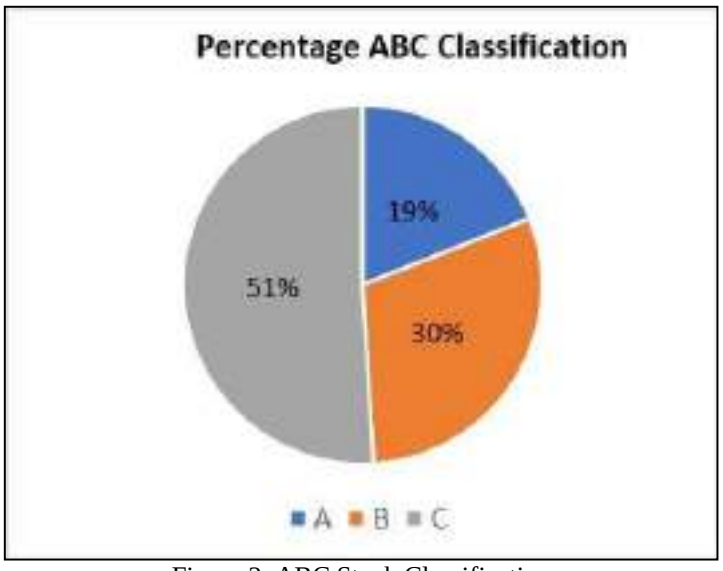

Figure 2. ABC Stock Classification

B. Safety Stock Calculation

Using formulation (2), the safety stock was calculated for each item. Therefore, average consumption, maximum usage, and lead time were counted in these steps.

Table 3. Example of Average, Maximum and Lead Time Calculation

No	Items	Avarage usage (units)	Maximum Usage (units)	Lead Time (month)
1	Bantex Pocket Transparan (A4)	4,731	21,519	0.1667
2	Amplop Coklat Custom	1,451	4,003	0.1667
3	Clear Sleeve Mal (A4)	1,290	2,848	0.1667
4	Map Coklat Berperekat	1,197	3,600	0.1667
5	Amplop Universitas	1,178	2,700	0.1667
6	Clear Sleeve Mal (F4)	878	2,624	0.1667
7	Kertas PaperOne (A4-80gr)	774	1,636	0.1667
8	Bantex Pocket Transparan (F4)	716	1,900	0.1667
9	Bantex Ordner 1465V01 (70mm)	479	1,156	0.1667
10	Kertas PaperOne (A4-70gr)	397	1,352	0.1667

The data from Table 3 was used to find safety stock value for each consumable good.

Table 4. Example of Safety Stock Calculation

No	Items	Attribute	Unit Type	Safety Stock
1	Bantex Pocket Transparan (A4)	Bening	Pcs	2799
2	Amplop Coklat Custom	Coklat	Pack	426
3	Clear Sleeve Map (A4)	Bening	Pack	7
4	Map Coklat Berperekat	Coklat	Pcs	401
5	Amplop Universitas	Coklat	Pcs	254
6	Clear Sleeve Map (F4)	Bening	Pack	292
7	Kertas PaperOne (A4-80gr)	Putih/A4	Rim	144
8	Bantex Pocket Transparan (F4)	Bening	Pcs	198
9	Bantex Ordner 1465V01 (70mm)	Biru	Pcs	113
10	Kertas PaperOne (A4-70gr)	Putih/F4	Rim	4

C. Min-Max Calculation

The Min-Max calculation stock method showed in Table 5 below. Min. Stock is used as a point where a reorder must be made to maintain stock at the warehouse, while Max. Stock is used to show the maximum amount of inventory that can be stored in the warehouse [5]. In addition, Min. Stock usually called as the Reorder Poin.

Table 5. Example Min-Max Calculation

No	Items	Safety Stock	Min. Stock	Max.Stock
1	Bantex Pocket Transparan (A4)	2799	3,588	4377
2	Amplop Coklat Custom	426	668	910
3	Clear Sleeve Map (A4)	7	476	691
4	Map Coklat Berperekat	401	601	801
5	Amplop Universitas	254	451	647
6	Clear Sleeve Map (F4)	292	439	585
7	Kertas PaperOne (A4-80gr)	144	274	403
8	Bantex Pocket Transparan (F4)	198	318	437
9	Bantex Ordner 1465V01 (70mm)	113	193	273
10	Kertas PaperOne (A4-70gr)	4	227	293

Based on Table 5, each type of item has a different value, this is because the needs for each item are different. Where at each period the number of requests for ATK goods varies depending on the needs of each user.

D. Inventory Cost Analysis

Inventory control activities will be related to ordering policies. This ordering activity is carried out to replenish stock that are close to the reorder point, this case is between the points of safety stock to minimum stock. But there is also some method of carrying out an ordering policy when the amount of inventory is approaching the minimum inventory limit. Determining the ordering policy using Equation (4) and carried out for each group. This activity will make it easier for Pertamina University in the determination process number of future orders.

Figure 3. Ordering Cost

Order quantity costs are costs incurred to carry out ordering ATK goods. The calculation of the cost is based on the price of each item of goods. This cost calculation does not consider costs of ordering or costs incurred to place an order for stationery goods. Based on the graph in Fig. 3 for the replenishment of inventory, the costs incurred for Class A are Rp. 71,595,499, while class B and C are Rp. 23,011,786 and Rp. 6,291,319. In addition, with the method of ABC class, order quantity costs can be more efficient. Table 6 showed an ordering cost comparison between the existing condition and Min-Max with the ABC class method.

Table 6. Ordering Cost Comparison

Ordering Cost Existing Condition	Ordering Cost using Min-Max with ABC Classification
Rp100,898,604	Rp71,595,499

From Table 6, can be concluded by Min-Max Method with the ABC classification, the cost of the order quantity is decreasing by 30% compared to the existing policy.

4. Conclusion

The conclusions of this study are as follows:

1. Inventory management carried out by Universitas Pertamina does not apply ABC Classification, so the items being managed will increase in number. From the inventory side, there are no stored stationery items, so it has the potential to delay the fulfillment of consumable items. So, the asset manager has had difficulties in tracking goods, this is due to the large number of items that must be handled.

2. The result of implementing the min-max policy with the ABC classification method, not all items will be stored in the warehouse, so it will streamline the cost of storing consumable items. With this classification process, the focus of managing goods will be more efficient because the number of goods will be less but have a greater value. From calculation results, it is shown that using Min-Max Method, the cost of the order quantity is decreasing by 30% compared to the existing policy.

References

[1]. Miski, R. The effect of Facilities and Infrastructure on Student Learning Outcome (Pengaruh Sarana dan Prasarana Terhadap Hasil Belajar Siswa). Jurnal Tadbir Muwahid, Vol.4, No.2, Hal. 17 – 21, 2015.
[2]. Lestari, N. D., & Yusmino, B. A. Analysis of the use of Facilities and Infrastructure to Support Student Learning Activities at University of PGRI Palembang (Analisis Penggunaan Sarana dan Prasarana Untuk Menunjang Kegiatan Belajar Mahasiswa Di Universitas PGRI Palembang Tahun Akademik 2016/2017). Jurnal Management, Kepemimpinan, dan Supervisi Pendidikan *(JMKSP)*, Vol. 3, No. 1, Hal. 41 – 51, 2018.
[3]. Matin, & Fuad, N. Management of Educational Facilities (Manajemen Sarana Prasarana Pendidikan). Jakarta: PT Raja Grafindo Persada, 2016
[4]. Kinanthi, A. P., Herlina, D., & Mahardika, F. A. Inventory Control Analysis of Raw Material using Min-Max (Analisis Pengendalian Persediaan Bahan Baku Menggunakan Metode Min - Max (Studi Kasus PT. Djitoe Indonesia Tobacco)). *Performa*, Vol. 15, No. 2, Hal. 87-92, 2016.
[5]. Sylvia, M. Inventory Control Using Min-Max Method at PT. Semen Tonasa (Pengendalian Persediaan Bahan Baku Menggunakan Metode Min - Max Stock pada PT Semen Tonasa di Pangkep). Makasar: Fakultas Ekonomi dan Bisnis, Universitas Hasanuddin, 2013.
[6]. Chatisa, I., Muslim, I., & Sari, R. P. Implementation of ABC Clasification Method at Warehouse Management System PT. Cakrawala Tunggal Sejahtera (Implementasi Metode Klasifikasi ABC pada Warehouse Management System PT. Cakrawala Tunggal Sejahtera). *JNTETI*, Vol. 8, No.2, Hal. 123 – 134, 2019.
[7]. A.C. Rădăşanu. Inventory Management, Service Level and Safety Stock. J Public Adm. 2016.
[8]. M.Rusănescu. Abc Analysis, Model for Classifying Inventory. HIDRAULICA.2014
[9]. D. Dhoka and Y.L Choudary. ABC Classification for Inventory Optimization. IOSR, J. Bus. Manag, 2013.
[10]. H.F. Afianti and H. H. Azwir. Inventory Control and Schedulling of Raw Material using ABC Method (Pengendalian Persediaan Dan Penjadwalan Pasokan Bahan Baku Import Dengan Metode Abc Analysis Di PT Unilever Indonesia), Cikarang, Jawa Barat. Journal IPTEK, 2017.
[11]. Yedida, C. K., & Ulkhaq, M. M. Raw Material Planning at CV. Endhigra Prima using Min-Max Method (Perencanaan Kebutuhan Persediaan Material Bahan Baku Pada CV Endhigra Prima dengan Metode Min-Max). Industrial Engineering Online Journal, Vol.6, No.1, 2017.
[12]. Redi, A. P., & Herdianti, I. K. Inventory Control of LPG Tube using Min-Max Analysis (Pengendalian Persediaan Tabung LPG dengan Menggunakan Metode Min - Max Analysis (Studi Kasus: Toko Retail di PT. XYZ)). Institut Supply Chain dan Logistik Indonesia, Hal. 107 – 129, 2020.

Biographies of Authors

Nurma Irfani Romadhon is a student of the Logistics Engineering Department at University of Pertamina. The author was born in Tegal on January 22, 1996. Before becoming a student, the author had completed his studies at SMA Negeri 24 Jakarta. During his time as a student, the author was active in several activities of the committee and campus organization, including being the PSDM Staff at the Logistics Engineering Student Association (HIMALOG UP) and being the coordinator of the Logistics Engineering Student Regeneration activities

Dr. Eng Iwan Sukarno graduated with a Bachelor's degree in Industrial Engineering at Andalas University Padang, a Master's Degree in Engineering, and a Doctor of Engineering at Toyohashi University of Technology, Japan. He has also taken the Certified Logistics Improvement Professionals (CLIP) Program Certificate and the Warehouse & Distribution Supervisor Competency Test Certificate from the National Professional Certification Agency (BNSP) related to Warehousing, Inventory, and Packaging. Before continuing his Master and Doctoral studies in Japan, he was involved in the Warehouse and Inventory Improvement Project at PT. Semen Padang, and PT. Semen Tonasa From 2005 to 2011. Currently focusing on areas of expertise and research related to Warehouse and Inventory Improvement, Energy Modeling, Halal Logistics, and System Dynamics. The results of these various studies have been presented at various seminars at home and abroad and published in Proceedings and Journals, both National and International.

Mirna Lusiani, ST, MT graduated with a Bachelor's degree in Industrial Engineering at the University of Indonesia in 2004. She obtained a Master's degree in Industrial Engineering from the University of Indonesia in 2011. Currently, she has obtained Lecturer Certification in 2014 and obtained Basic Level Mitigation Certification in the field of Procurement. She began to pursue the teaching profession and obtained a lecturer academic position in 2012 and since 2019 has joined Pertamina University as a permanent lecturer in the Logistics Engineering Study Program.

Vol. 1, No. 1, August 2022, pp. 63-74
p-ISSN: 2963-8577
DOI: 10.57102/jescee.v1i1.15

OVER CURRENT RELAY COORDINATION SYSTEM CONSIDERING DISTRIBUTED GENERATION

Teguh Aryo Nugroho[1], Muhammad Abdillah[1*], Helmi Fauzan[1], Nita Indriani Pertiwi[1], Herlambang Setiadi[2,3] Awan Uji Krismanto[4]

[1]Department of Electrical Engineering, Universitas Pertamina, Indonesia
[2]Faculty of Advanced Technology and Multidiscipline, Universitas Airlangga, Indonesia
[3]Institute for Systems and Computer Engineering Technology and Science (INESC-TEC), Portugal
[4]Department of Electrical Engineering, Institut Teknologi Nasional, Malang, Indonesia

Abstract
Today, electricity is one of the important components to drive the industrial process and other daily human activities. While the continuity of power supply through the power system grid is impressionable from disturbances such as a short circuit. In addition, the rapid development of distributed generation (DG) technology triggers the industry to use DG technology to maintain power quality and support for industrial processes. This paper proposed the coordination of over current relay (OCR) considering distributed generation (DG) to provide an extraordinary protection system in an electrical system network. The relay is coordinated with the other relay equipment to enhance the system more reliable, secure, and stable. To examine the efficacy of the proposed approach, the radial distribution system model is utilized in this paper where the DG is installed in bus 6. To compute the protection coordination index (PCI) and coordination time interval (CTI), the DG capacity is varied from 100 KVA to 1000kVA. From the simulation result, it could be seen that the installed DG that allowed in bus 6 was 900kVA because the CTI value reached convergence value as of 0.294 second for higher DC capacity than 900kVA. Moreover, the higher of DG capacity was injected to electrical system, the higher of PCI values was obtained.

Keywords:
Over current relay; distributed generation; CTI; PCI

Article History:
Received: July 31st, 2022
Revised: August 7th, 2022
Accepted: August 25th, 2022
Published: August 31st, 2022

Corresponding Author:
Muhammad Abdillah
Department of Electrical Engineering, Universitas Pertamina, Indonesia
Email:
m.abdillah@universitaspertamina.ac.id

1. Introduction

The growth of the industry in many countries is rapidly increasing in the last decade. So far, most of the industry is driven by generation sources using fossil fuels to supply the electricity in supporting the industrial processes. The continuity of good power supply in industry requires appropriate coordination of protection systems to avoid the electrical system from blackout events due to faults such as short circuit [1]. This fault has potential to cause severe damage to industrial equipment which can disrupt system production. To overcome this problem, a relay as an electrical safety device is utilized to protect the distribution system in the industry from a disturbance that can be localized quickly and prevented it to spread out to other areas.

Relay is a power system tool to protect the distribution system grid when the faults such as short circuit are occurred [2]. Moreover, many industries are now installing distributed generation to reduce the effect of fossil fuels on the environment and employed as backup power when there are any faults occurred. Generally, a short circuit occurring in the generator unit will increase its capacity by 6-8 times the existing generator rating. This condition will make the relay easily distinguish between normal conditions and any disturbances that occur to the distribution system due to the wide margin between loading situation and disturbance. Integration of DG to distribution system grid degrades the margin between the loaded system or under disturbance condition. The relay is difficult to distinguish between fault conditions or loading in this situation. In addition, this issue has significant impact to the power quality of electrical distribution system in industry. So far, to tackle this problem, it is required an appropriate protection system [3]. Several studies have been reported in according to the utilization of DG in electrical distribution system such as fault current limiter based [4], multi agent base protection scheme, dual setting protection scheme, voltage–current based protection [5]. Among studies mentioned above regarding to the

effect of DG to electrical distribution network, voltage–current based protection is renowned method over other approaches. In this study, radial distribution system is utilized as a test system with the main fault is occurred in generator where the current of short-circuit as of 6-8 times from current rating in normal condition.

The use of DG type such as photovoltaic (PV) in electrical distribution system trigger a thin margin between the normal rated current and fault current values. In this condition, the relay is difficult to recognize the system in normal loading or under fault conditions. When a disturbance occurs, the current flow in the electrical distribution system will increase 110% up to 150% more than in a normal condition. To overcome this issue, the coordination of the protection system relay is a must. This paper proposed the coordination of over current relay considering the effect of DG integration in the electrical distribution systems in the industry. To examine the proposed approach, the DG capacity about 100kVA to 1000kVA is employed to the electrical distribution system.

The rest of the paper is organized as follows. System modeling are explained in Section 2. Protection system coordination is described in Section 3. Simulation result and discussion are illustrated in Section 4. Conclusion is given in Section 5.

2. System Modelling

A. Distributed Generation

With the rapid growth of renewable energy technology and smart grids, distributed generation (DG) plays a key role in electrical distribution systems. DG is often utilized as supplementary power to maintain the electrical power network stable, reliable, and secure. Nowadays, DG is part of distributed energy resources (DREs) as energy storage and responsive loads [6]. The more advanced technology of renewable energy, the bigger the capacity size of DG for installation in a large-scale electrical distribution system. A brief overview of the most common DG technologies and their capacity sizes is illustrated in Table 1. DG can be applied to shave the peak load for a specific time, combined heat and power, continuous power, and emergency power.

Table 1. DG type and their capacity size

No	DG Type	Capacity Size
1	Combine cycle gas turbine	35 – 400 MW
2	Internal combustion engine	5kW – 10 MW
3	Combustion turbine	1 – 250 MW
4	Micro turbine	35 kW – 1MW
5	Fuel cell	200kW – 2MW
6	Battery storage	0.5 – 5MW
7	Small hydro	1 – 100 MW
8	Micro hydro	25kW – 1MW
9	Wind turbine	200W – 3MW
10	Photovoltaic array	20W – 100kW
11	Solar thermal	1 – 10MW
12	Biomass gasification	100kW – 20MW
13	Geothermal	5 – 100MW
14	Ocean energy	0.1 – 1MW

B. Electrical Distribution System

The electrical distribution system in this study consists of eleven generator units driven by a gas engine generator (GEG) and divided into 3 large sub-network areas. In existing normal conditions, the generator unit is utilized to supply the electrical load needs. Spinning reserve is also prepared as supplementary power if one of the generator units is interrupted from the distribution system grid to avoid load shedding [9]. The distribution system model has two voltage rating values of 0.38kV and 20kV. The distribution system with 0.38kV is utilized to supply the load with a small capacity. While the 20kV distribution system is especially employed to supply the feeder with load for high voltage. In addition, a distribution system with a high voltage of around 20kV is to maintain the reliability of its system.

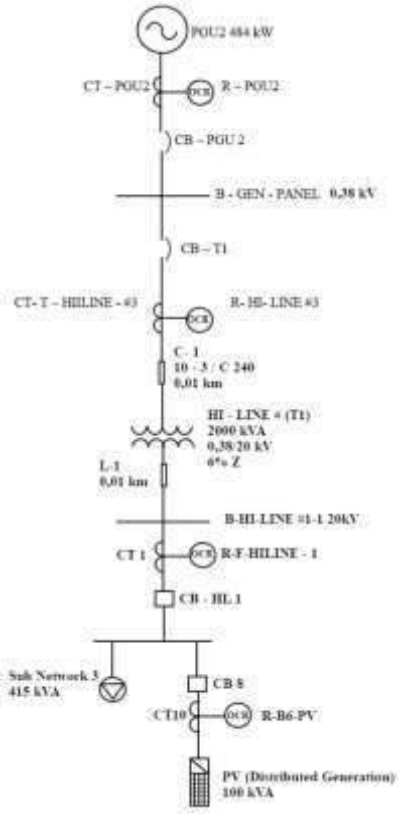

Figure 1. Proposed coordination of over-current relay (OCR)

The electrical distribution system network utilized in this study is depicted in Fig. 1. All data and distribution system models are taken from [7]. The coordinated over-current relay in this study is conducted in sub-network 3 with 484 kW of power supply PGU2 and connected through a 2000kVA of HI-LINE#(1) transformer which is located in HI-LINE #3. In this research study, over current relay R-B6-PV, over current relay R-F-HILINE-1, over current relay R-HI-LINE #3, and over current relay R-PGU2 will be coordinated to maintain the reliability of system due to integration of DG in this distribution network.

C. Over Current Relay

There are many types of relays utilized for electrical protection systems and one of important relays in industries is over current relay (OCR). OCR is a kind of relay working when there is any disturbance caused by a short circuit between phase to phase such as a three-phase or two-phase short circuit. These faults trigger an excessive current in the distribution system network.

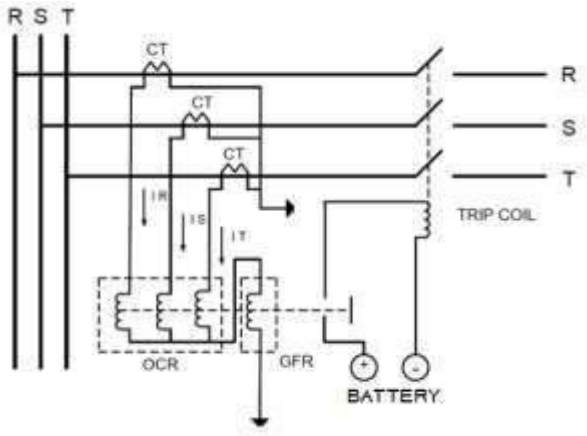

Figure 2. Over current relay (OCR) circuit installed in electrical distribution system grid

Over current relay (OCR) detects the current flow in the distribution network by working in conjunction with a current transformer (CT). The working principle of OCR is when the current transformer (CT) is reading abnormality conditions in the distribution system and the OCR will send signal to circuit breaker to disconnect a power from distribution system. when the current is over the current setting value (I_{set}). OCR only works as backup protection if there are any transformers with large capacity in the distribution line. Moreover, there are inverse time relay characteristics for OCR such as OCR with inverse time, OCR with definite time, and OCR with instantaneous time. The overcurrent relay circuit is depicted in Fig. 2.

D. OCR Setting

1. *OCR with definite time characteristic*

This OCR type is set based on its OCR's working time by neglecting the amount of current fault. It can be said that all currents through its pick-up set point will be disconnected by the pre-setting time of OCR. The OCR with definite time characteristic is shown in Fig. 3.

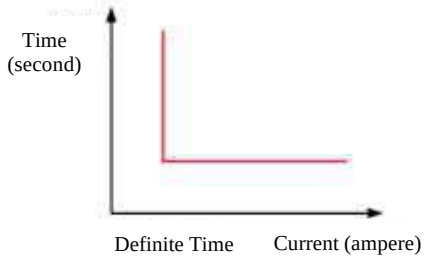

Figure 3. Over current relay (OCR) with definite time characteristic

2. *OCR with inverse time characteristic*

This OCR type works depending on its amount of current value reciprocal to time delay. The large current value through the OCR results in a fast time delay. This kind of OCR is figured out by the comparison current curve called the time current characteristic (TCC) to the IEC standard. The curve of OCR with inverse time characteristic has several types of curves including long time inverse, very inverse, short time inverse, dan extreme inverse [8]. This OCR type has two components that should be adjusted including the setting of pick-up current and the setting of time dial. In the setting of pick-up current, the OCR will select the larger current than the maximum load current during system operation. The pick-up current value is determined by the number of tap values as defined in (1).

$$Tap = \frac{I_{set}}{NCT} \tag{1}$$

where I_{set} is a pick-up current in ampere. The determination of pick-up current is based on the British BS-142 standard where it lies on intervals $1.05\, I_{FLA} < I_{SET} < 1.4\, I_{FLA}$. In addition, I_{FLA} is maximum equipment current.

While a time dial is utilized to determine the operating time of OCR where the determination of time dial for each curve of inverse time characteristic is computed by (2). Coefficient of inverse time dial is shown in Table 2.

$$td = \frac{k * T}{\beta * \left[\frac{I}{I_{set}}\right]^{\propto} - 1} \tag{2}$$

where, *td* is operating time (second), *T* is time dial, *I* is current (ampere), I_{set} is pick-up current (ampere), *k* is the 1-th inverse coefficient, α is the 2-nd inverse coefficient, and β is the 3-rd inverse coefficient.

Table 2. Coefficient of inverse time dial

Curve type	Coefficient		
	k	α	β
Standard inverse	0.14	0.02	2.970
Very inverse	13.50	1.00	1.500
Extremely inverse	80.00	2.00	0.808

3. *OCR with an instantaneous time characteristic*

This OCR type has a basis of operation without time delay, but it can work with a fast time. The coordination scheme of this OCR type for medium distribution system level is called instantaneous setting. This OCR type works based on the setting of the short circuit current, and the circuit breaker (CB) will be opened very fast around 80 ms. This OCR type is illustrated in Fig. 4.

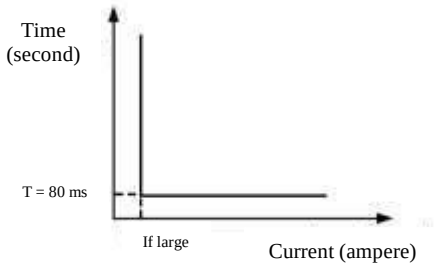

Figure 4. Over current relay (OCR) with instantaneous time characteristic

The OCR with an instantaneous time characteristic will work if there is a current flowing higher than a pre-setting pick-up current. The setting of pick-up current is determined by a minimum short circuit current such as two-phase fault. The setting of short circuit current is defined in (3).

$$I_{set} \leq 0{,}8\, I_{sc\,min} \tag{3}$$

The aims of coordination relay based on current, and time are to result in time delay for the over-current relay as an electrical distribution system. Moreover, to avoid the primary relay and backup relay working at the same time, it is required a time delay for a backup relay. The interval time for relay working time or grading time is set to 0.2 - 0,3 seconds.

3. Proposed Protection System Coordination

The procedures to coordinate the over-current relay in an electrical distribution network considering the distributed generation are described as follows [10]:

1) Collect the electrical distribution system data including generator, distribution line, transformer, and load.
2) Collect the appropriate DG capacity data for installation in the electrical distribution system.
3) Collect the data of OCR.
4) Design the electrical distribution system using ETAP 12.6.
5) Run a power flow program to obtain the voltage, active and reactive power, current, and power factor of the electrical distribution system.
6) Conduct a short circuit (SC) simulation to obtain the minimum value of SC current and SC fault current in each phase. Furthermore, the simulation of the star protection device is also carried out to determine the relay parameters along with the coordination system that has been modeled.
7) Calculate the coordination time interval value (CTI).
8) Compute the protection coordination index (PIC) value to determine the effect of DG.
9) There are two conditions that should be checked after obtaining all relay parameters in the simulation process as follow:
    a. Yes, if the simulation results show that the coordination of OCR matches the standard of IEEE 242.
    b. No, if the simulation results provide that the coordination of OCR doesn't fulfill the standard of IEEE 242. In this condition, the OCR parameters should be re-setting.
10) Print out the simulation results.

4. Simulation Result and Discussion

A. Time Current Curve (TCC) Curve Analysis

To simplify and easily read the plotting curve of time current curve (TCC) from the simulation results, the coordination strategy of OCR is divided into three stages. At stage 1, the coordination of OCR is conducted between the R-PGU2 relay and R-HI-LINE #1 relay. The current time curve of the OCR coordination is shown in Fig. 5.

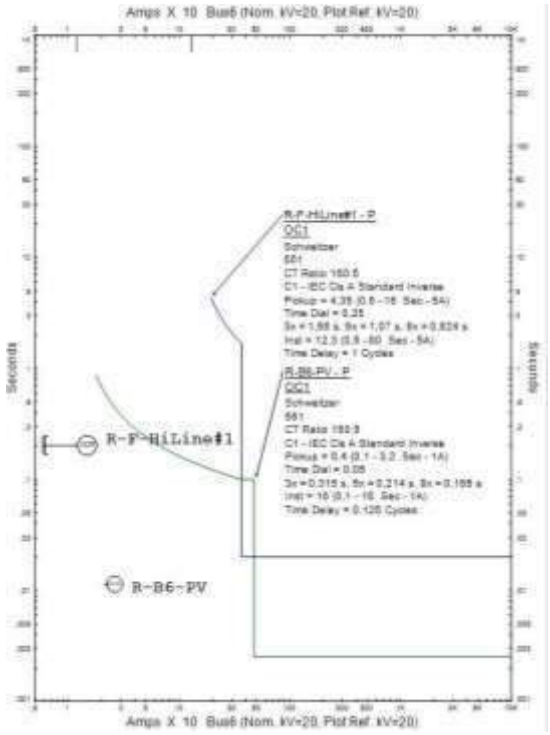

Figure 5. Plotting curve of OCR coordination at step 1

From TCC plotting curve as shown in Fig. 5, if there is a minimum short-circuit fault in the load (Bus 6), the R-F-HILINE #1 relay will react to protect the system where the instant value of its relay works at the same time with the inverse of the R-B6-PV relay. This condition is prohibited according to the cascade method and protection system standard. More than one OCR can't work at the same time because it will cause losses and the safe zone get the effect where it should be disconnected and didn't get the power flow.

At stage 2, R-F-HILINE#1 relay and R-HILINE #3 relay are coordinated, and the results are shown in Fig. 6.

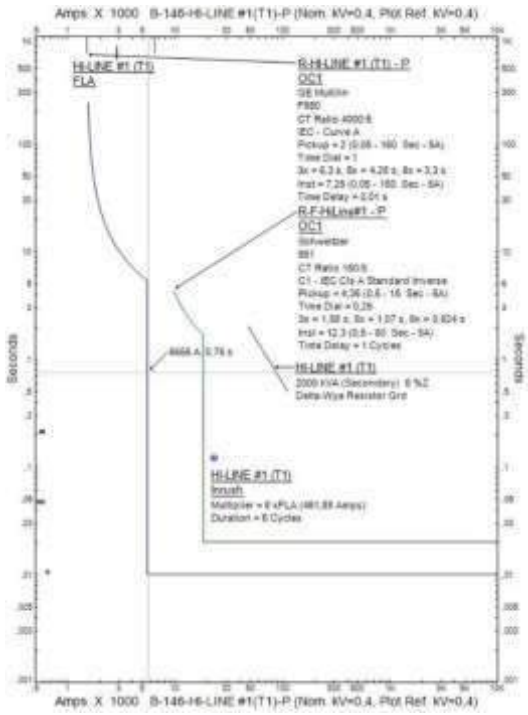

Figure 6. Plotting curve of OCR coordination at stage 2

It could be seen from Fig. 6 that if there is any short circuit current occurred at HI-LINE #1(T1) transformer at 5,655 kA, R-HILINE#3 relay will respond fastly as 0.75 seconds. If the R-F-HILINE#3 relay failed to respond to the faulted, R-F-HILINE #1 will work. TCC is on above the R-HILINE #3 relay and leads to the R-F-HILINE #1 relay. This condition is prohibited because it violates the arrangement of relay time working and may it should be conducted in the layered scheme.

At stage 3, R-HILINE #3 relay and R-PGU2 relay are coordinated. The results are illustrated in Fig. 7.

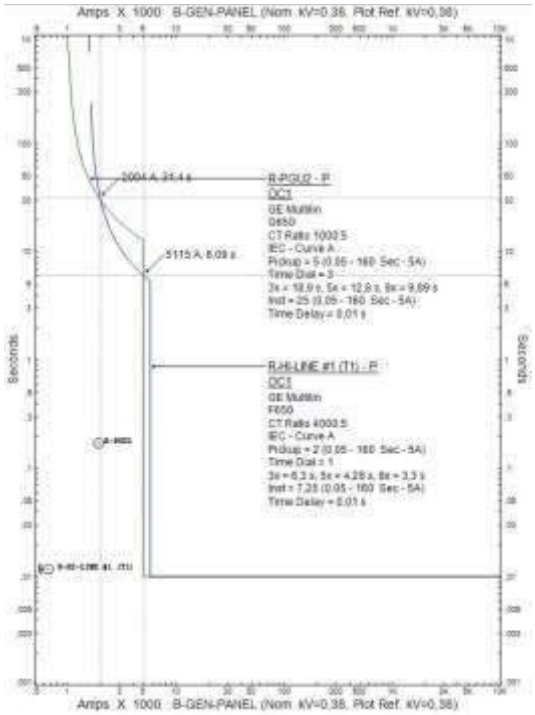

Figure 7. Plotting curve of OCR coordination at stage 3

Figure 8. Plotting curve of re-setting OCR coordination at stage 1

It could be seen from Fig. 7 that if there is a short circuit current of 2.004 kA, the R-HILINE#3 relay works with the R-PGU2 relay at the same time, this condition is prohibited because it violates the rules of the relay working time sequence.

It could be concluded that over current relay should be re-setting to obtain a good coordination relay. The computation of this condition is using ETAP software. TCC curve which are result in re-setting of OCR relay is defined in Figs. 9-10 for stage 1 to 3.

By re-setting of R-B6-PV relay and R-F-HILINE#1 relay values, the TCC curve is obtained as shown in Fig. 8. The OCR has worked in multi-stage and sequence. The grading time for the time delay between the primary relay and backup relay has complied with IEEE 242 standards as 0.2 s to 0.4 s. In the OCR relay for stage 1, the primary relay grading time with a backup relay is 0.2 s.

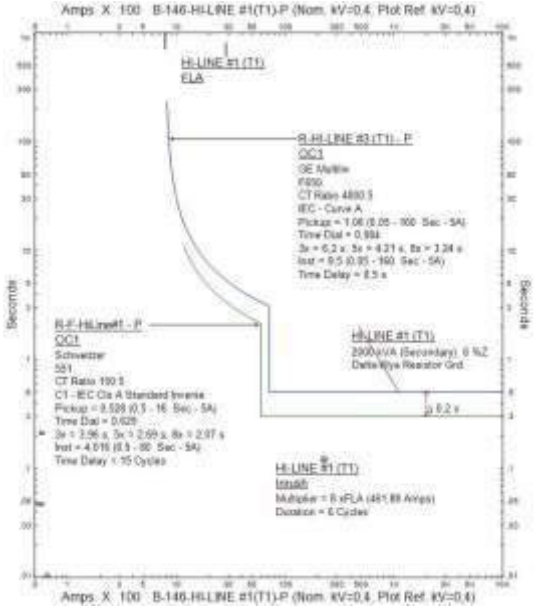

Figure 9. Plotting curve of re-setting OCR coordination at stage 2

At stage 2, after resetting the OCR as shown in Fig. 9, if there are faults at the transformer, the R-F-HILINE#1 relay will work first and the R-HILINE#3 relay will work as a backup relay when R-F-HILINE#1 relay fails to work. The time interval between primary and backup relays has matched the standards used by IEEE 242 as of 0.2s.

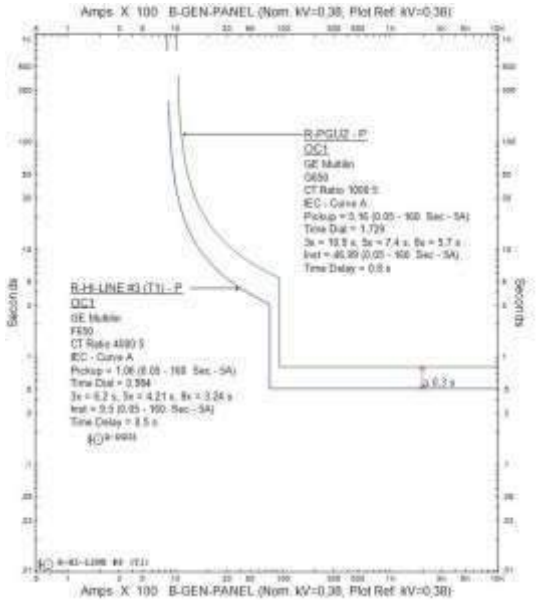

Figure 10. Plotting curve of re-setting OCR coordination at stage 3

At stage 3, after re-setting the OCR as shown in Fig. 10, if there are any faults occurred, R-HILINE#3 relay works firstly and R-PGU2 relay will work as a backup relay when R-F-HILINE#3 relay fails to work. The time interval between primary and backup relays has matched the standards used by IEEE 242 as of 0.3s.

B. Determination of DG Locations

The placement of DG in this study refers to the protection coordination index (PCI) value obtained by comparing the DG power to be added to the system with the total coordination time interval (CTI) value. The greater PCI value is obtained, the smaller possible changes to the protection system. The type of installed DG in this study is photovoltaic with100 kVA. To examine the effect of DG on the protection system short circuit test conducted and DG capacity is increased from 100 kVA to 1000 kVA. This condition is conducted to determine the PCI value. The data of the short-circuit current at the bus with injected DG power is depicted in Table 2. The CTI value can be seen in Fig. 11.

Table 3. Minimum short circuit current at Bus 6

DG Capacity (kVA)	Isc Min Bus6 (A)
100	654
200	660
300	668
400	673
500	678
600	683
700	687
800	692
900	695
1000	700

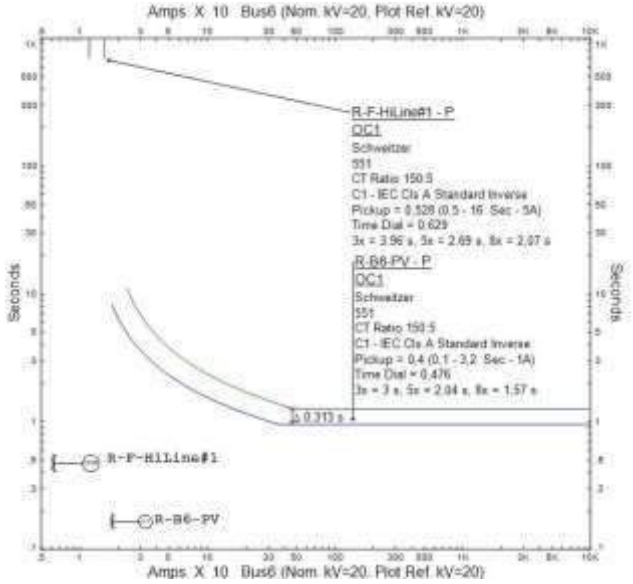

Figure 11. Plotting curve of CTI value

CTI value is illustrated in Table 3. The greater DG capacity is obtained, the smaller CTI value is achieved. It could be seen from Table 3 that the CTI value converges to 0.294 s after DG injected to the system with 900kVA. The maximum DG capacity is allowed to be injected to the electrical distribution system as 900KVA. The PCI value is depicted in Table 4.

Table 4. CTI Value at Bus 6

DG Capacity (kVA)	CTI (Second)
100	0.327
200	0.321
300	0.317
400	0.313
500	0.309
600	0.305
700	0.301
800	0.297
900	0.294
1000	0.294

Table 5. PCI Value at Bus 6

DG Capacity (kVA)	PCI
100	0.30581
200	0.62305
300	0.94637
400	1.27795
500	1.29449
600	1.96721
700	2.32558
800	2.69360
900	3.06122
1000	3.40136

A sequence of OCR operations for the electrical distribution system before and after installed DG could be seen in Tables 5-6.

Table 6. Sequence of OCR Operations at Bus 6 without DG

Time (ms)	ID	Condition
10	R-HILINE#3	Phase – OCI – 50
70	CBT1	Tripped by R-HILINE#3 Phase – OCI – 50
80	CBPGU2	Phase
817	R-F-HILINE#1	Phase – OCI – 50
917	CB-HL1	Tripped by R-F-HILINE#1 Phase – OCI – 50
1227	CBT1	Phase
31201	RPGU2	Phase – OCI – 50
31231	CBPGU2	Tripped by RPGU2 Phase – OCI – 50

Table 7. Sequence of OCR Operations at Bus 6 with DG

Time (ms)	ID	Condition
100	R-B6-PV	Phase – OCI – 50
200	CB8	Tripped by R-B6-PV Phase – OCI – 50
300	R-F-HILINE#1	Phase – OCI – 50
400	CB-HL1	Tripped by R-F-HILINE#1 Phase – OCI – 50
500	R-HILINE#3	Phase – OCI – 50
560	CBT1	Tripped by R-HILINE#3 Phase – OCI – 50
1227	CBT1	Phase
18877	RPGU2	Phase – OCI – 50
18907	CBPGU2	Tripped by RPGU2 Phase – OCI – 50

It could be seen from Tables 5-6 that there are differences in the working order of the OCR relay. In the existing system model, there is an error in the sequence of OCR working time. After adding the DG, it causes the OCR working time to be degraded.

5. Conclusions

This paper has investigated the effect of DG on protection systems in the electrical distribution systems. There are many errors related to relay working order and violate the standard of the protection system. It is complex to determine the locations of DG to match the protection system standard. Resetting of OCR causes getting slower OCR operating time, but standard grading time and CTI already meet standard. DG injection at distribution system caused resetting protection systems component for almost 50% based on this study. For Future research needs more parameter such as voltage drop, loadability and stability system.

References

[1] PLN, P. (2013). Pedoman dan Petunjuk Sistem Proteksi Transmisi dan Gardu Induk JawaBali. Jakarta; PT PLN (Persero) Penyaluran dan Pusat Pengatur Beban Jawa Bali

[2] Champa S, Vyas S R, *Protection of Industrial System Using Over Current Relay Co-Ordination*-Review International Journal of Advanced Research in Electrical, Electronics and Instrumentation Engineering, 2017; 6(2); 923 – 931

[3] Pepermans, G., Driesen, J., Haeseldonck, D., Belmans, R. & D'haeseleer, W. (2005) 'Distributed generation: definition, benefits and issues', *Energy Policy*, 3(6), pp., 787–798.

[4] Enriquez, A. C., Martinez, E. V., & Altuve-Ferrer, H. J. (2013). A Time Overcurrent Adaptive Relay. International Journal of Electrical Power & Energy Systems, 25(10)., 841–847.

[5] Saleh, K. A., Zeineldin, H. H., Al-Hinai, A., & El-Saadany, E. F. (2015). Optimal Coordination of Directional Overcurrent Relays Using a New Time–Current–Voltage Characteristic. IEEE Transactions on Power Delivery, 30(2)., 537–544

[6] Lazar, Irwin, "*Electrical System Analysis and Design for Industrial Plant*", McGraw-Hill Inc., USA., Ch. 1, 1980

[7] Wahyudi, "*Diktat Kuliah Pengaman Sistem Tenaga Listrik*", Teknik Elektro, ITS, Surbaya, Bab 2, 2004

[8] IEEE std 242-2002, "*IEEE Recommended Practice for Protection and Cordination of Industrial and Commercial Power System"*The institute of Electrical and Electronic Engineering, Inc, New York, Ch 15, 2002.

[9] Juergen Schlabbach, "Power System Engineering: Planning, Design, and Operation of Power Systems and Equipment"Willey, 2008.

[10] J.Sahebkar Farjhani et.al, "Coordination of Directional Overcurrent Protection Relay for Distribution Network With Embedded DG".IEEE.2019 5th Conference on Knowledge Based Engineering and Innovation (KBEI), 2019.

Biographies of Authors

Teguh Aryo Nugroho was born in Surabaya, Indonesia, on 1991. He received his B.Eng, and M.T. degrees in Electrical Engineering from Institut Teknologi Sepuluh Nopember Surabaya, in 2013 and 2015. His research focuses on electrical material insulation and high voltage engineenring. Currently, he is working as lecturer at Electrical Engineering Department, Universitas Pertamina, Jakatrta

Muhammad Abdillah was born in Pasuruan. He received Sarjana Teknik (equivalent to B.Eng.), and Magister Teknik (equivalent to M.Eng.) degrees from Department of Electrical Engineering, Institut Teknologi Sepuluh Nopember (ITS), Surabaya, Indonesia in 2009 and 2013, respectively. He obtained Dr. Eng. degree from Graduate School of Engineering, Hiroshima University, Japan in 2017. He is currently working as lecturer at Department of Electrical Engineering, Universitas Pertamina, Jakarta, Indonesia. As author and coauthor, he had published 70 scientific papers in different journals and conferences. He was a member of IEEJ, IAENG and IEEE. His research interests are power system operation and control, power system optimization, robust power system security, power system stability, intelligent control and system, and artificial intelligences (optimization,
machine learning, deep learning)

Helmi Fauzan was born in jakarta, he received Sarjana Teknik from Departement of Electrcal Engineering, Universitas Pertamina in 2022. Currently he is graduate student at Electrical Engineering Universitas Pertamina. His research interest in Power System Protection.

Nita Indriani Pertiwi holds a Sarjana Teknik (equivalent to B.Eng) in 2013 and Magister Teknik (equivalent to M.Eng) in 2015 from Department of Electrical Engineering, Institut Teknologi Sepuluh Nopember (ITS). She is currently an Academician at Department of Electrical Engineering, Universitas Pertamina, Jakarta, Indonesia. Her research is mainly focused on Power System Operation,
Electrical Machines, and Renewable Energy

Herlambang Setiadi was born in Sidoarjo, on November 29, 1990. He received a bachelor degree from Sepuluh Nopember Institute of Technology (Surabaya, Indonesia) majors in Power System Engineering in 2014. Then, master degree from Liverpool John Moores University (Liverpool, United Kingdom), majors in Electrical Power and Control Engineering in 2015. Furthermore, he received a Doctoral degree from The University of Queensland, majors in Electrical Engineering in 2019. Currently, He is a lecturer at School of Advanced Technology and Multidisciplinary, Universitas Airlangga. His research interest includes small signal stability in power systems, renewable energy integration

Awan Uji Krismanto was born in Malang, Indonesia. He completed his B.Sc. and M.Sc. in Electrical Engineering from Brawijaya University and Sepuluh Nopember Institute of Technology (ITS), Indonesia in 2004 and 2010 respectively, and the Ph.D. degree in electrical engineering from The University of Queensland, Brisbane, Australia, in 2018. Currently, He is a faculty member in the Department of Electrical Engineering National Institute of Technology (ITN) Malang, Indonesia from 2005. His research interests include microgrid, smart grid, power system stability, distributed generation, power electronic and power quality.

Vol. 1, No. 1, August 2022, pp. 75-83
p-ISSN: 2963-8577
DOI: 10.57102/jescee.v1i1.8

TEMPERATURE CONTROL USING PI CONTROLLER

Muhammad Zidane Wahyudi[1], Dhika Wahyu Pratama[1], Ansya Fitrian[1], Muhammad Abdillah[1*]
Herlambang Setiadi[2]
[1]Department of Electrical Engineering, Faculty of Industrial Engineering, Universitas Pertamina
[2]Department of Engineering, Faculty of Advanced Technology and Multidiscipline, Universitas Airlangga

Abstract
Indonesia is a large archipelago with a tropical climate consisting of dry and wet seasons. Indonesia has had high rainfall and temperature over the year because this country lies on the equator lines. Moreover, severe global warming occurs because of the depletion of the ozone which affects the inclement weather, air, and temperature over the years. Therefore, special equipment is required to obtain appropriate thermal conditions by controlling the temperature. This paper proposed the PI controller to maintain the temperature in their nominal values and its temperature stability is analyzed using pole placement. In this study, the system model is 1st order, called first order plus dead time (FOPDT). Pole placement is utilized to improve the output signal to obtain the gain of the PI controller. The gain of the PI controller obtained is K_p as of 0.36095 and K_i is as of 0.00072231. The percentages of overshoot and steady-state error are 29.98% and 1.5% for the Ziegler Nichols method while 1.28% and 0.26% for the PI Tuner, respectively. PI controller is robust for this system where the pole's position is on the left side of the real axis and has small values of overshoot and steady-state error.

Keywords:
Temperature; PI; Pole Placement stability; Tools; Thermal Conditions.

Article History:
Received: July 31st, 2022
Revised: August 7th, 2022
Accepted: August 25th, 2022
Published: August 31st, 2022

Corresponding Author:
Muhammad Abdillah
Department of Electrical Engineering, Universitas Pertamina, Indonesia
Email:
m.abdillah@universitaspertamina.ac.id

1. Introduction

The increase in global temperature makes people need additional tools to get suitable thermal conditions [1]. With the increase of global temperature, the controlling temperature is needed which aims to design a system and control the temperature according to the desired temperature using a 1st order system which has been widely used in system settings [2]. This is due to the temperature control having transient response characteristics of 1st order, these characteristics consist of time constant (τ), rise time (τr), settling time (t_s), and delay time (t_d). The difference between 1st order and 2nd order is that the response of 2nd order doesn't have a time constant [3].

In addition, a PI controller with pole placement stability analysis is employed to stabilize the system model. PI controller has characteristics such as reducing rise time, increasing overshoot, descending time, and eliminating steady-state error. If the system already gives a good response to increase or reach the desired signal using only the PI controller, there is no need to add a derivative (D) controller. So, the PI controller is simpler and only has K_p gain and K_i gain values. The steady state error can't be eliminated if the K_p gain is greater than the K_i gain [4]. The use of pole placement analysis on temperature control is to observe the stability of the output response system [5].

Ziegler-Nichols method is one example of a traditional method to determine gain for the system. However, the result of this method was made the overshoot high and made the tunning result bad. To increase the performance and make less overshoot from the system, PI tunning using PI-Tuner can help to determine the gain with auto computing and this method will help to get the optimum result.

The output for this paper is comparing the resulting temperature controlling using PI between tunning gain with the Ziegler-Nichols method and PI-Tuner. The result was expected to see the effectiveness and stability from the system with these two methods.

2. Modelling

A. Temperature Modeling using First Order Plus Dead Time (FOPDT)

This experiment utilized a first-order system to determine the transfer function of system model. The mathematical model of system in this study is represented by (1).

$$\frac{T(s)}{U(s)} = \frac{K}{\tau s + 1} e^{-tds} \quad (1)$$

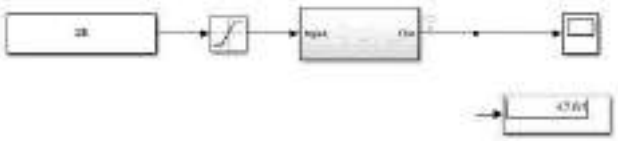

Figure 1. Block diagram of FOPDT

K is a gain value, τ is time delay, and *td* is time constant [4]. The block diagram for determining the parameter of the transfer function can be seen in Fig. 1. The method for finding the gain K can be obtained by (2).

$$K = \frac{T_{SS} - T_0}{\Delta u} \quad (2)$$

Meanwhile, to find τ, it is necessary to know the temperature value at T_τ which is obtained using (3).

$$T_\tau = \frac{63.2}{100}(T_{SS} - T_0) + T_0 \quad (3)$$

Thus, a temperature T_τ is obtained when temperature point is determined through curve model. Then, time at the current point T_τ can be determined. The predetermined time based on the temperature T_τ is τ value.

3. Method

MATLAB/Simulink is used as the main supporting software in modeling this temperature in regulation system. There are several methods used to adjust the temperature namely duty ratio and determining the gain. Then, this model is implemented directly using hardware in Arduino and used to develop a temperature control tool.

A. *Temperature Checking*

The adjustment of the modeling temperature is conducted by checking the real temperature surrounds, one example is the real temperature in the room. The real temperature is checked using DHT11 on Arduino UNO. So, the ambient temperature can reach as of 31.40° where it can be seen in Fig. 2.

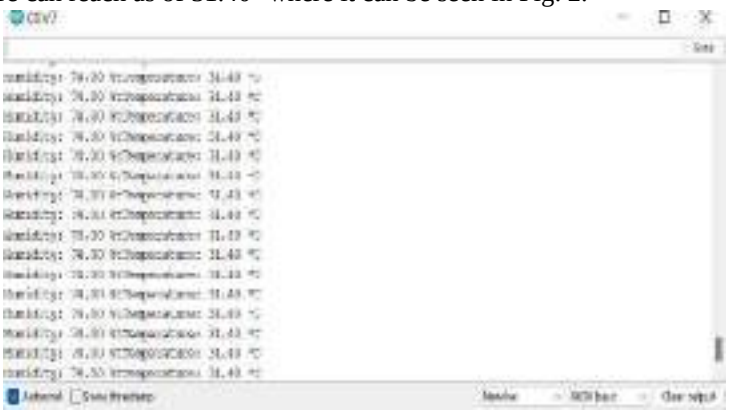

Figure 2. Temperature checking with DHT11

B. LM35 Calibration

In this temperature modeling, the sensor for temperature control is LM35. The real room temperature obtained previously is used to obtain the gain value which will be used for temperature conversion. The software circuit and the Simulink block diagram circuit of the LM35 calibration are shown in Fig. 3.

Figure 3. *Software* circuit LM35

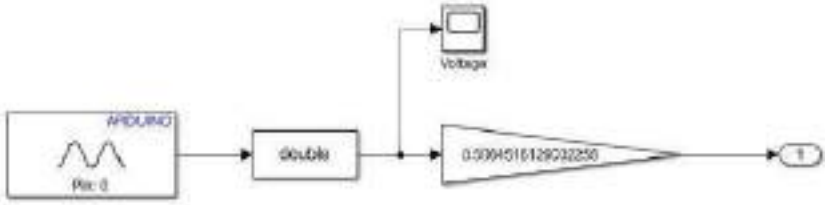

Figure 4 Block diagram of LM35

From Fig. 4, the voltage obtained when calibrating LM35 is 62mV as shown in Fig. 5

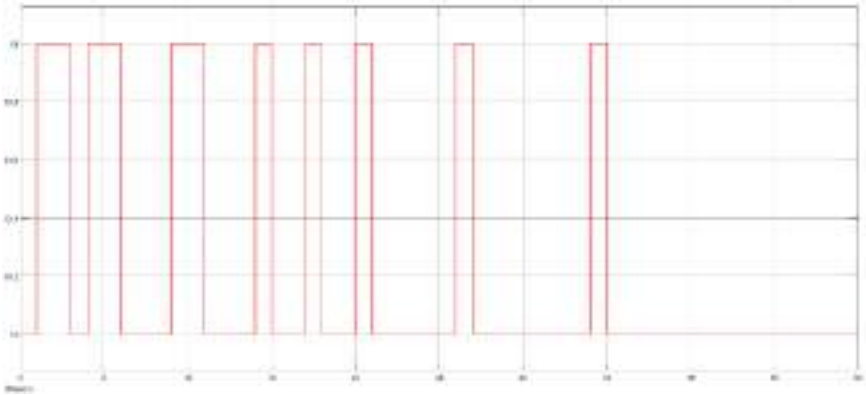

Figure 5. Output voltage of LM35

So, based on Fig. 5, the results of gain calibration are obtained by (4).

$$K_{LM35} = \frac{Real\ Temperature}{Calibrate\ Voltage} \quad (4)$$

$$K_{LM35} = \frac{31.40}{62mV}$$

$$K_{LM35} = 0.506\ ℃/mV$$

C. Duty Ratio

The use of duty ratio is carried out as a measure of the maximum temperature released by the power resistor as measured by the LM35 sensor. The temperature measurement is done by designing a block diagram on Simulink as shown Fig. 6.

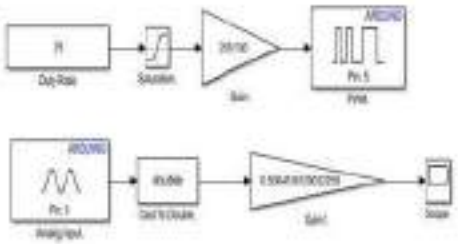

Figure 6. Block diagram using duty ratio in MATLAB/Simulink

The saturation given in the block diagram above is the highest voltage value from the power supply. In this design, the power supply has a maximum voltage of 12 V DC.

D. Gain Determination

D.1. Ziegler-Nichols

Ziegler-Nichols method is the conventional method to get the gain. The K_P and the K_I will get from the calculation which needs some information. The time constant (τ) and delay time (td) was needed to get the calculation of K_p and K_I. The K_I value can get from the calculation between K_P and T_I.

D.2. PI Tuner

In determining the PI gain values, the method used is PI tuner. This method simplifies modeling with K_p and K_I values that have been automatically calculated by the computer. This PI tuner is also used to refine the results obtained in real-time testing. The following is an adjustment of the gain settings using the PI tuner to obtain a fast rise time but less overshoot.

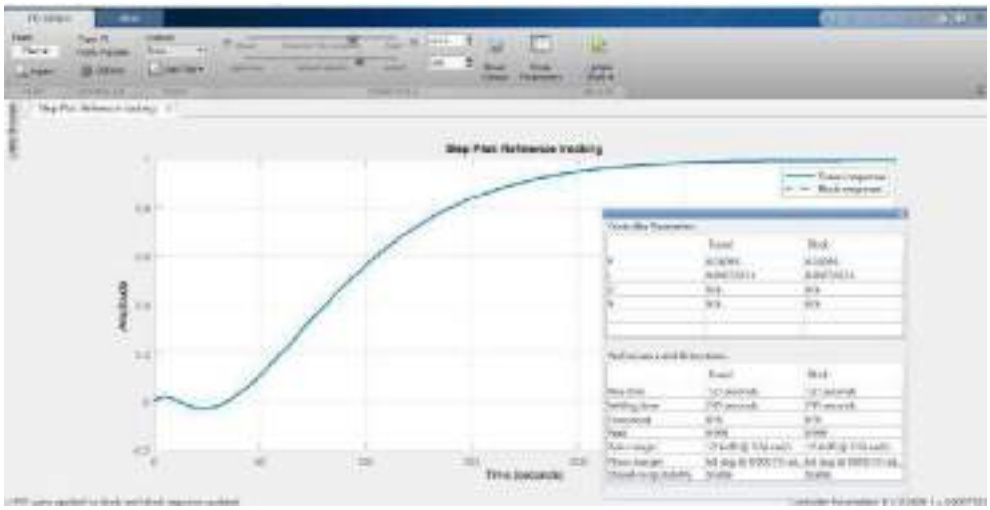

Figure 7. PI tuner gain determination

4. Results

MATLAB/SIMULINK is the environment to support this experiment and the system is using first order plus dead time (FOPDT) for temperature control. A modification was made to the system by using the PI controller in Fig 7.

A. Gain Determination

A.1. Ziegler-Nichols

In this section, a sample is taken that implements the gain from setting from Ziegler-Nichols method to temperature control to 60°C. The following is a graph of the results of temperature control for 60°C while the time constant was known using the *Kp* and K_I that has been determined by calculation in (5).

Table 1. ZN Method Gain

Control	K_P	Ti
PI	$= 0.9\frac{T}{L}$ $= 0.9\frac{481}{40}$ $= 10.8225$	$= \frac{L}{0.3}$ $= \frac{40}{0.3}$ $= 133.33$

Then the K_I can get from the calculation between K_P and T_i.

$$K_I = \frac{K_p}{K_i} \quad (5)$$
$$K_I = 0{,}08117$$

The following is a graph of the results of temperature control for 60°C using the K_I and K_P that has been determined is shown in Fig. 8.

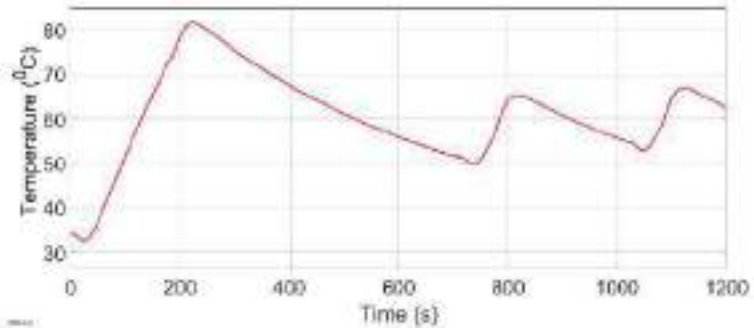

Figure 8. Temperature control using *Ziegler-Nichols* method

Based on the graph on the implementation, the peak value and the temperature value are not steady with overshoot is 81.73° C.

A.2. PI tuner

The use of the PI controller was assisted by computing automatically on SIMULINK while there is a PI tuner feature to improve the output signal and reduce the overshoot obtained from the experiment. The results of tuning using the PI tuner, the K_I value is 0.00072231 and the K_P is 0.36095. In this section, a sample is taken that implements the gain from setting via the PI tuner to reach 50°C. The following is a graph of the results of temperature control for 50°C using the K_I and K_P that has been determined.

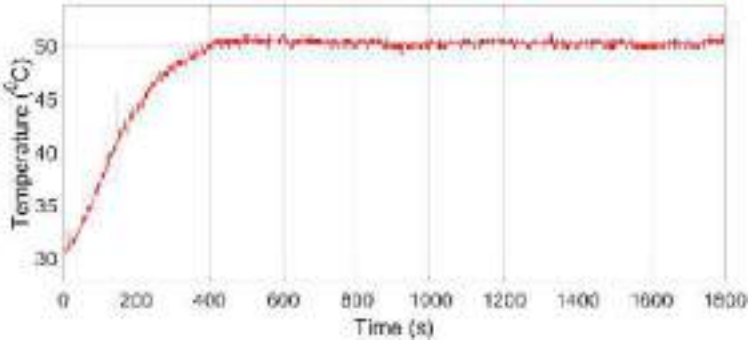

Figure 9. Temperature control

Based on the graph on the implementation, the peak value and the temperature value are not steady with overshoot is 50.64° C.

B. Comparison of Experiment and Simulation

B.1. Zigler-Nichols

The following chart is a comparison of the between simulation and experiment for temperature control of 60° Celsius.

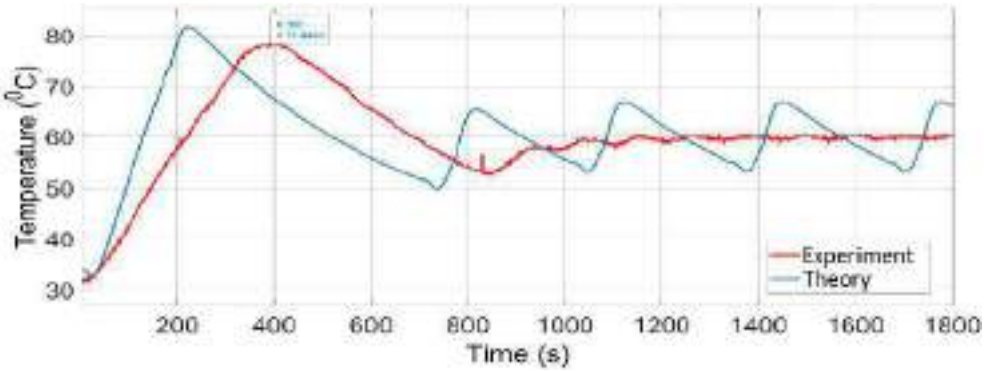

Figure 10. Comparison Graph of Experiment with Simulation

Based on the results obtained for controlling the temperature of 60° C, it is possible to find the amount of overshoot and the steady state error as follows.

$$Overshoot = \frac{Overshoot\ Temp - Reference\ Temp}{Reference\ Temp}\ x\ 100\% \quad (6)$$

$$Overshoot = \frac{77.99 - 60}{60}\ x\ 100\%$$

$$Overshoot = 29.98\ \%$$

Then the following is the calculation of the obtained SSE value

$$SSE = \frac{SSE\ Temp - Reference\ Temp}{Reference\ Temp}\ x\ 100\% \quad (7)$$

$$SSE = \frac{60.9 - 60}{60}\ x\ 100\%$$

$$SSE = 1.5\ \%$$

B.2. PI Tuner

The following chart is a comparison of the between simulation and experiment for temperature control of 50° Celcius.

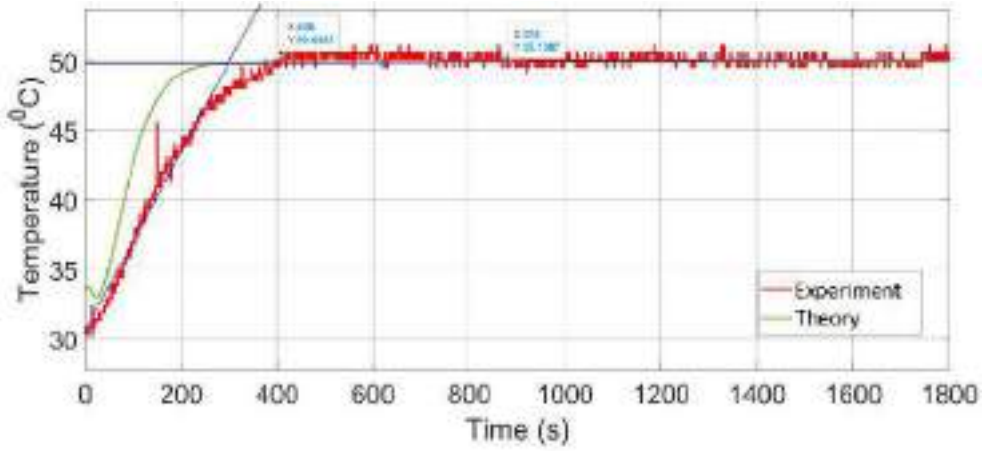

Figure 11. Comparison graph of experiment and Simulation

Based on the results obtained for controlling the temperature of 50° C, it is possible to find the amount of overshoot and also the steady state error as follows.

$$Overshoot = \frac{Overshoot\ Temp - Reference\ Temp}{Reference\ Temp}\ x\ 100\%$$
$$Overshoot = \frac{50.64 - 50}{50}\ x\ 100\%$$
$$Overshoot = 1.28\ \%$$

Then the following is the calculation of the obtained SSE value

$$SSE = \frac{SSE\ Temp - Reference\ Temp}{Reference\ Temp}\ x\ 100\%$$
$$SSE = \frac{50.13 - 50}{50}\ x\ 100\%$$
$$SSE = 0.26\ \%$$

C. Determine The Effective Method

The determining the effective method can be easily with those calculation and experiment before. The aim for this experiment is to see the less overshoot and SSE between Ziegler-Nichols method and PI tuner to determine the more effective method. If we look at the calculation and the experiment before, PI tuner more effective with less overshoot and less Steady State Error.

D. Pole Placement Stability Analysis

Based on the modelling of the design results on temperature modelling using first order plus dead time (FOPDT), the results obtained on FOPDT are as follows.

$$\frac{T(s)}{U(s)} = \frac{1.\ 57}{481s + 1}e^{-40s}$$

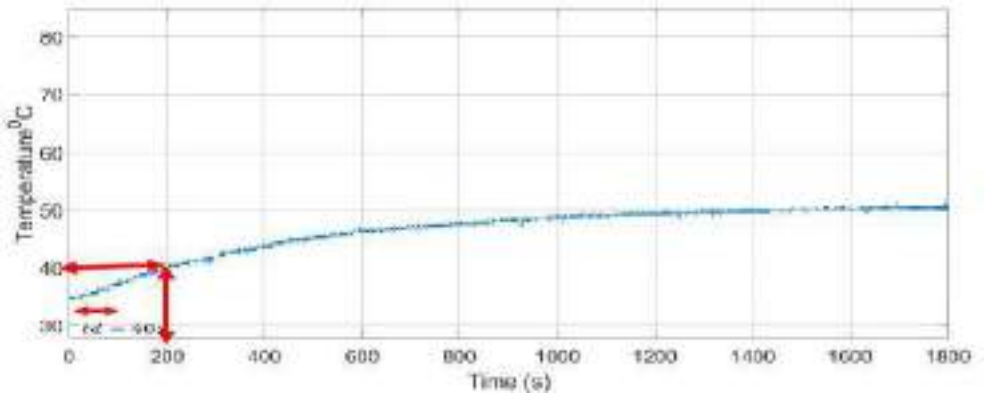

Figure 12. Calculation FOPDT

So based on the value above, it is possible to find the positions of the poles and zeros in this system. The following are the positions of the poles and zeros in this system which can be found using the following equation.

$$\frac{T(s)}{U(s)} = \frac{Zeros}{Poles}e^{-tds} \quad (10)$$

so,

- Poles

$$481s + 1 = 0$$
$$481s = -1$$
$$s = -\frac{1}{481}$$
$$s = -0.00207$$

- Zeros

None

Thus obtained the position of the poles on the real axis at the point -0.00207 and zeros that do not exist, this is due to the absence of s in the zero's equation. Therefore, the system can be said to be stable. This is based on the absence of the poles on the right side of the Cartesian diagram, and the poles on the left side of the real and imaginary axes. So there are no poles on the right side

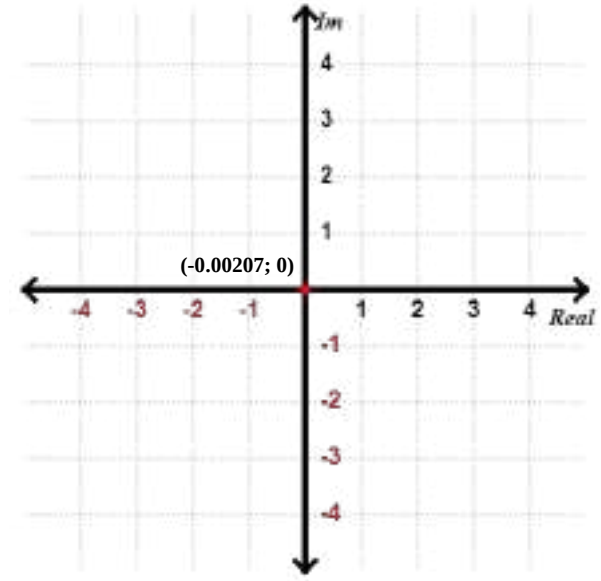

Figure 13. Cartesian Poles and Zeros Diagram

5. Conclusions

This paper focuses on the implementation of temperature control modeling using the PI controller with stability analysis by pole placement. Based on the results of the experimental and simulation figures obtained, it can be concluded that there is a difference between the experiment and the simulation. Where the difference is shown in the rise time, steady-state error, and overshoot. In the simulation the results look ideal, this is because the simulation does not care about external interference, while in the real experiment many external disturbances cause noise to appear in the resulting signal. Determining gain with PI tuner is more effective than determining gain with Ziegler Nichols method with more less overshoot and steady state error. The resulting overshoot from Ziegler-Nichols is 29.98% and the Steady State Error is 1.5 % while overshoot from PI tuner is 1.28% and the steady-state error is 0.26%. Control using a PI controller is proven stable. This can be seen from the poles position which is to the left of the real axis on the cartesian diagram and the small overshoot and steady state error value.

References

[1] D. T. W. S. M. Muhammad Nuruzzaman Alkautsar, " The Effect of Air Temperature and Room Humidity with Air Conditioning on Subjective Response and Thermal Comfort In Men," 2015. [Online]. Available: http://etd.repository.ugm.ac.id/penelitian/detail/82236. [Accessed 05 Juli 2022].

[2] F. F. Ardiansyah, " First-order system is a system in which the denominator of the transfer function has the highest rank equal to one," [Online]. Available: https://id.scribd.com/doc/312900076/Sistem-Orde-Satu-Adalah-Sistem-Dimana-Penyebut-Fungsi-Alihnya-Memiliki-Pangkat-Tertinggi-Sama-Dengan-Satu#:~:text=Sistem%20orde%20satu%20adalah%20sistem%20dimana%20penyebut,fungsi%20alihnya%20memiliki%20pangkat%20terti. [Accessed 05 Juli 2022].

[3] F. Arifin, " Time Response and Frequency Response," Faculty of Engineering, Yogyakarta State University, Yogyakarta, 2015.

[4] I. Z. T. Dewi, "PID Controller (Proportional Integral Derivative Controller)," 23 February 2020. [Online]. Available: https://imeldaazahraa.medium.com/kontrol-pid-proportional-integral-derivative-controller-c173086724af. [Accessed 3 Juli 2022].

[5] M. Dr. Fatchul Arifin, " System Stability Analysis," Faculty of Engineering, Yogyakarta State University, Yogyakarta, 2014.

[6] M. P. R.G. Kanojiya, “Tuning of PID controller using Ziegler-Nichols method for speed control of DC motor,” IEEE-International Conference on Advances in Engineering, Science and Management, ICAESM-2012. 117-122, 2012

[7] Yucelen . T, “Self-Tuning PID Controller using Ziegler-Nichols Method for Programmable Logic Controllers”. IFAC Proceedings Volumes. 39. 11-16. 10.3182/20060830-2-SF-4903.00003, 2006

[8] K. H. A. G. C. y. C. Yun Li, "PID Control System Analysis and Design," *IEEE control systems*, 2006.

[9] Patra. Ashis, “Application of Ziegler-Nichols Method For Tuning the PID Controller”. 2018

[10] M. a. C. S. a. B. P. a. V. D. Huba, "Making the PI and PID Controller Tuning Inspired by Ziegler and Nichols Precise and Reliable," *Sensors*, vol. 21, no. 10.3390/s21186157, p. 6157, 2021.

Biographies of Authors

Dhika Wahyu Pratama is a student in Department of Electrical Engineering, Universitas Pertamina, Indonesia

Ansya Fitrian is a student in Department of Electrical Engineering, Universitas Pertamina, Indonesia

Muhammad Zidane Wahyudi is a student in Department of Electrical Engineering, Universitas Pertamina, Indonesia

Muhammad Abdillah was born in Pasuruan. He received Sarjana Teknik (equivalent to B.Eng.), and Magister Teknik (equivalent to M.Eng.) degrees from Department of Electrical Engineering, Institut Teknologi Sepuluh Nopember (ITS), Surabaya, Indonesia in 2009 and 2013, respectively. He obtained Dr. Eng. degree from Graduate School of Engineering, Hiroshima University, Japan in 2017. He is currently working as lecturer at Department of Electrical Engineering, Universitas Pertamina, Jakarta, Indonesia. As author and coauthor, he had published 70 scientific papers in different journals and conferences. He was a member of IEEJ, IAENG and IEEE. His research interests are power system operation and control, power system optimization, robust power system security, power system stability, intelligent control and system, and artificial intelligences (optimization

Herlambang Setiadi Herlambang Setiadi was born in Sidoarjo, on November 29, 1990. He received a bachelor degree from Sepuluh Nopember Institute of Technology (Surabaya, Indonesia) majors in Power System Engineering in 2014. Then, master degree from Liverpool John Moores University (Liverpool, United Kingdom), majors in Electrical Power and Control Engineering in 2015. Furthermore, he received a Doctoral degree from The University of Queensland, majors in Electrical Engineering in 2019. Currently, He is a lecturer at School of Advanced Technology and Multidisciplinary, Universitas Airlangga. His research interest includes small signal stability in power systems, renewable energy integration

ISSN 2963-8577

Faculty of
Industrial Technology
Universitas Pertamina
Jl. Teuku Nyak Arief, RT.7/RW.8, Simprug, Kec. Kby. Lama, Kota Jakarta Selatan, Daerah Khusus Ibukota Jakarta 12220